A GENERAL MECHANISM OF MARTENSITIC NUCLEATION

BY

GREGORY BRUCE OLSON

S.B., S.M. Massachusetts Institute of Technology

1970

Submitted in partial fulfillment of the requirements

for the degree of

DOCTOR OF SCIENCE

at the

Massachusetts Institute of Technology

June, 1974

Signature Redacted

Signature of Author _____
Department of Metallurgy and Materials
Science, June, 1974

Signature Redacted

Certified by _____
Thesis Supervisor

Signature Redacted

Accepted by _____
Chairman, Departmental Committee on
Graduate Students

A GENERAL MECHANISM OF MARTENSITIC NUCLEATION

BY

GREGORY BRUCE OLSON

Submitted to the Department of Metallurgy and Materials Science on May 3, 1974, in partial fulfillment of the requirements for the degree of Doctor of Science.

ABSTRACT

Consideration of the martensitic nucleation process as a sequence of small steps which take the particle from maximum to minimum coherency leads to the hypothesis that the first step in martensitic nucleation is faulting on planes of closest packing. It is further postulated that the faulting displacements are derived from an existing defect, while matrix constraints cause all subsequent processes to occur in such a way as to leave the fault plane unrotated, thus accounting for the observed general orientation relations. Mechanisms for accomplishing these processes are described for the major lattice changes which occur in metal systems. For the specific case of the fcc→hcp transformation in Fe-Ni-Cr alloys and the fcc→bcc transformation in Fe30%Ni, the energetics of the proposed mechanisms are examined using a theory of stacking-fault energy developed from the basic concepts of classical nucleation theory. The theory predicts that, under the known thermodynamic conditions for martensitic nucleation, the fault energy decreases with increasing fault thickness. Spontaneous formation of martensitic embryos can occur by the simultaneous dissociation of 4 to 5 properly spaced lattice dislocations to produce a fault of sufficient thickness that the fault energy can be zero or negative. Thus, the function of the nucleating defect is to provide a group of appropriate partial dislocations of the proper spacing. Typical lattice defects, such as grain-boundary segments, incoherent twin boundaries and inclusion-particle interfaces, are considered as possible sites which can fulfill this function. Examples of martensitic nucleation at each of these sites by the proposed faulting mechanism are found in available experimental observations.

Thesis Supervisor: Professor Morris Cohen

       Title: Ford Professor of Materials Science and Engineering

TABLE OF CONTENTS

LIST OF FIGURES

Figure
Number

Page
Number

LIST OF TABLES

ACKNOWLEDGMENTS

The author is greatly indebted to Her Majesty Ms. Jane E. Black for making life worth the hassle.

1. INTRODUCTION

Having made practical use of martensitic transforma-
tions for over 3000 years, man's lack of an adequate explanation
of how these transformations come about has represented an
uncomfortable situation to those who like to consider metallurgy
a science. While phenomenological approaches to the
crystallography have produced a satisfying description of the
growth aspect of these transformations, the mystery largely
remains in the mechanism of nucleation; this is the problem we
address here.

It is now well recognized that classical homogeneous
nucleation theory cannot account for martensitic nucleation[1];
small-particle experiments have demonstrated convincingly that
the transformation is nucleated heterogeneously on rather
sparsely distributed special sites[2]. Proposed theories of
martensitic nucleation as they stand today are largely
concerned with the initial growth start-up of an existing
martensitic embryo. These theories were mainly developed to
explain bulk kinetic behavior. Kaufman and Cohen[1] and
Raghavan and Cohen[3] extended a model proposed by Knapp and
Dehlinger[4], and considered the formation of interfacial
dislocation loops as the rate-limiting step in martensitic
nucleation. Magee[5] later proposed that the motion of such
interfacial dislications might be rate-limiting. Subsequently,
Raghavan and Cohen[6] showed that the ideas of dislocation

formation and dislocation motion were interdependent: either may initiate the growth process depending on the size and shape of the embryo. . Mechanisms of how the embryos first come into existence have not been developed in detail. A possible exception might be the recent attempts to account for embryo production through soft phonon-mode concepts[7,8]. Though nucleation at free surfaces is predicted and there is recent indication from electron microscopy[9] that soft modes may have some relevance to nucleation in thin films, these theories are unable at this time to account for the known heterogeneous nature of martensitic nucleation in bulk material.

Knapp and Dehlinger[4] and Kaufman and Cohen[3] consider that embryos might be produced by some type of dislocation rearrangement above T_o, the parent-product equilibrium temperature. A conceptual difficulty with this approach is that, if such rearrangements are difficult below T_o when the chemical driving force is favoring embryo formation, it is hard to imagine how they can readily occur above T_o when opposed by the driving force. Experiments designed to detect the presence of such high-temperature embryos have not provided convincing support for their existence[10,11,12].

Magee[5] and Christian[13] suggested that such dislocation rearrangements could occur below T_o. By interaction with a suitable defect, the energy versus particle size may be "downhill" from the start and, further, a large critical nucleus size (implicit in the Knapp-Dehlinger and Kaufman-Cohen

approaches) may not be necessary. However, a specific defect and mechanism of defect-particle interaction has not been described. Thus, although the basic <u>energetic</u> scheme necessary to account for martensitic nucleation has been outlined by Magee[5] and Christian[13], a consistent nucleation mechanism has yet to be developed. A basic question in the martensitic nucleation problem today is thus one of <u>mechanism</u>, and that is the issue chosen for this thesis.

While the previous treatments of the martensitic nucleation mechanism have worked <u>backward</u> from the structure of a fully-developed martensitic unit with emphasis on explaining available <u>kinetic</u> information, the approach we will take here is to develop a nucleation sequence working <u>forward</u> from the very formation of the embryo and making use of available <u>structural</u> information. The latter consists primarily of (a) the known heterogeneous nature of the transformation, (b) the crystallography of the transformation (particularly the orientation relations), (c) established concepts of dislocation mechanics, and (d) hitherto unexplained results of transmission electron microscopy. We will also attempt here to deal with the nucleation process in sufficient generality to encompass many martensitic systems, thereby permitting the observations on one system to be incorporated in an understanding of others. Though we will discuss the critical step in nucleation for purpose of examining energetic feasibility, our main concern is actually with the development

of a general mechanism for the sequential stages in the overall process of embryo formation without emphasis on any particular stage as rate-limiting. Various possibilities will be explored in light of available experimental evidence, but we do not exclude the possibility that different stages may be rate-limiting in different systems and under different nucleation conditions.

2. BASIC CONCEPTS FOR A GENERAL MECHANISM

Theories of martensitic nucleation which consider the initial growth stage of a martensitic unit, starting with essentially the same structure as a fully developed macroscopic plate, are closely tied to the phenomenological theories[14,15] of the martensite crystallography, designed to account for the structure and morphology of the fully grown macroscopic product. However, if we consider the total nucleation process (that is, the process which includes the stage during which the first structure recognizable as the new lattice comes into existence), the phenomenological theories may not be entirely relevant.

The phenomenological theories assume that the interface plane (habit) of a martensitic plate must be an invariant plane (i.e. the shape change of the transformation is an invariant-plane strain). Recognizing that the lattice deformation which transforms the parent to the product lattice is not by itself an invariant-plane strain, a lattice-invariant deformation is added which, in combination with the lattice deformation*, fulfills the requirement that there be a plane which is macroscopically invariant. The processes which accomplish these deformations are envisioned as occurring simultaneously at a semicoherent interface, and the propagation of this interface accomplishes the growth of the martensitic plate.

---

* As in the Bowles and Mackenzie[15] formulation the total lattice deformation here includes a "Bain strain" relating the two lattices plus a rigid-body rotation.

In the case of <u>nucleation</u>, however, these processes need not occur simultaneously. The strain energy of a macroscopic plate is minimized if its interface plane is an invariant plane. On the other hand, if the shape of the particle at the earliest stage of nucleation is other than plate-shape, or by virtue of its small size, if coherency-strain energy is favored over surface energy, then the invariant-plane condition, and hence the lattice-invariant deformation, may not be necessary. But the <u>lattice deformation</u> per se is necessary if the particle is to be recognizable as a region of new lattice. Unlike the growth process which has been developed from the phenomenological theories, the total nucleation process might then be considered as some <u>sequence of steps</u> arranged in a logical order. Further, the phenomenological theories, though specific about the mechanism of the lattice-invariant deformation, do not consider the actual mechanism of the lattice deformation. Where the lattice deformation is of such importance in nucleation, the mechanism of the lattice deformation may constitute the very essence of the nucleation problem.

It is also apparent that, even in the total transformation process, there are additional constraints beyond those involved in the phenomenological theories. The success of the latter has largely been in demonstrating that, for the majority of martensitic transformations, a simple lattice-invariant deformation system can be found which, in combination with a logical lattice deformation (smallest principal strains), can

produce the observed total shape change and orientation relations. However, these theories do not explain why the observed lattice-invariant shear system is chosen over other possible systems which could also lead to invariant-plane shape strains (but differing from observed habit and orientation relations). These theories do not, therefore, account for such general observations as the tendency of the orientation relations to involve parallelism of planes of closest packing.

Still operating within the essential framework of the phenomenological theories, we will here examine other possible details of the transformation process with particular attention to the constraints existing at the nucleation stage. It is hoped that the result will be useful in understanding not only the nucleation problem, but also those problems dealt with by the phenomenological theories as well; though constraints in the growth stage (invariant plane) may not exist at nucleation, constraints operating at the nucleation stage may conceivably persist throughout the entire transformation process.

If we now consider the total nucleation process as a sequence of small steps, a reasonable order for these steps would be, by analogy with other phase transformations, one which takes the particle from maximum to minimum coherency. Moreover, the observed parallelism of closest-packed planes common to the orientation relations of all martensitic transformations is a rather special condition. It is improbable that such a condition would be attained by coincidence after all of the steps which

account for the total transformation process, but more likely
would be maintained throughout the total sequence, starting from
the first step. In addition, if we assume that the easiest
(lowest-energy) systems for the displacements in the lattice
deformation are the same as those for conventional plastic
deformation by slip, it seems probable that the first (most
coherent) step in the nucleation process would be faulting on
the closest-packed planes. Furthermore, there is considerable
evidence that the martensitic transformation is heterogeneously
nucleated[2]. If we assume that the function of the nucleating
defect is to provide the displacements of the first faulting
step, and consider the subsequent steps to be generated without
benefit of such pre-existing displacements, we can then
explain the observed general orientation relations by recognizing
that the constraint of the surrounding parallel close-packed
planes will tend to make these subsequent processes occur in
such a way as to leave the fault plane unrotated. These
considerations lead to the following concepts which we postulate
as the basis for a general mechanism of martensitic nucleation:

(1) Unlike the growth process developed from the
phenomenological theories, the total nucleation process can be
considered as a sequence of steps which take the particle from
maximum to minimum coherency.

(2) The first nucleation step consists of faulting
on the closest-packed planes; the fault displacement is derived
from an existing defect.

(3)   The subsequent steps in the nucleation process occur in such a way as to leave the fault plane unrotated.

We will here describe specific mechanisms consistent with these requirements for each of the major martensitic transformations occurring in metals. The energetic feasibility of these mechanisms will be examined in specific alloys under the conditions for which martensitic nucleation is known to occur (Chapters 4 to 6). Implications relative to kinetic behavior will also be explored (Chapter 7). Having defined the function of the nucleating defect, possible nucleation sites will be investigated in light of available experimental observations (Chapter 8).

In order to treat the energetics of general faulting mechanisms, we will first establish a procedure for the calculation of stacking-fault energy consistent with the underlying concepts of classical nucleation theory.

3. PRINCIPLES OF STACKING-FAULT ENERGY

There is often a certain skepticism regarding proposals of out-of-the-ordinary dislocation dissociations. Consideration of dislocation self-energies and interaction energies alone are not enough to decide whether a particular dissociation is possible. Once it is established that these energies are favorable, the deciding factor is the stacking-fault energy. To date there appears to be no unified theory for the calculation of stacking-fault energies in order to settle such questions. This problem is addressed here not only because we will be invoking rather special partial dislocations in the proposed nucleation mechanisms, but also because the concept of fault energy represents a realistic way of taking into account the basic concepts of classical nucleation theory in order to evaluate the energetic feasibility of nucleation by a general faulting mechanism.

3.1 General Principles

Attempts at thermodynamic calculation of stacking-fault energy usually treat the fault either as a surface[16,17] or as a small volume with only volume free energy[18,19]. However, if we recognize that a stacking fault represents a second-phase embryo, we find, consistent with classical nucleation theory, that the stacking-fault energy consists of both volume-energy and surface-energy contributions.

To identify the structure constituted by a particular fault, we use the following simple rule:

If 1 dislocation per x planes produces a bulk structure, then m such dislocations of the proper spacing produces an embryo of that structure n = m·x planes thick.

Figure 1 illustrates the structure of stacking faults in the fcc lattice. Figure 1a shows the normal ABC stacking of the fcc close-packed planes. Figures 1c and d indicate the stacking sequence for intrinsic and extrinsic faults, respectively. Inasmuch as an intrinsic fault can be formed by the motion of a single Shockley partial dislocation, while the motion of such a dislocation on every second plane would produce a bulk hcp crystal, an intrinsic stacking fault is actually an hcp embryo, two planes in thickness (n = 2). An extrinsic fault can be generated by the motion of Shockley partial dislocations on two consecutive planes. Since the motion of such dislocations on every plane would produce an fcc twin, we conclude that an extrinsic fault is a twin embryo, two planes in thickness (n = 2).

As in classical nucleation theory, the free energy of such second-phase embryos relative to the perfect lattice can be expressed in terms of the chemical free-energy difference between parent and product phases, ΔG^{chem}, a strain energy, E^{str}, and a true surface energy, σ. The fault energy, γ, expressed as an energy per unit area of fault (in the fault plane), for a fault n planes in thickness can be written as:

C	A	A	B
B	C	C	A
A	B	B	C
C	—A—	A	—B—
B	B'	—C—	C
A	A'	A	—A—
C	—C—	C	C
B	B	B	B
A	A	A	A

| (a) | (b) | (c) | (d) |
| Normal FCC Stacking | FCC→BCC Intermediate Structure | Intrinsic Fault | Extrinsic Fault |
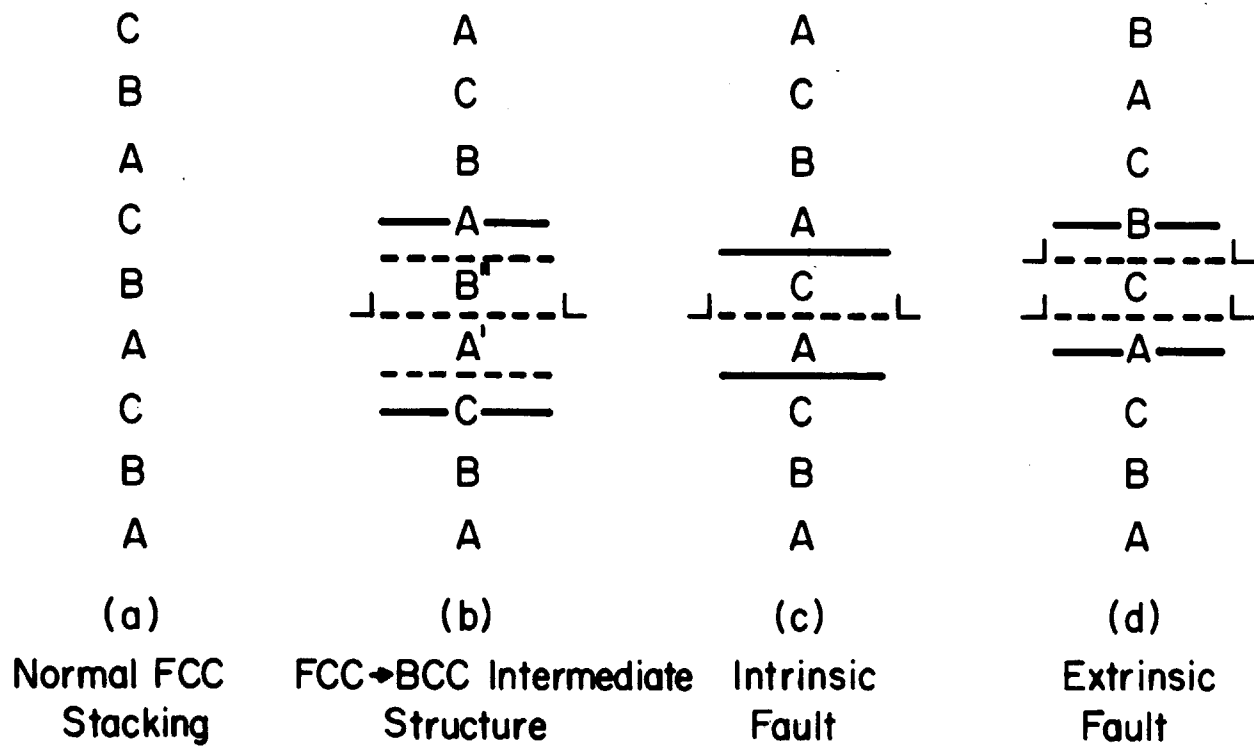
FIGURE 1. STACKING SEQUENCE OF CLOSE-PACKED PLANES OF FCC STACKING-FAULT STRUCTURES.

$$\gamma = n\rho_A \left(\Delta G^{chem} + E^{str} \right) + 2\sigma(n) \tag{1}$$

where ρ_A is the density of atoms in a close-packed plane in moles per unit area, ΔG^{chem} and E^{str} are defined here as molar quantities, and $\sigma(n)$ is the free energy per unit area of the particle-matrix interface. ΔG^{chem} and E^{str} refer to bulk properties defined in an infinite crystal and so are independent of the size of the embryo*.

By definition, then, the differences between "bulk" and "embryo" properties are included in the surface energy, σ, and we must allow for a possible dependence of σ, on the fault thickness (n), i.e. surface interactions at small separations. This approach represents a straightforward application of the basic definition of surface energy established by Gibbs[20]. Unlike other more approximate or qualitative approaches to fault-energy calculations, Equation (1) is a rigorous statement of the total energy of the fault.

3.2   Intrinsic Stacking-Fault Energy

Reliable measurements of intrinsic stacking-fault energy by the extended-node method are now available for many fcc alloys. When the bulk thermodynamic properties of the fcc and hcp phases of an alloy are well established, the stacking-fault energy determinations furnish, by the arguments presented here, an evaluation of the fcc-hcp coherent surface energy at

---

* E^{str} may be shape dependent, but will not depend on size per se.

two planes of separation. Lecroisey and Pineau[21,22] have measured the intrinsic fault energy as a function of temperature by the extended-node method in several Fe-Cr-Ni alloys. They demonstrated that their measurements correspond to equilibrium fault energies by showing that the observed node configurations were reversible upon heating and cooling.

The chemical free-energy differences between the fcc (γ) and hcp (ϵ) phases, $\Delta G^{\gamma \to \epsilon}$, were calculated for three of Lecroisey and Pineau's alloys, using the regular-solution thermodynamics of Breedis and Kaufman[23]. Values of $\Delta G^{\gamma \to \epsilon}$ are available for iron over the temperature range of interest, while linear extrapolations of high-temperature data to room temperature were adopted for pure chromium and nickel[23]. A third law correction for $\Delta G^{\gamma \to \epsilon}$ of chromium and nickel below 300°K was made by fitting the free-energy curves to Debye free-energy functions*. The resulting free-energy curves for the three alloys are shown in Figure 2.

Measurements[22] of the lattice parameters of the ϵ phase in Fe-Cr-Ni alloys indicate that the fcc-hcp transformation in these alloys is accompanied by a contraction along the hcp c-axis on the order of 1 percent. A calculation of the coherency strain energy associated with this contraction for the extended-node configurations on which the fault-energy measurements were made reveals that this energy represents less

---

* Knowing the Debye temperature of one phase, an "effective" Debye temperature of the other phase was determined from the measured high-temperature entropy difference. The Debye free-energy function thus defined was joined to the linear extrapolation at 300°K by adjusting $\Delta G_{o}^{\gamma \to \epsilon}$.
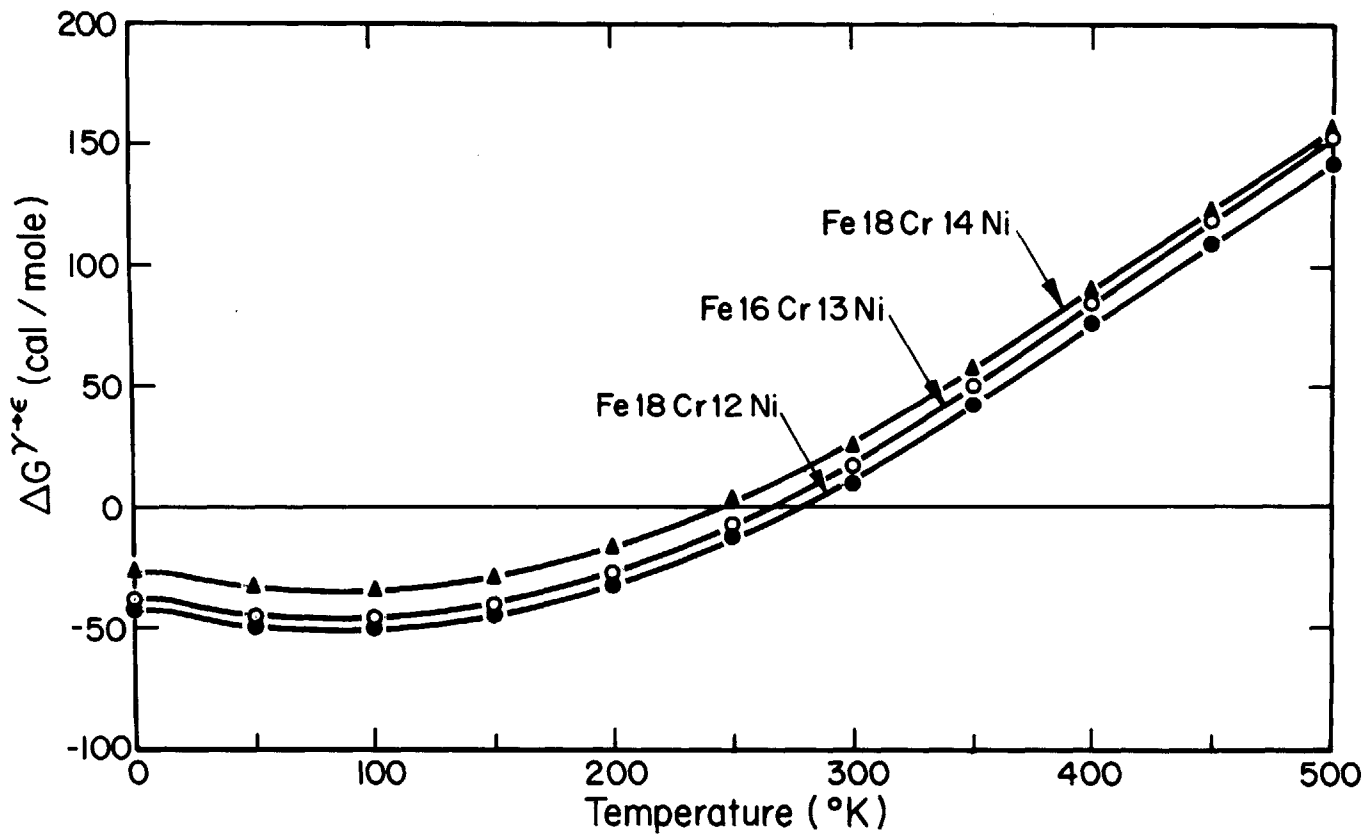
FIGURE 2. Calculated FCC-HCP free energy differences vs. temperature for the three Fe-Cr-Ni alloys examined by Lecroisey and Pineau[21].

than 0.1 percent of the measured fault energy. The contribution of coherency strain energy can thus be neglected.

Subtracting the volume chemical free-energy contribution of two planes of hcp from the measured intrinsic stacking-fault energies leaves (through Equation 1) a value which represents twice the fcc-hcp coherent surface energy at a separation of two planes. The stacking-fault energy measurements of Lecroisey and Pineau and the surface energy values thus obtained are shown in Figure 3. The surface energies for these three alloys are found to lie between 10 and 15 ergs/cm^2, and are relatively insensitive to temperature. Hence, the temperature dependence of the stacking-fault energy in these alloys arises principally from the fcc-hcp entropy difference, $\Delta S^{\gamma \to \varepsilon}$, as suggested by Lecroisey and Pineau.

Similar results have been obtained for Co and Co-Ni alloys. Ericson[24] has shown that the temperature dependence of the intrinsic stacking-fault energy in such alloys can be correlated with $\Delta S^{fcc \to hcp}$ in the same manner, and further, there is an additional contribution to the fault energy besides the volume chemical free energy, inasmuch as the fault energy still has a positive value at T_o, the fcc-hcp equilibrium temperature. By the formalism developed here, Ericson's measurements are consistent with fcc-hcp coherent surface energies of 5 - 10 ergs/cm^2.

Similarly, for a variety of other alloys[23,25], wherever data are available, comparison of measured intrinsic
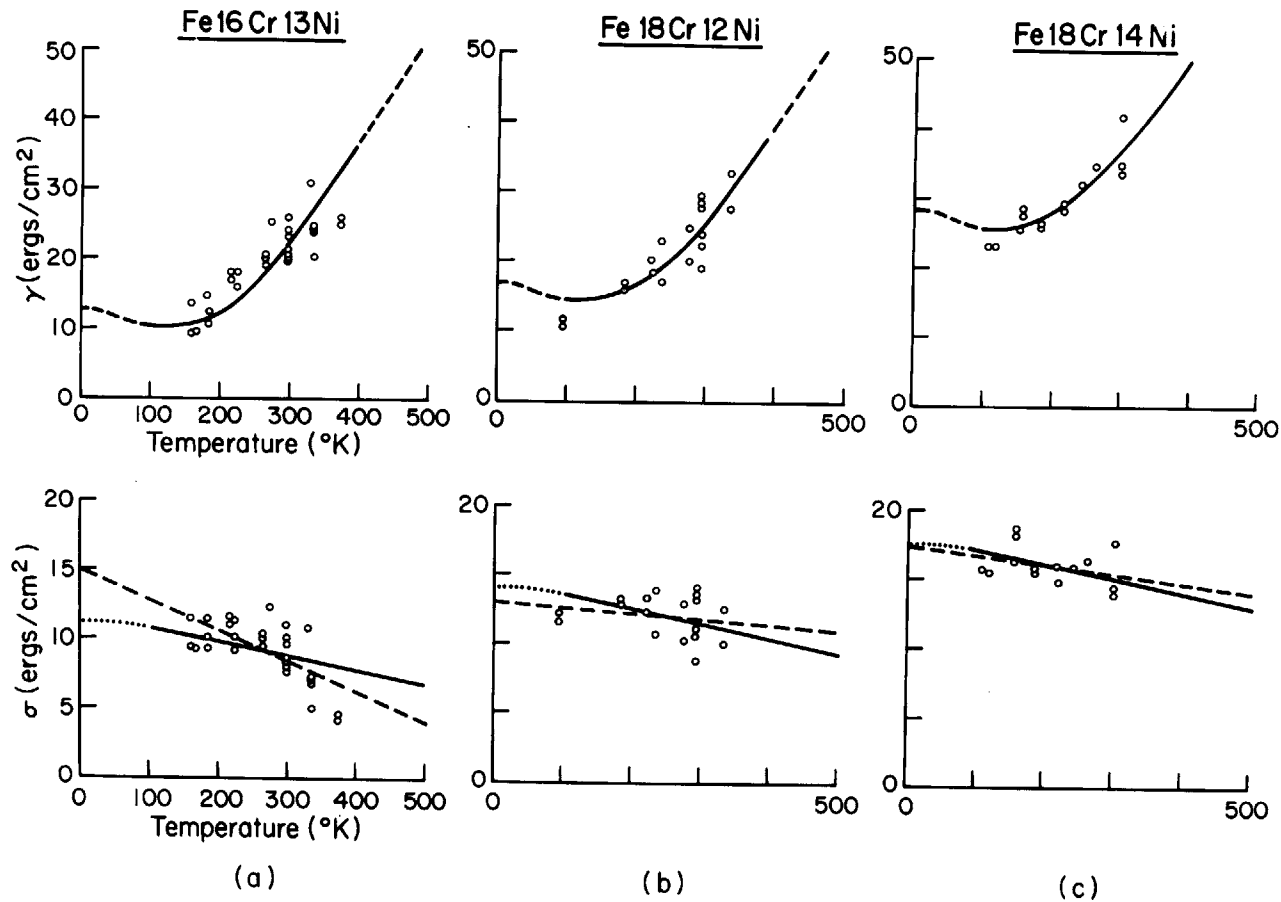
FIGURE 3. INTRINSIC STACKING-FAULT ENERGY, γ, AND COHERENT SURFACE ENERGY, σ, VS. TEMPERATURE FOR THE THREE ALLOYS OF FIGURE 2. MEASURED γ VALUES AND COMPUTED σ VALUES ARE REPRESENTED AS POINTS. DASHED σ CURVE REPRESENTS LEAST-SQUARES FIT THROUGH THE COMPUTED VALUES. SOLID CURVES REPRESENT BEST FIT USING A COHERENT SURFACE ENTROPY OF $S_A = 0.01$ ERGS/CM^2 - °K. (A) FE16CR13NI (B) FE18CR12NI (C) FE18CR14NI.

fault energies, and bulk thermodynamic data indicate a small
additional positive energy contribution which can be ascribed
to fcc-hcp coherent surface energy.

In the absence of surface adsorption effects, the
fcc-hcp coherent interface is expected to have a positive
surface entropy. The surface energies of Lecroisey and Pineau's
high-purity alloys (Figure 3) should, therefore, decrease with
increasing temperature. The dashed lines in the surface-energy
plots of Figure 3 represent least-squares fits to the data and
indicate that, though the actual magnitude of the slope may not
be statistically significant, there is a consistent decrease
with increasing temperature for all three alloys. The solid
curves show the best fit, using the average slope of the three
alloys which corresponds to a surface entropy of 0.01 ergs/cm^2-$^{\circ}$K
(the curves are flattened at very low temperatures to be
consistent with the Third Law). Adding the calculated volume
free-energy contributions to the surface-energy curves in
Figure 3 yields the calculated fault energies represented by the
solid curves through the measured fault-energy values. A
coherent surface entropy of 0.01 ergs/cm^2-$^{\circ}$K seems reasonable
since the ratio of the surface entropy to surface energy is
then of roughly the same magnitude as that for free surfaces
in metals. The influence of the coherent surface entropy on the
temperature dependence of the fault energy, is, of course,
small in comparison to the large effect of $\Delta S^{\gamma \rightarrow \varepsilon}$ in these alloys.
However, recent measurements in Co-Ni-Cr alloys[25], where

$\Delta S^{fcc \to hcp}$ is significantly smaller, indicate a discrepancy between the measured temperature dependence and that predicted by $\Delta S^{fcc \to hcp}$ alone, this being consistent with a coherent surface entropy of roughly the same magnitude.

The strong influence of $\Delta S^{fcc \to hcp}$ on the observed temperature dependence of the intrinsic stacking-fault energy, the consistent evidence for a positive surface energy, and the indications of a positive surface entropy, all represent excellent agreement between experiment and theory. Accordingly, where the bulk fcc-hcp thermodynamics of an alloy are known, calculation of the intrinsic stacking-fault energy as a function of temperature requires only one measurement to establish the appropriate fcc-hcp surface energy. In the absence of such a measurement, the range of observed surface energy values (5 to 15 ergs/cm^2) suggests that the use of a surface energy of 10 ergs/cm^2 can provide an estimate of intrinsic stacking-fault energy within $\pm$ 10 ergs/cm^2.*

3.3   Extrinsic Stacking-Fault Energy

Treating an extrinsic stacking fault (Figure 1d) as a twin embryo two planes in thickness predicts that the extrinsic fault energy represents twice the coherent twin-boundary energy at two planes of separation, since the volume thermodynamic contribution in this case will be zero in the absence of

---

* Provided $\Delta G^{fcc \to hcp}$ is known within $\pm$ 40 cal/mole.

applied stress. Experimental measurement of the extrinsic fault energy and the energy of isolated coherent twin boundaries in the same alloy would provide an interesting experimental determination of the extent of interaction of these interfaces at two planes of separation.*

3.4   Comparison with the Pair-Wise Central-Force
          Interaction Approach

The predictions of the thermodynamic approach to stacking-fault energy described here are compared with those obtained using the approximation of pair-wise central-force interactions in Appendix A. It is concluded that the relations obtained by the latter approach are not as precise as those of the more rigorous thermodynamic approach, but may provide some additional qualitative information beyond that available from the thermodynamics alone.

---

* An intrinsic fault, in addition to representing an hcp embryo
  two planes thick, can be considered as a twin embryo one plane
  in thickness. Where measured intrinsic and extrinsic fault
  energies are generally not equal, there is clearly a signifi-
  cant interaction of the coherent twin boundaries at one plane
  of separation. Treating an intrinsic fault in this manner is
  not a fruitful approach for fault-energy calculation.

4.   THE FCC→HCP TRANSFORMATION

The fcc→hcp martensitic transformation is the simplest case for examining the concept of nucleation by a faulting mechanism, in that the entire transformation can be achieved by simple faulting. In other words, a bulk hcp crystal can be created from fcc merely by the passage of a Shockley partial dislocation on every second close-packed plane. Moreover, the observation of such partial dislocations in the fcc-hcp martensitic interface[26], as well as the direct observation of splitting of lattice dislocations upon cooling into the transformation region[27], support the likelihood that the transformation actually occurs by this mechanism.

4.1   Basic Energetics

The measured values of the fcc-hcp coherent surface energy at two planes of separation are not very different from that expected for isolated fcc-hcp coherent interfaces, suggesting that the surface interaction beyond two planes of separation is not large. This provides a basis for adopting the approximation of classical nucleation theory that the surface energy is independent of particle size.

We can now examine the possibility of spontaneous nucleation by faulting. Equation (1) predicts that, under conditions where the volume-energy change, $\Delta G^{chem} + E^{str}$, is negative, the fault energy, γ, decreases with increasing fault

thickness, n. The volume-energy change will be negative when the magnitude of the chemical driving force, ΔG^{chem}, is greater than the strain energy, E^{str}; this will occur below T_o^{coh}, the equilibrium temperature for the parent and coherent-product structures. The fault thickness can be increased by "overlap"* of partial dislocations, and so we can consider the simultaneous dissociation of a group of dislocations rather than the dissociation of a single dislocation. The simplest configuration for this purpose is a finite symmetric tilt-boundary segment (or "superdislocation") where the dislocations are of the proper spacing. For fcc→hcp nucleation, such a defect would consist of a tilt boundary segment where the dislocations are spaced two planes apart. A distribution of sizes of such defects can be expected to exist in a crystal. Figure 4 is a schematic representation of the expected temperature dependence of the fault energies associated with the dissociation of defects of various thicknesses. At T_o^{coh}, all the faults have the energy, 2σ, but the energies diverge at lower temperatures because the energy of the thicker faults decreases more rapidly. Thus, under conditions where the intrinsic stacking-fault energy (n=2) is still positive, the energy of thicker faults can be zero or negative.

The dissociation of fcc lattice dislocations into Shockley partial dislocations lowers the total strain energy of

---

* "Overlap" here refers to the overlapping of the faults produced by the partial dislocations.
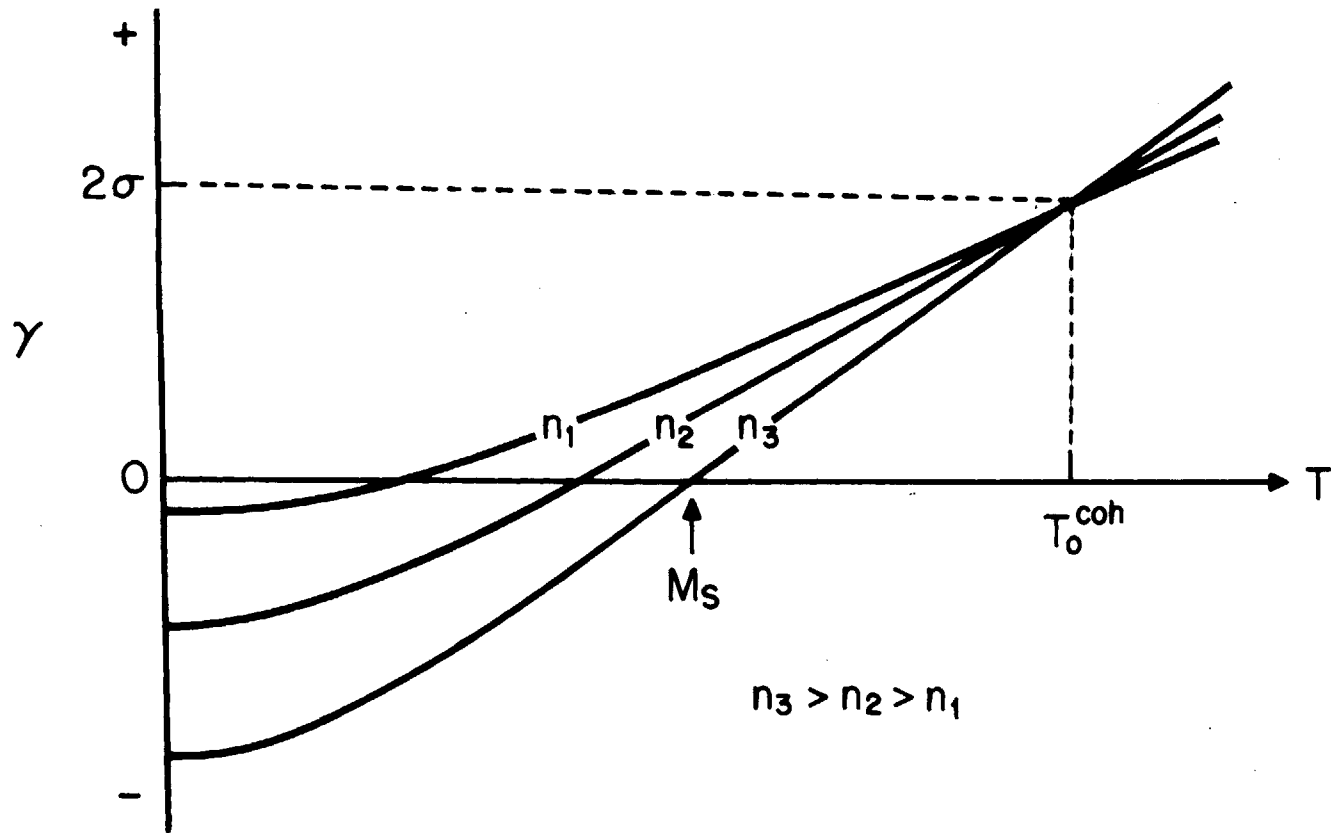
FIGURE 4. SCHEMATIC REPRESENTATION OF THE TEMPERATURE DEPENDENCE OF THE FAULT ENERGY, γ, FOR THREE FAULT THICKNESSES, n_1, n_2, AND n_3.

the dislocations (Frank criterion) and the partials repel each other. This is also true, in general, for the dissociations to be considered in subsequent chapters. In considering a finite tilt-boundary segment containing m dislocations of Burgers vector b dissociating into two finite boundary segments of Burgers vectors b_1 and b_2, the elastic interaction of the two segments can be approximated by treating them as superdislocations of Burgers vectors mb_1 and mb_2. For parallel dislocations of infinite length and line sense ξ, the energy (per unit length of dislocation) of moving such superdislocations from a separation r_o to r is given by[28]:

$$E_\perp(r) - E_\perp(r_o) = -\frac{\mu m^2}{2\pi}\left[(b_1 \cdot \xi)(b_2 \cdot \xi) + \frac{(b_1 \times \xi)(b_2 \times \xi)}{1-\upsilon}\right]\ln\frac{r}{r_o}. \qquad (2)$$

When the interaction of dislocations of Burgers vectors b_1 and b_2 is repulsive, the interaction of the superdislocations mb_1 and mb_2 is also repulsive.

At small separations, the interaction of the two finite boundary segments will not be as severe as that of the superdislocation analog but will still be repulsive in nature. Thus, the total dislocation energy will decrease monotonically with increasing separation. This dislocation energy actually represents the surface energy of the end interfaces bounding a thin second-phase embryo. The total free energy per unit

length of such an embryo formed by the dissociation of such
dislocations of infinite length is given by:

$$G(r) = E_{\perp}(r) + \gamma \cdot r . \tag{3}$$

Since the dislocation interaction is repulsive and $E_{\perp}(r)$ decreases
monotonically with r, the restraining force necessary to provide
a stable configuration (separation) of the partial dislocations
arises from a positive stacking-fault energy.* On the other
hand, if the stacking-fault energy is zero or negative, the
defect will be unstable.

Figure 5 is a schematic representation of the total
free energy of the system as a function of the separation, r,
of the partial dislocations bounding a faulted region. When
the fault energy is positive, there is an equilibrium separation,
r_{eq}, of the partial dislocations where the dislocation repulsion
is balanced by the "attractive" force associated with the fault
energy. Lowering the temperature to where the fault energy is
zero, the only force acting is the dislocation repulsion, and
the equilibrium separation becomes infinite. Lowering the
temperature further, the fault energy is negative, and provides
an additional force pushing the dislocations apart. Under such
conditions, the actual details of the short-range repulsive
dislocation interaction is relatively unimportant since, when
the fault energy is negative, the defect is clearly unstable

---

*   In assuming dislocations of infinite length, line-tension
    effects may be ignored for the time being.
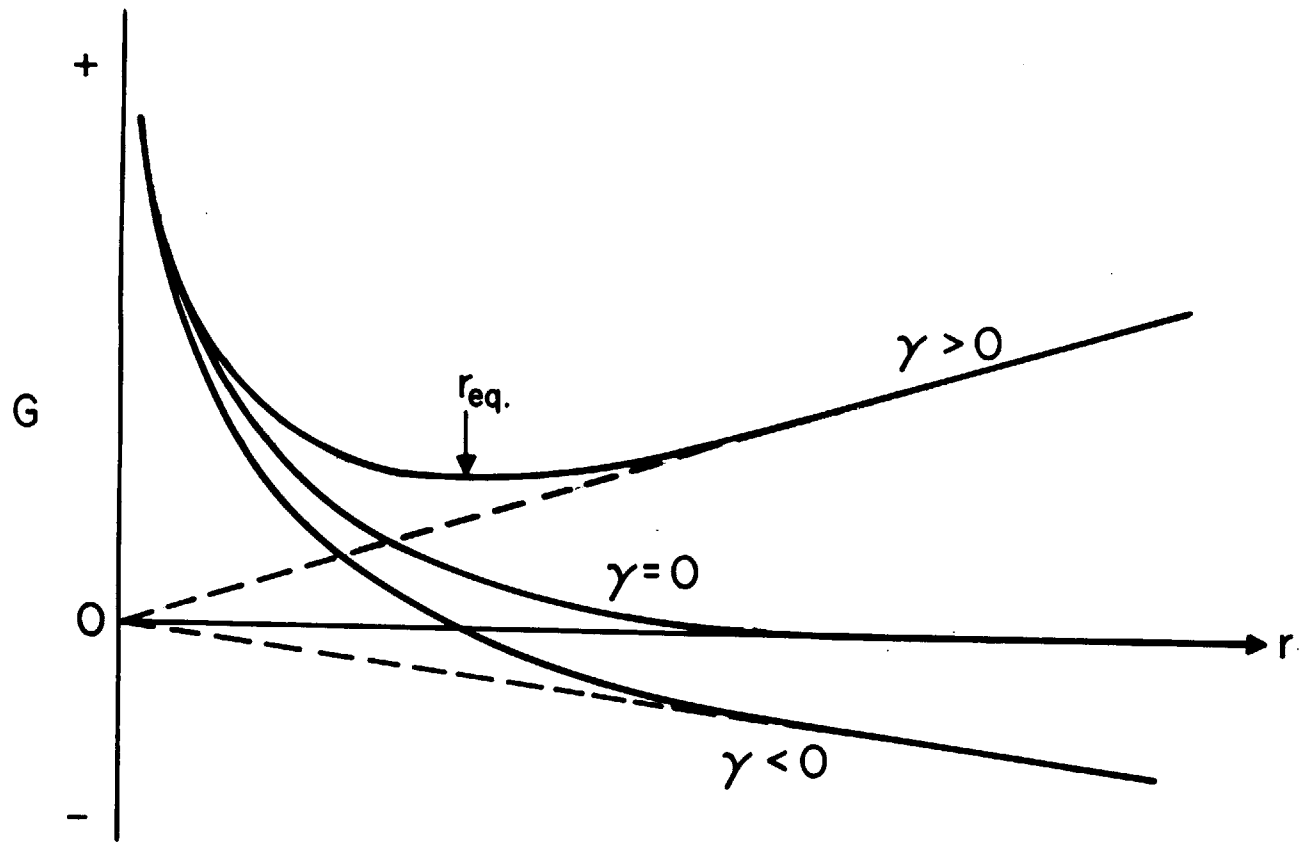
FIGURE 5. Schematic representation of total free energy, G, as a function of the separation, r, of the partial dislocations bounding a faulted region for the three conditions $\gamma > 0$, $\gamma = 0$, and $\gamma < 0$.

with respect to the formation of a thin martensitic embryo.

Once the embryo can attain a large size in the plane of

faulting, there is a reasonable chance of thickening by

incorporating other existing dislocations on parallel slip

planes (or possibly encountering pinned screw dislocations

crossing the plane which can thicken the particle by a pole

mechanism). We here regard the formation of the initial thin

embryo as "nucleation."

As indicated in Figure 5, when γ is zero or negative

there is no barrier to nucleation in the proposed model. Such

nucleation by the dissociation of a group of dislocations of the

proper spacing (normal to the fault plane) is thus an athermal

process. The overall energy scheme represented by Figure 5 is

similar to that suggested by Magee[5] and by Christian[13] for

martensitic nucleation from a defect. In terms of classical

nucleation theory, the situation considered here can be regarded

as heterogeneous nucleation on an existing interface where the

total energy of the two particle-matrix interfaces produced is

lower than that of the original interface they replace. As

long as the remaining terms contributing to the total particle

energy (here represented by the fault energy) do not increase

with particle size ($\gamma \leq 0$), the particle is unstable and there is

no barrier to nucleation. We will later treat the possibility

that a force provided by a somewhat negative fault energy is

required to drive the partial dislocations to large separations.

But for now, we will let $\gamma = 0$ represent the critical condition

for spontaneous nucleation from such a defect.

Given that there will be a distribution of sizes of the defects under consideration here, the M_s temperature will be determined by the largest (most potent) defect which is available in sufficient numbers to produce detectable transformation. We here define the size of the defect by the parameter n, the number of atomic planes in the thickness dimension of the fault (embryo) produced by the dissociation of the defect. The M_s temperature thus determined is indicated in Figure 4 where n_3 corresponds to the size or potency of the existing defect that defines M_s. We next compute the size of the defect necessary to account for nucleation under the known conditions for the fcc→hcp martensitic transformation in Fe-Cr-Ni alloys.

4.2   Energetics of the Transformation in Fe-Cr-Ni Alloys

4.2.1   Surface Energy

Two of the alloys studied by Lecroisey and Pineau[21,22] and discussed in Chapter 3 displayed a spontaneous ε martensitic transformation on cooling. The M_s temperatures for this transformation in the alloys Fe16Cr13Ni and Fe18Cr12Ni were found to be -95°C and -65°C, respectively. Referring to Figure 2, $\Delta G^{\gamma \to \varepsilon}$ at M_s for the two alloys is -34 cal/mole and -30 cal/mole, respectively. Assuming surface interaction to be small beyond two planes of separation (as previously justified), we can obtain the coherent fcc-hcp surface energy for these alloys from Figure 3, giving σ values of 10 ergs/cm^2 for Fe16Cr13Ni and 12 ergs/cm^2 for Fe18Cr12Ni.

4.2.2   Coherency Strain Energy

The coherency strain energy associated with the ~1%
contraction normal to the hcp basal plane for the "stress-free"
fcc-hcp transformation in these alloys can be neglected for the
extended-node configurations on which the intrinsic stacking-
fault energy measurements were made, since this configuration
is a shape which tends to minimize the coherency-strain energy.
However, at the critical stage of nucleation, it is expected
that the shape of the particle will not be one which minimizes
the strain energy, inasmuch as the shape should be established,
rather arbitrarily, by the geometry of the original defect.

Assuming isotropic elasticity, and a shear modulus,
μ, and Poisson's ratio, ν, for both particle and matrix, the
strain energy per unit volume, E_v, of a coherent particle in a
matrix where the stress-free transformation strain of the
particle is a pure dilatation, $\frac{\Delta v}{v}$, is given by Eshelby[29] as:

$$E_v = \frac{2(1 + \nu)}{9(1 - \nu)} \mu \left(\frac{\Delta v}{v}\right)^2 .$$ (4)

This result is independent of shape. Eshelby[29] also showed
that the strain energy per unit volume of a particle whose
stress-free transformation strain is a pure shear, $\varepsilon_{13} = \varepsilon_{31}$,
is shape dependent and is given by:

$$E_v = 2\eta\mu(\varepsilon_{13})^2$$ (5)

where $2\mu(\epsilon_{13})^2$ is the energy per unit volume necessary to pull the particle back to its original shape in the absence of the matrix or, alternatively, the strain energy per unit volume of the particle if it transformed in a perfectly rigid matrix. The η factor is a shape-dependent parameter which is the fraction to which the total energy per unit particle volume is reduced by accommodation of the transformation strains in the matrix. For a thin plate in the plane of shear, η approaches zero. The accommodation factor for a sphere is given by[29]:

$$\eta = \frac{7 - 5\nu}{15(1 - \nu)} \tag{6}$$

and for a rod[29] $\eta = 1/2$. For $\nu \approx 1/3$ the values for a sphere and a rod turn out to be very nearly the same.

If we consider nucleation by dissociation of infinitely-long dislocations in a tilt-boundary segment (Figure 6a), the shape of the particle in the early stages of dissociation will be rod-like. However, if the dissociation occurs by the bowing out of a finite length of such a segment where the spacing of the pinning points, ℓ, is comparable to the segment dimension, n (Figure 6b), the nucleating shape can be more nearly spherical. In view of the fact that the accommodation factors for these two shapes are nearly identical, we will assume a spherical shape for purposes of strain-energy estimates.

The spherical shape favors some additional simplifications. For spherical symmetry, the strain energy is independent
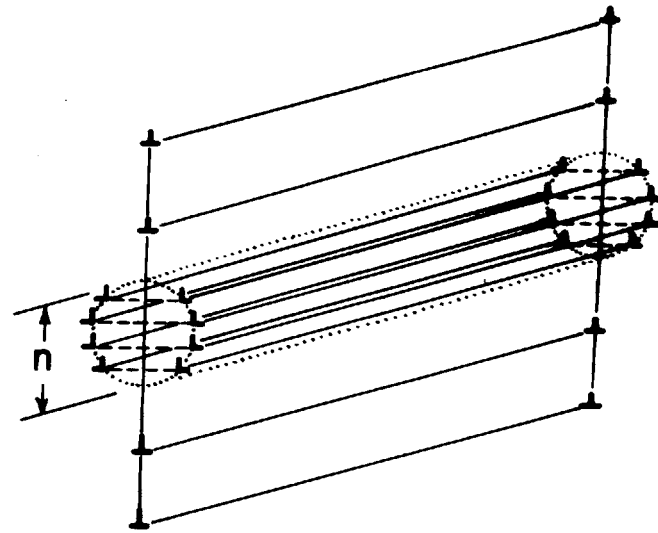
(a)
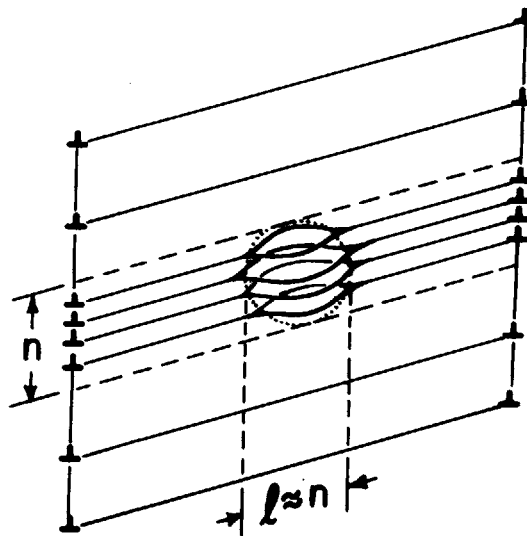
(b)

FIGURE 6. POSSIBLE PARTICLE SHAPES AT THE CRITICAL STAGE OF NUCLEATION FROM
THE TILT-BOUNDARY SEGMENT, (A) ROD SHAPE, CORRESPONDING TO
DISSOCIATION OF A GROUP OF INFINITE DISLOCATIONS, (B) SPHERICAL
SHAPE, CORRESPONDING TO THE BOWING OUT OF PINNED DISLOCATIONS
WITH SPACING OF PINNING POINTS, ℓ , COMPARABLE TO BOUNDARY
SEGMENT HEIGHT, N.

of the orientation of the shear. Hence, we assume that, for a
complex shear or deviatoric strain, the accommodation factor
will be about the same as for the simple shear (Equation 6)
and the total strain energy per unit particle volume can be
obtained by replacing $(\varepsilon_{13})^2$ in Equation (5) with the second
tensor invariant[30]:

$$\frac{1}{6} [(\varepsilon_{11}-\varepsilon_{22})^2 + (\varepsilon_{22}-\varepsilon_{33})^2 + (\varepsilon_{33}-\varepsilon_{11})^2] + \varepsilon_{12}^2 + \varepsilon_{23}^2 + \varepsilon_{13}^2.$$

The procedure adopted here and in subsequent chapters to estimate
the coherency strain energy at the earliest stages of nucleation
is to divide the transformation strains into dilatational and
deviatoric components. The strain energy associated with the
deviatoric component is to be evaluated by the procedure just
outlined, while the dilatational strain-energy component can be
determined through Equation (4).

To determine the transformation strains relevent to
the coherency strain energy in the type of heterogeneous nuclea-
tion we are considering here, we must subtract from the total
stress-free transformation strain matrix describing the total
transformation process those strains which are accomplished by
the motion of the existing dislocations. The total stress-free
strain describing the fcc-hcp transformation in these Fe-Cr-Ni
alloys consists of a shear $\varepsilon_{13} = \varepsilon_{31}$ equal in magnitude to one-
half an fcc twinning shear, and a small contraction ε_{33} normal
to the basal plane of approximately 1%. If we were to consider

fully coherent nucleation without benefit of an existing defect, all these strains would contribute to the coherency strain energy. However, in the defect-assisted nucleation we are treating here, the $\varepsilon_{13} = \varepsilon_{31}$ shear strain does not appear in the coherency strain energy contributing to the fault energy, γ, since the energy associated with this shear is in the form of interfacial energy associated with the existing dislocation array and is already accommodated in the matrix.

Accordingly the stress-free transformation strains appropriate to the coherency strain energy (per unit volume) simply reduces in this case to ε_{33}. Taking $\varepsilon_{33} = -.01$ and using an Fe-Cr-Ni austenite shear modulus of 7.4 x 10^{11} dynes/cm^2, [22] we obtain a deviatoric strain-energy component of 4.45 cal/mole and a dilatational component of 5.56 cal/mole to give a total coherency strain energy of 10 cal/mole at the early stages of nucleation by the proposed mechanism.

4.2.3   The Critical Defect

The size of the defect necessary to account for spontaneous nucleation of ε martensite at the observed M_s temperatures for these alloys according to the considerations represented in Figure 5 can now be calculated by setting $\gamma=0$ in Equation (1) and rearranging:

$$n = \frac{2\sigma}{-\rho_A(\Delta G^{chem} + E^{str})} .$$

(7)

Substituting the derived quantities in Equation (7), we obtain defect sizes of n=7 for Fe16Cr13Ni and n=10 for Fe18Cr12Ni. Since each partial dislocation produces two atomic planes of hcp, the existing defect which is responsible for the M_s temperature consists of 4 or 5 dislocations.

As an approximate estimate of the probability of such dislocation groups being available in sufficient abundance to account for observable transformation, we treat the probability of such groups existing as segments of larger inhomogeneous tilt boundaries. For a simple tilt boundary in which a fraction, f, of the slip planes crossing the boundary are randomly* occupied by dislocations, the probability that any m planes will be simultaneously occupied by dislocations is f^m.

If we consider all the dislocations in an annealed polycrystal with a dislocation density ρ (cm/cm^3) to be arranged as boundaries of subgrains of average diameter D, the length of dislocations per unit boundary area (or number per unit length) will be 1/3 ρD. The fraction of slip planes in the boundaries occupied by dislocations is then f = 1/3 ρDd, where d is the interplanar spacing. The probability of any arbitrary group of m planes being occupied by dislocations is thus $(1/3\ \rho Dd)^m$. The number of groups of m dislocations of a given configuration

---

* Dislocations in isolated finite tilt boundaries or in such
  segments of inhomogeneous tilt boundaries will experience
  climb forces. The assumption of a <u>random</u> distribution of
  the dislocations in such boundaries carries with it the
  assumption of restricted dislocation climb.

per unit length of boundary (or the length of such groups per unit boundary area) is given by the product of this probability and the number of possible positions of such groups per unit boundary length, d^{-1}. The number per area of such groups of length D is then $1/Dd$ $(1/3 \; \rho Dd)^m$ and the number per unit volume of sample, N_V, is given by

$$N_V = \frac{\rho}{D} \left(\frac{1}{3} \rho Dd\right)^{m-1}. \tag{8}$$

Taking $d = 2\text{Å}$, $D = 10\mu$ and $\rho = 10^9$ cm/cm^3 (including grain boundary dislocations) as representative of annealed polycrystalline austenites, the number per unit volume of groups of 4 dislocations of the appropriate spacing is 10^6 per cm^3. This agrees well with the expected density of initial martensitic nucleation sites which is generally taken to be between 10^5 to 10^7 per cm^3 on the basis of small particle experiments.[5]

The rapid variation of N_V with m indicated by Equation (8) is also consistent with the observed sharpness of the M_s temperature. The number per volume of more potent nucleation sites involving 6 dislocations is only 10^2 per cm^3.

Thus we see that the probability of a group of dislocations being arranged with a particular spacing decreases rapidly with the number of dislocations required for the nucleation event. The idea that 4 or 5 dislocations could happen to be spaced by two planes is sufficiently probable to be realistic, and at the same time sufficiently improbable (in

terms of the expected number of such defects per unit volume

of parent phase) to account for the known sparseness of the

initial nucleation sites which trigger the martensitic

transformation.

5. THE FCC→BCC TRANSFORMATION

We will now demonstrate that the fcc→bcc lattice change, despite an increased complexity of the atom motions, can also be accomplished by a faulting mechanism and treated with the same basic energetic considerations developed for the fcc→hcp transformation.

5.1   Mechanism

To consider the nucleation of the fcc→bcc martensitic transformation, we first develop a mechanism which is consistent with the concepts postulated in Chapter 2. A convenient place to start is the "double shear" mechanism developed by Bogers and Burgers[31] for the fcc→bcc conversion of a hard-sphere structure.

Figure 7a and d* illustrates an fcc packing of spheres lying in $\{111\}_{fcc}$ planes. Before dealing with the transition to a bcc structure, it is instructive to visualize the configuration of spheres after a regular fcc twinning shear, shown in Figure 7c and f, wherein successive layers parallel to the close-packed plane PVQ have shifted by $\frac{a_{fcc}}{6}$ <112> in the direction QT perpendicular to PV. The result of this twinning shear is that the shear plane PVQ and its

---

* Figure 7d-f are sections through the hard-sphere model in Figure 7a-c, corresponding to $\{110\}_{fcc}$ planes. Such planes are normal to the shear plane PVQ and contain both the shear direction QT and the dilatational direction.
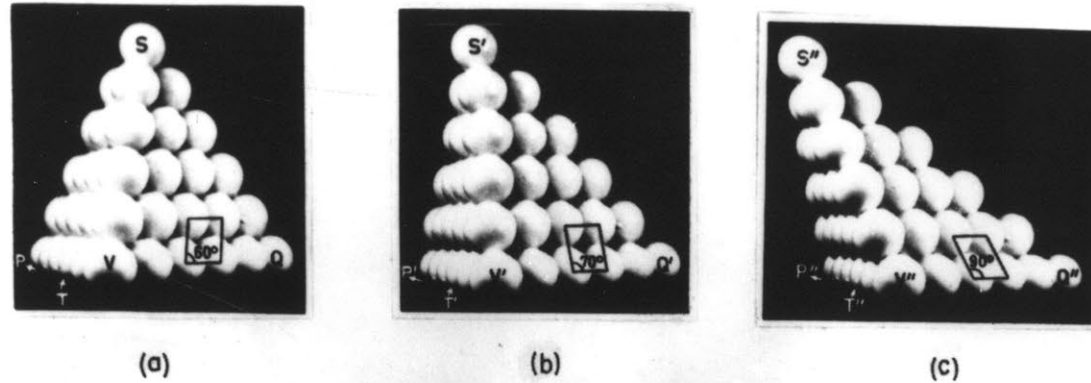
(a) Original tetrahedral arrangement with four {111} planes.

(b) Intermediate position after 1/3 of normal twin shear. The distance between successive {111} planes parallel to P'V'S' and P'V'Q' has increased by 5.4%.

(c) Final position after complete twin shear.
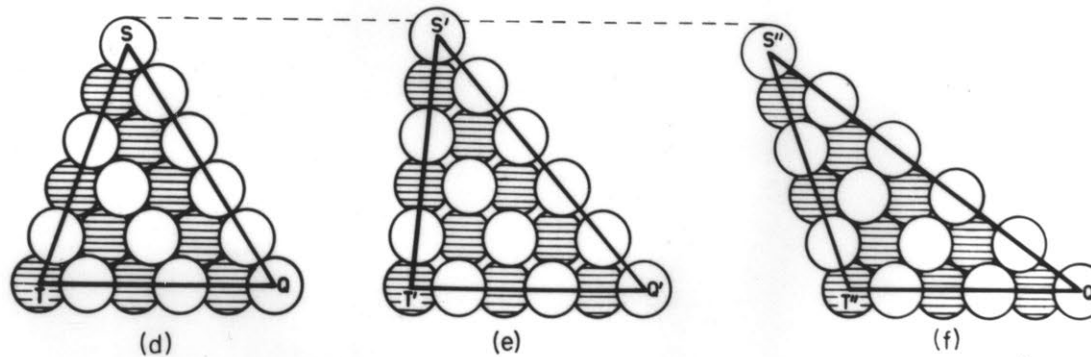
(d-e-f) Cross section through the {110} plane TQS perpendicular to PV.

FIGURE 7. HARD-SPHERE MODEL ILLUSTRATING TWINNING SHEAR $A_{FCC}/6 <112>$ IN AUSTENITE AND THE INTERMEDIATE POSITION CORRESPONDING TO $A_{FCC}/18 <112>$ WHERE THE INITIALLY CLOSE-PACKED PLANE QSV TAKES ON THE GEOMETRY OF A ${110}_{BCC}$ PLANE IN Q'S'V'. BOGERS AND BURGERS[31].

conjugate plane PVS remain as close-packed $\{111\}_{fcc}$ planes, whereas the other two close-packed planes QSV and QSP become $\{100\}_{fcc}$ planes. Thus, the 60° angle denoted in Figure 7a is enlarged to 90° in Figure 7c.

If we now trace the paths taken by the hard spheres during the transition from Figure 7a and d to 7c and f, each sphere must ride up to a saddle-point position between the initial and final states. Hence, a dilatational component normal to the shear plane is involved; this expansion amounts to 5.4 percent at <u>one-third of the twinning shear,</u> $\frac{a_{fcc}}{18}$ <112>, as shown in Figure 7b and e. Figure 7b further indicates that the shear plane PVQ and its conjugate plane PVS are still dimensionally unchanged, but the planes QSV and QSP are distorted in such a way that the 60° angle in Figure 7a is enlarged to 70° 32' in Figure 7b, thus attaining the geometry of a $\{110\}_{bcc}$ plane. The stacking sequence of these planes is not correct for a true bcc structure, but the latter can be obtained if successive planes (parallel to QSV or QSP) are sheared according to Figure 8. Referred to the bcc structure, this shear corresponds to a displacement of $\frac{a_{bcc}}{8}$ <110> on each plane, or $\frac{a_{fcc}}{16}$ <112> referred to the fcc structure. Again, because of the hard-sphere packing, there is a dilatation (3.6%) normal to the shear plane. Since each of the above shears entails a dilatational component, they are more accurately described as invariant-plane strains. By the Bogers-Burgers model, then, a bcc structure can be generated from an fcc structure by two

(a)   (b)
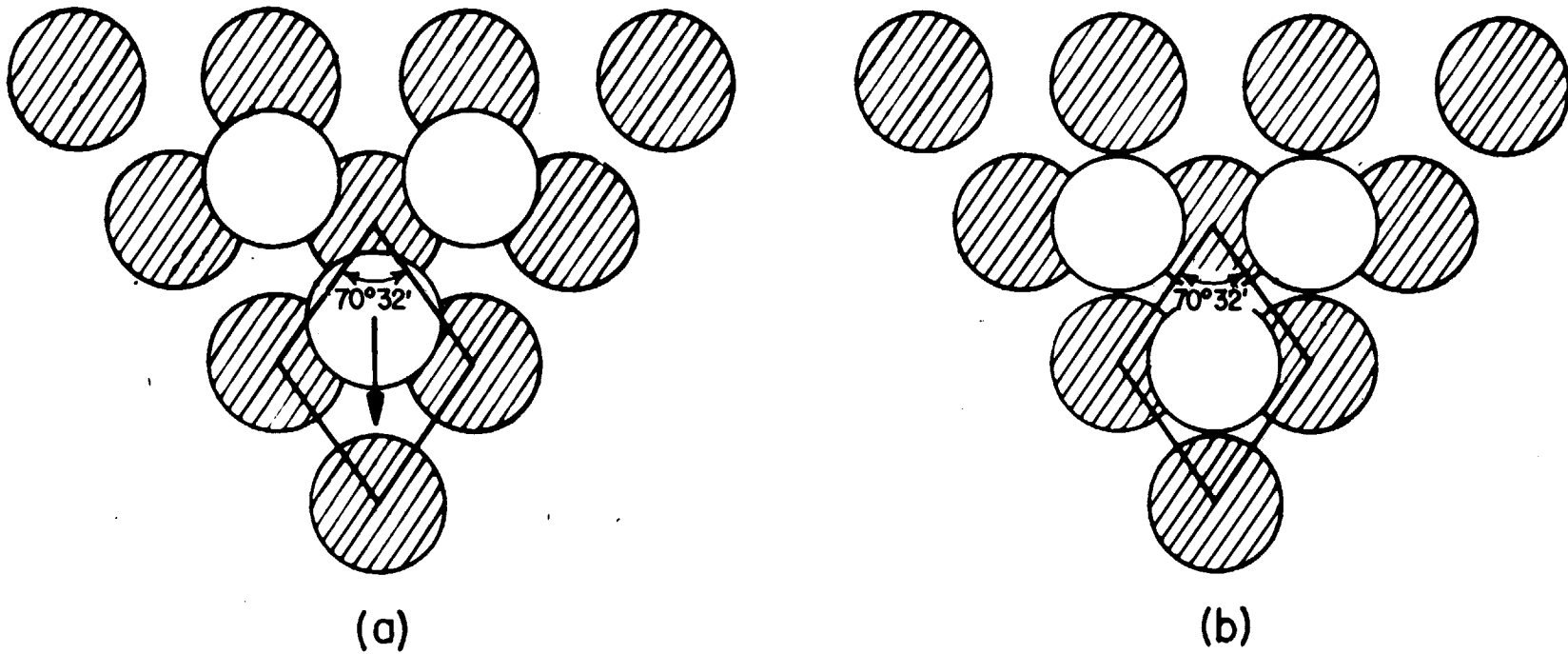
FIGURE 8.   STACKING OF $\{110\}_{BCC}$-TYPE PLANES IN HARD-SPHERE MODEL (A) AFTER THE
$A_{FCC}/18 <112>$ SHEAR IN FIGURE 7B AND E, AND (B) AFTER THE SUCCESSIVE
SHEARING OF THESE $\{110\}_{BCC}$-TYPE PLANES TO ACHIEVE THE PROPER STACKING
IN A REGULAR BCC STRUCTURE.   BOGERS AND BURGERS[31]

invariant-plane strains; for convenience, we will still refer to these deformations as "shears."

The first shear of the Bogers-Burgers model must involve displacements on each $\langle 111 \rangle_{fcc}$ plane of $\frac{a_{fcc}}{18} \langle 112 \rangle$, the latter being one-third the Burgers vector of a Shockley partial dislocation, $\frac{a_{fcc}}{6} \langle 112 \rangle$. Bogers and Burgers suggest that such partial displacements might occur by the "spreading" of a Shockley partial dislocation over a number of successive $\langle 111 \rangle_{fcc}$ planes. The concept is not difficult to imagine because, in the conventional glide motion of an $\frac{a_{fcc}}{6} \langle 112 \rangle$ partial dislocation, the atoms pass through appropriate positions for the first Bogers-Burgers shear. Under thermodynamic conditions where these positions are energetically favorable, the atoms may tend to stay in these positions (Figures 7b and e) rather than continue through to the full Burgers-vector twinning displacement of $\frac{a_{fcc}}{6} \langle 112 \rangle$ (Figure 7c and f). However, the full Burgers vector can be conserved if the atoms in an adjacent plane are concurrently "dragged along" to the same type of position. The concept is illustrated in Figure 1b. Since the effect of a Shockley partial displacement is to move atoms from A to B positions (and B to C, etc.) we can denote the positions obtained by dividing this displacement into thirds as A' and A" (also B' and B", etc.). The Shockley partial displacement which produced the intrinsic stacking fault in Figure 1c has moved the atoms in the plane immediately above the slip plane from B to C positions. In this process, the atoms moved through B" positions. If the intermediate

configuration is energetically favorable, this plane of atoms may

stay in the B" position, as in Figure 1b; the Burgers vector

is conserved if the A plane below is "dragged" to A' while

the planes above move through the full Shockley partial

displacement. In this manner, a single Shockley partial

dislocation can produce a fault with the structure of the

first Bogers-Burgers shear configuration, three planes in

thickness. Such a fault is actually bounded by $\frac{a_{fcc}}{18}$ <112>

dislocations on each plane, and we can say the original

Shockley partial dislocation has "spread" its core over three

planes. Just as the fcc→hcp lattice deformation can be

derived from a Shockley partial dislocation spaced every

second plane, the first shear of the Bogers-Burgers fcc→bcc

mechanism can thus be derived from Shockley partial disloca-

tions spaced three planes apart.

If we now examine the second shear of the Bogers-

Burgers mechanism occurring in a crystal lattice, we find

that it must be modified to conform to our postulate that the

initial fault plane will be left unrotated. Figure 9

represents the plane Q'V'S' of Figure 7b on which a simple

shear by the displacement "a" (as in Figure 8) on each plane

is required to convert the structure to bcc. The dashed line

XY is parallel to Q'V' and thus represents the line of

intersection of the two shear planes. The component of "a"

which is normal to XY will rotate the initial shear plane PVQ
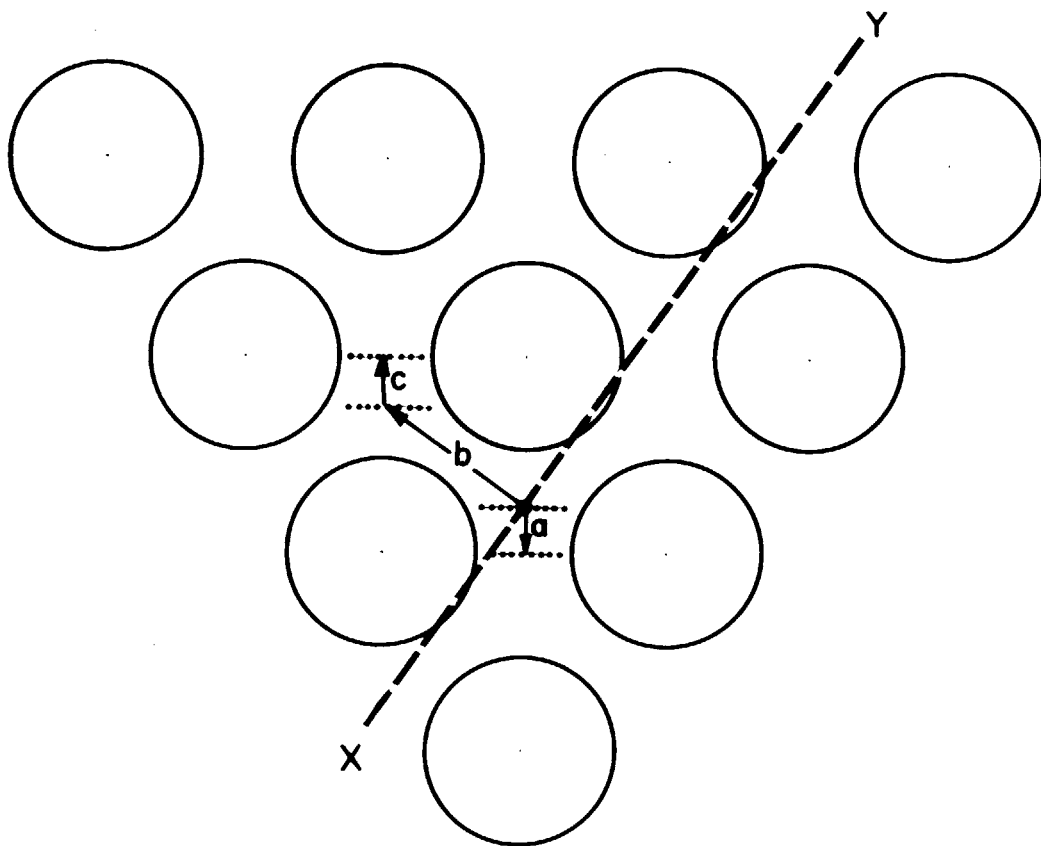
FIGURE 9. $\{110\}_{BCC}$-TYPE PLANE SHOWING ALTERNATE SHEAR
DISPLACEMENTS FOR CONVERTING THE STRUCTURE
PRODUCED BY THE FIRST BOGERS-BURGERS SHEAR TO
A BCC STRUCTURE. XY REPRESENTS THE LINE OF
INTERSECTION OF THE TWO BOGERS-BURGERS SHEAR
PLANES. SEVEN "A" DISPLACEMENTS FOLLOWED BY
A "B+C" DISPLACEMENT PRODUCES NO NET ROTATION
ABOUT XY.

about XY. This rotation will be opposed by the constraint of the close-packed planes of the matrix surrounding (parallel to) the faulted region. The rotation can be eliminated if every eighth Q'V'S' plane moves to a bcc position by the displacement "b + c" of Figure 9 instead of "a". The component of "b + c" normal to XY is seven times that of "a" and is oppositely directed. Thus, a displacement of "a" for seven planes followed by a "b + c" displacement* every eighth plane (on the average) can convert the configuration of the first Bogers-Burgers shear to bcc without a rotation of the initial shear (fault) plane. The displacement "c" is of the same magnitude as "a" ($\frac{a_{bcc}}{8}$ <110>) but is of opposite sign. The "b" displacement is $\frac{a_{bcc}}{4}$ <211> referred to the bcc lattice; referred to the fcc lattice, it represents a Shockley partial displacement. When these displacements occur in the faulted region left by the motion of the partial dislocations which accomplish the first Bogers-Burgers shear, they will leave the corresponding partial dislocations in the particle-matrix interface.

The proposed mechanism of fcc→bcc martensitic nucleation is outlined in Figure 10. Figure 10a represents an $\frac{a_{fcc}}{2}$ [1$\bar{1}$0] screw dislocation lying normal to the plane of the diagram ([1$\bar{1}$0] here corresponds to QV in Figure 7).

---

* The same result can be obtained by a homogeneous shear of "a" per plane with a displacement of a total lattice vector (-a+b+c) every eighth plane. However, such a description involves unnecessary additional atom motions.

(a) $\dfrac{a}{2}\left[1\bar{1}0\right]$ ⊥

(b) $\dfrac{a}{18}\left[1\bar{2}1\right]$ ⌐————————⌐ $\dfrac{a}{18}\left[2\bar{1}\bar{1}\right]$

(c) $\dfrac{a_{fcc}}{6}\left[112\right]+\dfrac{a_{bcc}}{8}\left[0\bar{1}1\right]$

$\dfrac{a_{bcc}}{8}\left[0\bar{1}\bar{1}\right]$
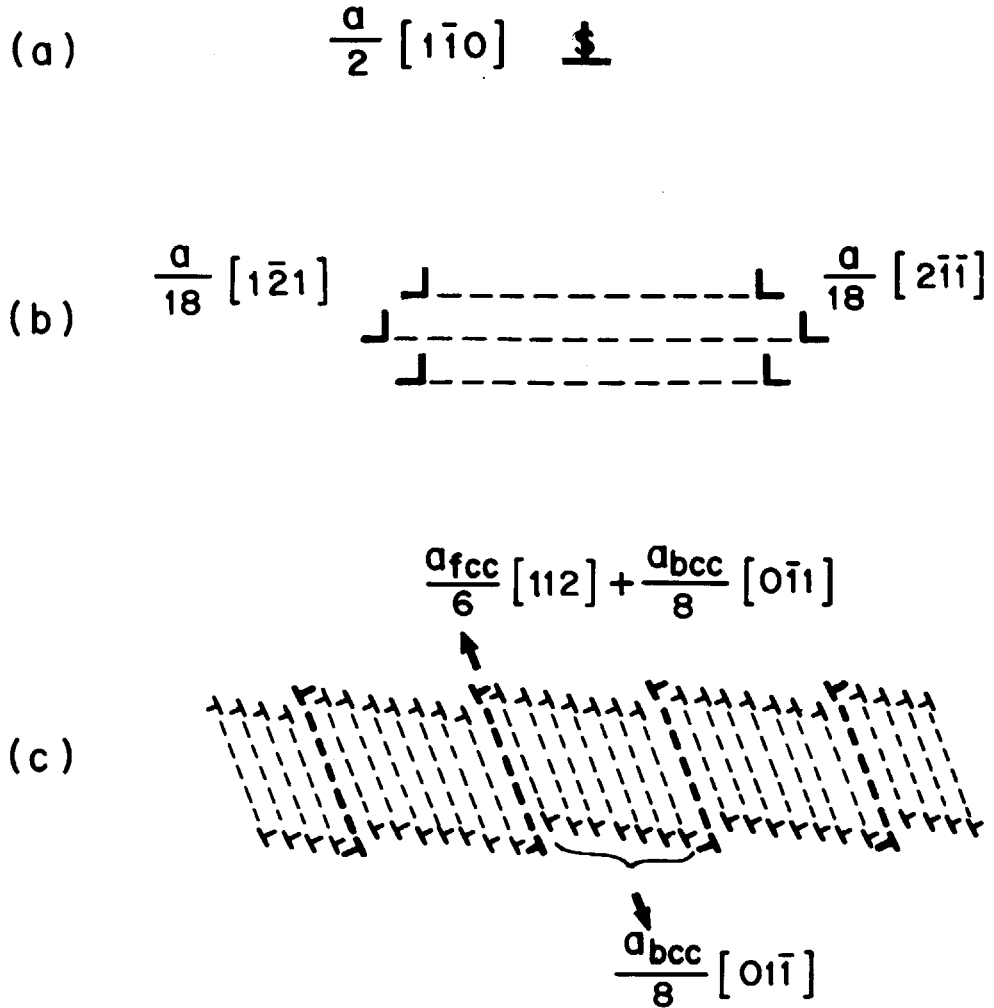
FIGURE 10. Sequence of steps for the formation of a semicoherent BCC embryo from an FCC lattice dislocation. (A) Existing $A_{FCC}/2\left[1\bar{1}0\right]$ screw dislocation. (B) Dissociation of dislocation with spreading of cores over consecutive planes to produce a fault with the structure of the first Bogers-Burgers shear configuration. (C) Spontaneous relaxation of fault of (B) to BCC structure producing new partial dislocations in the fault interface.

Dissociating on the (111) plane (corresponding to PVQ in Figure 7) and "spreading" over three planes, this dislocation can produce three $\frac{a_{fcc}}{18}$ [1$\bar{2}$1] and three $\frac{a_{fcc}}{18}$ [2$\bar{1}\bar{1}$] partial dislocations as in Figure 10b. The fault produced by this operation alone has the structure of the first Bogers-Burgers shear configuration. Thicker faults can be produced by the simultaneous dissociation of an $\frac{a_{fcc}}{2}$ [1$\bar{1}$0] dislocation every three planes. From this structure, atoms can slide to bcc positions by the modified second shear mechanism just described. This shear occurs on (11$\bar{1}$)$_{fcc}$ = (011)$_{bcc}$ (corresponding to QVS in Figure 7), and will produce an interfacial structure (Figure 10c) consisting of seven $\frac{a_{bcc}}{8}$ [01$\bar{1}$] partial dislocations followed by an $\frac{a_{bcc}}{8}$ [0$\bar{1}$1] partial dislocation and an $\frac{a_{fcc}}{6}$ [112] Shockley partial dislocation every eighth plane. In this way, a semicoherent bcc martensitic embryo is produced in the Kurdjumov-Sachs orientation:

$$(111)_{fcc} \quad || \quad (101)_{bcc}$$
$$[1\bar{1}0]_{fcc} \quad || \quad [11\bar{1}]_{bcc} \ .$$

Accordingly, we are proposing a model for the fcc→bcc lattice deformation where the transformation strains are principally derived from the shears associated with two sets of partial dislocations; one set is derived from an existing defect, while the other is spontaneously generated. Additional strains necessary to produce a perfect bcc structure are obtained from dilatations (normal to the shear plane) which

accompany these partial shears, owing to the "hard-sphere" nature of the atoms. To arrive at the correct lattice parameter of the product phase, however, a uniform dilatation must be superimposed. Inasmuch as the semicoherent embryo represented in Figure 10c still has a high degree of coherency with the matrix, it will not be able to relax completely to its equilibrium structure at this early stage. There is no "invariant line" or "invariant plane"; these are established in later stages of the total sequence which leads the particle from maximum to minimum coherency (and hence decreasing strain energy). The conditions which may determine how the "invariant line" and "invariant plane" are established in these later stages (thus influencing macroscopic morphology) are examined in Appendix B. We will now consider the energetic feasibility of the formation of a semicoherent bcc nucleus by the mechanism just discussed.

5.2   Energetics of the fcc→bcc Lattice-Deformation

To examine the energetics of the proposed nucleation mechanism, we will deal with the specific case of the fcc→bcc martensitic transformation in Fe30Ni, since the conditions under which martensitic nucleation occurs in this alloy are well established. We first consider the energetic feasibility of the fault produced by the first Boger-Burgers shear alone (represented in Figures 10b and 1b) existing in significant sizes. The distorted structures of such a fault is midway between

fcc and bcc since it can be visualized as fcc which has been sheared 24 percent along [1$\bar{2}$1] on (111) or bcc which has been sheared 25 percent along [0$\bar{1}$1] on (011). Hence, the structure represents a specific model for the old "strain embryo" concept so often discussed in connection with martensitic nucleation. The view is generally held that such a structure is of too high a strain energy to exist in any significant size[1,32]. Where the chemical driving force at M_s for Fe30Ni is about 300 cal/mole, the strain energy of such a defect, regarding it as distorted bcc, must be approximately of this magnitude or less for the structure to exist in appreciable size. The isotropic elastic constants of Fe30Ni martensite at M_s have been measured by Goldman and Robertson[33]. Assuming the same elastic anisotropy as for pure iron, the appropriate modulus for [0$\bar{1}$1] (011) shear is 4 x 10^{11} dyne/cm^2 [34]; and if all the strain is confined to the particle, linear anisotropic elasticity predicts a strain energy of 2100 cal/mole. If we consider an elastically relaxed form of the particle such that some of the distortion is accommodated in the matrix, an isotropic linear elastic calculation using the shape considerations discussed in Chapter 4 can lower the energy by as much as 1/2; but this is still much too high in relation to the chemical driving force.

A shear strain of 25 percent is large enough that nonlinear elastic effects might be substantial. To estimate the magnitude of such effects, the strain energy of the unrelaxed

configuration of the first Bogers-Burgers shear (referred to
the bcc lattice) was computed using various interatomic
potentials available for pure iron. These calculations are
discussed in detail in Appendix C. The results indicate that
the strain energy is not significantly different from that
predicted by linear elasticity. Thus, it appears that the
strain energy of this configuration, even in some elastically
relaxed form, will not be much less than 1000 cal/mole. With
a chemical driving force of 300 cal/mole, this corresponds
(through Equation (1)) to a fault energy for the fault of
Figures 1b and 10b of roughly +350 ergs/cm^2 per plane of fault.
Therefore, it is expected that the motion of the partial
dislocations which produce the first Bogers-Burgers shear
configuration will only occur under conditions where the
fault structure thus produced can move spontaneously to the
configuration of Figure 10c immediately as the dislocations
pass. As discussed further in Appendix C, the high-energy
configuration of Figure 10b then need only exist at the cores
of the partial dislocations which make up the interfaces
that bound the ends of the fault (embryo).

The consideration of such fcc-bcc intermediate
configurations in Appendix C indicates that the high-energy
configuration of the first Bogers-Burgers shear should be
unstable and an unconstrained particle in this configuration
would move spontaneously to bcc without barrier. For a
constrained particle in a matrix, however, spontaneous

relaxation to the configuration of Figure 10c can occur when the fault energy of this configuration is zero or negative. We now estimate the energy of this complex fault.

5.2.1 Surface Energy of the Semicoherent bcc Embryo

The surface energy of the fault in Figure 10c arises principally from the partial dislocations produced in the interface. Picturing these dislocations as lying along $[1\bar{1}0]_{fcc}$, the Burgers vectors can be separated into screw and edge components* and the energies of these components evaluated separately. The energy per unit area, $\gamma_{\perp}^{screw}$, of a single set of screw dislocations of Burgers vector magnitude b and spacing D, can be computed as one half the energy of forming two such arrays of opposite sign and moving them to infinite separation; the energy is set to zero at a separation of $r_o = b/\alpha$, where α is the core-energy cut-off parameter designed to take core energy into account in the integration.[28] Integrating from r_o to ∞ gives an infinite energy for such an array because its stress field produces a constant strain at large distances. However, at an interphase interface where such an array is matching two structures, this constant strain puts atoms in equilibrium positions with no associated strain energy. Thus, for the case of a single set of screw dislocations matching two structures at an interface, a constant stress term, ϕ, must be added to the normal dislocation stress field, $\sigma_{yz}(x)$, as in the

---

* These components are best seen in Figure 9 where the vectors indicated represent the Burgers vectors in question and XY the dislocation line.

energy calculation for a misfit edge-dislocation interface by

Brooks[35]. The energy of such a boundary is then given by:

$$\gamma_{\perp}^{screw} = \frac{1}{2D} \int_{r_o}^{\infty} [\sigma_{yz}(x) + \phi] \, bdx \qquad (9)$$

Substituting the appropriate expression[28], $\frac{\mu b}{2D} [\coth (\frac{\pi x}{D}) - 1]$,

for $\sigma_{yz}(x) + \phi$ and integrating, we obtain,

$$\gamma_{\perp}^{screw} = \frac{\mu b^2}{4\pi D} \left[(\frac{\pi r_o}{D}) - \ln \left| \sinh (\frac{\pi r_o}{D}) \right| \right]. \qquad (10)$$

Goldman and Robertson[33] have measured the isotropic shear

moduli of the fcc and bcc phases of Fe30Ni at M_s as 6.5×10^{11}

dynes/cm^2 and 5.5×10^{11} dyne/cm^2, respectively. Taking particle

and matrix to be in parallel, we use an "effective modulus" of

$\mu = 6 \times 10^{11}$ dyne/cm^2. Approximating the screw component of the

dislocation interface of Figure 10c as a homogeneous array

consisting of one dislocation per plane with the appropriate

Burgers vector to produce the required overall displacement.,

we obtain a screw-component contribution to the interfacial energy

of 27 ergs/cm^2.

The edge component of the interfacial dislocation

array can be considered as two sets of dislocations: one

consisting of a small partial dislocation on each plane, and

the other consisting of a larger oppositely directed dislocation

every eighth plane. Where the function of the second set is to

cancel the effect of the first (so that there is no rotation of

the fault plane), the array represents two skewed tilt boundaries

stabilized by the cancellation of their (long-range) stress fields. An upper limit of their energy can be estimated by regarding them as two separate symmetric tilt boundaries. The energy of a symmetric tilt boundary is given by[28]:

$$\gamma_{\perp}^{edge} = \frac{\mu b^2}{4\pi(1-\nu)D} \left[\frac{\pi r_o}{D} \coth \frac{\pi r_o}{D} - \ln \left(2 \sinh \frac{\pi r_o}{D}\right) \right]$$

$$\dots \dots (11)$$

The energy of the two sets of edge dislocations then comes out to be 50 ergs/cm^2 and 236 ergs/cm^2, respectively, giving a total edge-component contribution of 286 ergs/cm^2 to the interfacial energy.

However, since the tendency of the two sets of dislocations in the interface is to cancel each other, there will be a strong interaction between them. A better estimate might be simply to sum the core energies of the dislocations. Taking a core energy per unit length of $\frac{\mu b^2}{4\pi(1-\nu)}$ [28] gives energies of 42 ergs/cm^2 and 180 ergs/cm^2, or a total edge-component contribution of 222 ergs/cm^2,

Overlap of the cores of the two sets of edge dislocations might lower their energy contribution even further. If we allow the second set of edge dislocations to "spread" their cores over consecutive planes to produce a continuous distribution, the basic structure of the embryo is unaffected.* In this case there would be a total cancellation

---

* In considering the structure of a martensitic interface, Frank[36] suggests that his interfacial screw dislocations might spread their cores in this manner.

of the two sets of edge dislocations and their energy

contribution would be zero. Allowing for some extent of core

overlap, therefore, we will say that the contribution of the

edge component of the interfacial dislocation array is between

zero and 222 ergs/cm^2.

Summing up the screw- and edge-component contributions

to the energy of the interface dislocation array and adding an

estimate of 20 ergs/cm^2 as the contribution of the fcc-bcc

coherent surface energy, we obtain a total surface energy, σ,

for the fault of Figure 10c of between 50 and 270 ergs/cm^2.

We will adopt a value of $\sigma = 150$ ergs/cm^2 for further

calculations; the surface energy of a fully developed

martensite interface is generally estimated as $\sim$200 ergs/cm^2,

while the structure considered here represents a more coherent

form.

5.2.2   Coherency Strain Energy

As in Chapter 4 we obtain the transformation strains

relevent to the coherency strain-energy contribution to the

fault energy, γ, of the semicoherent embryo by subtracting from

the total stress-free transformation strain matrix the shear

strain in the fault plane which can be derived from the existing

defect and which is therefore already accommodated in the form

of existing (dislocation) interfacial energy. In addition,

shear displacements associated with the partial dislocations

in the (111)$_{fcc}$ interfaces which are produced by the spontaneous

motions of the atoms within the fault from unstable to stable

positions are also accommodated in the form of the interfacial

energy just calculated. Hence, the volume coherency strain

energy here arises principally from the dilatations which

must accompany the shear displacements of the partial

dislocations owing to the hard-sphere nature of the atoms in

the model. A 5.4 percent expansion normal to the fault plane

is associated with the first shear, and there is a 3.6 percent

expansion normal to the plane of the second shear. Since the

"hard-sphere" model produces a bcc structure with too large a

lattice parameter, a uniform contraction of 2.3 percent in all

directions must be superimposed to produce the final structure.

Referring these strains to the same coordinate system, where

x_1 is $[1\bar{1}0]_{fcc}$, the close-packed direction common to the two

shear planes, and x_3 is $[111]_{fcc}$, the normal to the fault

plane, gives the following result for ε_{ij}^T, the remaining

"stress-free" transformation strains:

$$\varepsilon_{ij}^T = \begin{bmatrix} 0 & 0 & 0 \\ 0 & 0 & 0 \\ 0 & 0 & .054 \end{bmatrix} + \begin{bmatrix} 0 & 0 & 0 \\ 0 & .032 & .011 \\ 0 & .011 & .004 \end{bmatrix} + \begin{bmatrix} -.023 & 0 & 0 \\ 0 & -.023 & 0 \\ 0 & 0 & -.023 \end{bmatrix} = \begin{bmatrix} -.023 & 0 & 0 \\ 0 & .009 & .011 \\ 0 & .011 & .035 \end{bmatrix} \quad (12)$$

With the procedure outlined in Chapter 4 and again using

$\mu = 6 \times 10^{11}$ dynes/cm^2, we obtain deviatoric and dilatational

strain energies of 105 cal/mole and 18 cal/mole, respectively.

The total volume coherency-strain energy, E^{str}, is thus 123

cal/mole. In view of the fact that this energy is significantly

less than the magnitude of the chemical driving force of 300

cal/mole at M_s, the fault energy will decrease with increasing

fault thickness.*

5.2.3   The Critical Defect

To examine the energetic feasibility of the proposed

mechanism of formation of a semicoherent bcc embryo, we now

assume that the formation of this embryo fault represents the

critical step in fcc→bcc nucleation as in fcc→hcp nucleation.

Following the same energetic considerations represented in

Figure 5 of Chapter 4, we first take the condition that $\gamma = 0$

for the most potent defect (available in detectable quantity)

to represent the condition which defines the M_s temperature.

(This condition of $\gamma = 0$ will be relaxed in Chapter 7.)

Substitution of the estimates of σ, E^{str}, and ΔG^{chem}

in Equation (7) results in a critical defect size for the

spontaneous formation of the proposed nucleus at M_s of n = 13.5.

Since three planes of fault can be derived from one lattice

dislocation, the nucleating defect again corresponds to 4 to 5

dislocations of the proper spacing. The similarity of this

result with that obtained for the fcc→hcp transformation is note-

worthy in terms of the generality of the proposed mechanism of

nucleation by faulting.

---

* Since the surface energy here arises principally from the
   interfacial dislocations, the extent of interaction between
   the two opposite surfaces can be calculated. Such a calcula-
   tion reveals that the range of interaction is on the order of
   the dislocation spacing in the interface. Surface interaction
   is, therefore, negligible for the fault thicknesses we are
   considering.

The long experimental search for martensitic embryos
in Fe-Ni austenities by electron microscopy has provided numerous
hitherto unexplained observations[5,37,38] which support the
proposed mechanism of initial nucleation by faulting on close-
packed planes. Such a fault on $(111)_{fcc}$ reported by Magee[5]
is shown in Figure 11. The fault was observed in an Fe33.1Ni
foil which had been partially transformed to martensite. Such
faults were found in a variety of Fe-Ni-Mn-C austenites under
similar conditions. Diffraction-contrast experiments revealed
that the faults were neither conventional (intrinsic or
extrinsic) stacking faults or twins.* Further, it was noted
that the faults had some thickness and the dislocations
associated with them were not coplanar. Magee also observed
isothermal growth of such units along $(111)_{fcc}$ at a temperature
where the bulk alloy exhibited isothermal transformation
behavior. Such findings provide strong support for the
contention that the formation of martensitic embryos in the
form of thin faults on close-packed planes represents the first
stage in martensitic nucleation.

Similar fault structures were reported earlier by
Gaggero and Hull[37] and Dash and Brown[38]. Some of their
observations will be discussed in detail in Chapter 8 when
specific nucleation sites are examined.

---

* Thermodynamic calculations also indicate that the formation
  of intrinsic faults or ε martensite in these alloys is
  extremely unlikely.

FIGURE 11. $\{111\}_{FCC}$ FAULT OBSERVED IN FE-33.1NI FOIL AFTER PARTIAL MARTENSITIC TRANSFORMATION OF SPECIMEN. MAGEE[5]

6. OTHER MARTENSITIC TRANSFORMATIONS

We now extend the proposed mechanism of martensitic nucleation to less familiar cases.

6.1 The bcc-fcc Transformation

The bcc→fcc lattice deformation can be accomplished by running the Bogers-Burgers fcc→bcc mechanism in reverse. A homogeneous shear of $\frac{a_{bcc}}{8}$ [0$\bar{1}$1] on each plane of (011)$_{bcc}$ (corresponding to Q'V'S' of Figure 7b) converts (101)$_{bcc}$ to the configuration of (111)$_{fcc}$ (P'V'Q' of Figure 7b). An fcc structure is then obtained by a shear on each of the latter planes of $\frac{a_{fcc}}{18}$ [$\bar{1}$2$\bar{1}$]. Again dilatations accompany these shears in a hard-sphere model.

An $\frac{a_{bcc}}{2}$ [1$\bar{1}$1] lattice dislocation on (011)$_{bcc}$ can dissociate by the reaction:

$$\frac{a_{bcc}}{2} [1\bar{1}1] \rightarrow \frac{a_{bcc}}{8} [0\bar{1}1] + \frac{a_{bcc}}{4} [2\bar{1}1] + \frac{a_{bcc}}{8} [0\bar{1}1]$$

$$\ldots\ldots\ldots (13)$$

where the three partial dislocations correspond to "-a," "b," and "c," respectively, in Figure 9. If a group of such dislocations, one on every second plane, dissociate in this manner, the $\frac{a_{bcc}}{8}$ [0$\bar{1}$1] partial dislocations can accomplish the first shear of the inverse Bogers-Burgers mechanism by spreading over successive planes to produce a homogeneous shear.

If the second shear necessary to convert the fault structure thus produced to fcc is then presumed to occur spontaneously, we must again modify the displacements to leave the $(011)_{bcc}$ fault plane unrotated. Figure 12 represents the $(101)_{bcc}$ plane that has been transformed to $(111)_{fcc}$ and is the plane of the second shear. The $\frac{a_{fcc}}{18}$ $[\bar{1}2\bar{1}]$ displacement (per plane) required to convert the structure left by the $\frac{a_{bcc}}{8}$ $[0\bar{1}1]$ partial dislocations to fcc is indicated by the displacement "a." Again, the dashed line represents the line of intersection of the two shear planes, and it is the component of "a" normal to this line that would cause a rotation of the fault plane $(011)_{bcc}$. This rotation can be eliminated if, after eight planes of the "a" displacement, every ninth plane is displaced by "b + c." The "c" displacement corresponds to Shockley partial dislocation and "b" corresponds to 2/3 of a Shockley partial. Superimposing a uniform dilatation to adjust the lattice parameter, we thus achieve a semicoherent fcc embryo in the form of an $(011)_{bcc}$ fault with an interface structure similar to that of the bcc embryo discussed in Chapter 5.

Very few "fcc" martensites actually have a true fcc structure. If $\Delta G^{fcc \rightarrow hcp}$ is small, such that we might expect the close-packed structure to be relatively "indifferent" to stacking sequence, there is a simpler way that the embryo fault can relax to avoid rotation of the fault plane. If the second "shear" occurs by a displacement of "a" in Figure 12 for two planes, followed by a "b" displacement every third plane, the
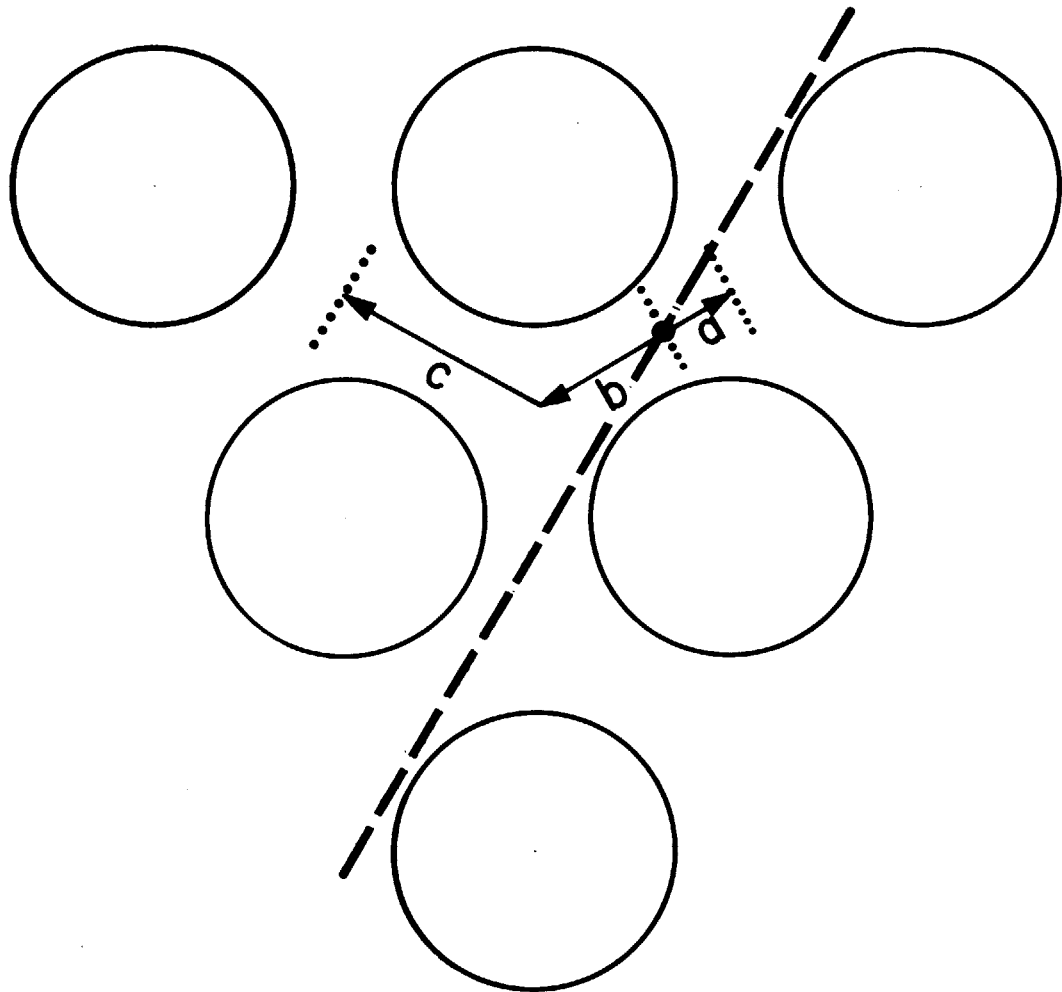
FIGURE 12. $\{111\}_{FCC}$-TYPE PLANE SHOWING SHEAR DISPLACEMENTS FOR PRODUCING AN FCC STRUCTURE FROM THAT OF THE FIRST SHEAR OF THE INVERSE BOGERS-BURGERS MECHANISM. DASHED LINE REPRESENTS THE LINE OF INTERSECTION OF THE TWO SHEAR PLANES. EIGHT "A" DISPLACEMENTS FOLLOWED BY A "B+C" DISPLACEMENT PRODUCES AN FCC STRUCTURE WITH NO ROTATION OF THE INITIAL FAULT PLANE.

fault plane is unrotated and a close-packed structure is generated with the stacking sequence ABCBCACAB. This is the samarium structure and can be considered as fcc with a fault every third $(111)_{fcc}$ plane. There is evidence that this is actually the basic structure of the "fcc" martensites in copper-, silver-, and gold-base alloys[39,40].

This high-period structure is often described with an orthorhombic unit cell taking the close-packed plane as the basal plane. Such structures in Cu-Al and other Cu-base alloys are often quoted as apparent exceptions to the general parallelism of closest-packed planes in the parent-martensite orientation relations, since the orthorhombic basal plane is deviated from the nearest $\{1\bar{1}0\}_{bcc}$ plane by about $4°$[41]. However, this observation does not violate our basic concepts here when we note that, by the proposed mechanism, the orthorhombic basal plane is the plane of the second shear of the lattice deformation and not the original fault plane which is maintained unrotated in establishing the orientation relations.

That the suggested general faulting mechanism applies to this type of lattice transition is supported by the transmission electron microscopy of Ferraglio and Mukherjee[42] in Au-47.5 at.% Cd shown in Figure 13. The transformation in this alloy is from ordered bcc to an ordered samarium structure. The presence of long-range order does not affect the applicability of the proposed mechanism, since the same partial

(A)
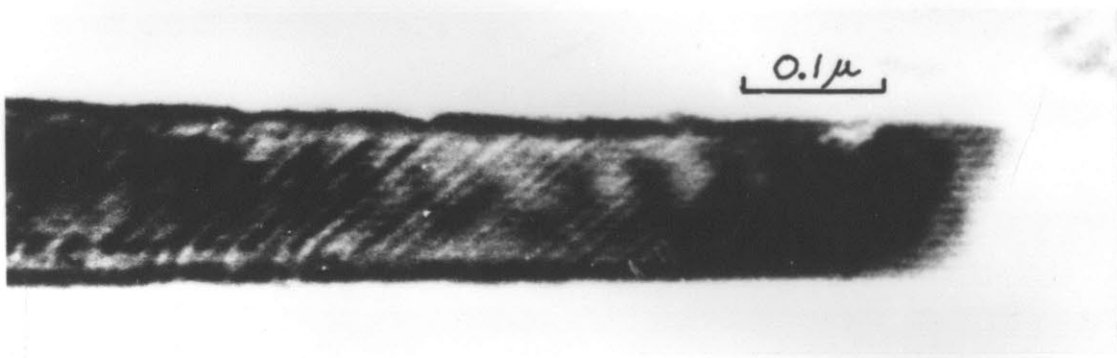
(B)

FIGURE 13. $\{011\}_{BCC}$ FAULT OBSERVED IN ORDERED Au-Cd ALLOY
DURING _IN SITU_ MARTENSITIC TRANSFORMATION. FAULT
EMANATING FROM GRAIN BOUNDARY IN (A) IS ENLARGED
IN (B) TO SHOW STRIATIONS IN FAULT IMAGE. FERRAGLIO
AND MUKHERJEE[42].

dislocations will simply transform the ordered parent to an ordered product. The fault shown in Figure 13 is on $(011)_{bcc}$ and was made to appear and extend reversibly ("thermo-elastically") by thermal stressing through control of the intensity of illumination in the electron microscope. When such faults grew beyond a certain size, they assumed the habit of the macroscopic product in this alloy and were identified as martensite by electron diffraction. The striations in the fault of Figure 13 suggest a second deformation has occurred within the fault in addition to the displacements in the fault plane, as proposed. Ferraglio and Mukherjee's observations will be discussed further in Chapter 8.

Since the embryo structure considered here is very similar to that of the bcc embryo discussed in Chapter 5, we can expect that the coherency strain energy and the energy of the dislocation interface, compared to that of the iron-base fcc$\rightarrow$bcc transformation, will roughly scale with the shear modulus. The shear modulus of copper-base alloys is about one-half that of iron-base alloys. If we assume that the size of the available structural defects for nucleation is the same, Equation (7) predicts that the chemical driving force at M_s should be one-half that of Fe30Ni or roughly 150 cal/mole. Thermodynamic calculations[43] show that this is actually the

magnitude of the chemical driving force at M_s for this transformation in copper-rich (disordered*) Cu-Al alloys.

6.2 The bcc→hcp Transformation

If a group of $\frac{a_{bcc}}{2}$ [$1\bar{1}1$] dislocations, one on every second (011)$_{bcc}$ plane dissociate by the reaction of Equation (13) and produce a true fcc structure by the mechanism described, the $\frac{a_{bcc}}{4}$ [$2\bar{1}1$] partial dislocations produced in the dissociation do not participate in the lattice deformation. Inasmuch as these dislocations correspond to $\frac{a_{fcc}}{6}$ [112] Shockley partial dislocations in the fcc structure and there is one such dislocation on every second close-packed plane, the passage of these partial dislocations through the fcc embryo will convert it to hcp. The bcc→hcp lattice deformation can, therefore, be accomplished by a sequence in which fcc appears as an intermediate structure**. If the Shockley partial dislocations follow closely behind the $\frac{a_{bcc}}{8}$ [$0\bar{1}1$] partial dislocations while

---

* Ordered Cu-Al alloys which exhibit thermoelastic behavior appear to involve lower chemical driving forces. Observations in Fe-Pt[44] reveal that long-range order has a profound influence on martensitic kinetics promoting such thermoelastic behavior, although the influence of the order on the basic parameters relevant to nucleation is not yet established. Although the ordered Au-Cd observations indicate that the proposed nucleation mechanism is still applicable, we will limit our discussion of energetics to disordered alloys.

** This mechanism may account for the observation[45] of fcc-type martensites as artifacts in thin foils of titanium-base alloys which display bcc→hcp martensitic transformations in the bulk.

the additional spontaneous displacements are occurring, the sequence may be very close to simultaneous and so the fcc structure need not ever exist in any significant amount.

In this transformation, the basal plane of the hcp structure is the plane of the fault. The embryo thus formed conforms to the observed orientation relations for the bcc-hcp transformation.

6.3   Additional Distortions

The bcc, fcc, and hcp structures considered herein represent the basic structure of the majority of the martensites which occur in alloy systems. Various tetragonal and orthorhombic structures which are observed can be derived from these basic structures by small additional distortions. These distortions can come about from the presence of interstitial atoms as in the case of the bct martensites in iron-base alloys containing carbon*, or the distortions may arise from ordering of substitutional atoms (either long- or short-range) in the parent phase. Cahn and Rosenberg[46] have shown that such distortions can result from an anisotropy of atomic pair correlations brought about by the transformation of a parent phase with short-range order.

---

*   The lattice deformations produced by the proposed mechanisms are of course equivalent to the assumed Bain strains of the phenomenological theories. Accordingly, any theoretical considerations based on the assumption of a Bain strain will still apply.

6.4   Mechanical Twinning

In the present context, mechanical twinning can be viewed as a special class of martensitic transformation where the parent and product phases have the same structure but differ in orientation. The driving force in this case will consist entirely of a mechanical work term derived from the applied stress acting through the transformation shape change*. The similarity of fcc twinning to the fcc→hcp transformation is obvious since the twinning merely requires the passage of a Shockley partial dislocation on every close-packed plane rather than every second plane. Accordingly, the defect necessary for the nucleation of an fcc twin involves a denser array of dislocations.

The formation of a bcc (112) twin requires the passage of an $\frac{a_{bcc}}{6}$ [11$\bar{1}$] partial dislocation on each (112) plane. Such dislocations can be derived from a group of $\frac{a_{bcc}}{2}$ [11$\bar{1}$] lattice dislocations by the spreading of their cores over successive planes as invoked in the case of fcc→bcc nucleation (Chapter 5). The concept of core spreading for twinning has some prior basis, in that it has been proposed[48] that the cores of $\frac{a_{bcc}}{2}$ [11$\bar{1}$] screw dislocations will adopt a symmetrical "star-shaped" configuration involving dissociation to form $\frac{a_{bcc}}{6}$ <111> type partial dislocations on three (different) {112} type planes. The kind of core spreading suggested here for twin nucleation

---

* Such a work term can also be included in the general case of martensitic nucleation when considering nucleation under applied stress[47].

can be derived from the latter type of spreading if we consider
the simultaneous dissociation of a group of dislocations of
the proper spacing and allow all the $\frac{a_{bcc}}{6}$ <111> screw dislocations
thus generated to move on the same set of {112} planes.
Consequently, the existing defect required for bcc twin
nucleation is similar to that proposed for the fcc→bcc trans-
formation in that it requires a lattice dislocation on every
third plane.

7. KINETICS OF MARTENSITIC NUCLEATION

In order to examine the energetic feasibility of a
general faulting mechanism of martensitic nucleation in
specific systems, we have treated the spontaneous formation of
embryo faults as a critical event. However, the possibility
remains that later stages in the total sequence of the
development of a martensitic unit might actually represent the
critical stage which determines the nucleation rate. In
exploring the consequences of a resistance to the motion of
partial dislocations, we will here consider the possibility
that their thermally-activated motion may be rate-limiting in
isothermal martensitic nucleation. Other possible rate-
limiting steps will be compared.

7.1   Resistance to Dislocation Motion

We have so far allowed $\gamma=0$ to represent the critical
condition for the spontaneous production of a martensitic embryo
from an existing defect. We now consider the possibility of a
resistance to the motion of the dislocations bounding the ends
of the fault such that a stress, τ_o, is required to move them.
The fault in question is bounded by n dislocations of Burgers
vector b, and so the force per unit length (of interface)
necessary to move such a dislocation array will then be $n\tau_o b$.
A stacking-fault energy γ exerts a force per unit length on
this array of $-\gamma$. Accordingly, the critical condition for a

defect to become unstable with respect to the formation of a martensitic embryo is then:

$$\gamma = -n\tau_o b \quad . \tag{14}$$

The critical resolved shear stress for slip near the M_s temperature has been measured by Breedis and Robertson[49] in single crystals of Fe30Ni as well as Fe-Cr-Ni alloys exhibiting the fcc→hcp transformation. The critical shear stress can be interpreted as the stress necessary to move total lattice dislocations, and the value obtained for Fe30Ni is expected to arise principally from "invar strengthening" and solid-solution strengthening. It is difficult to extract from this information the shear stress appropriate for the motion of the partial dislocations considered here, but the observed critical shear stress can certainly be taken as an upper limit ($\sim$8kg/mm^2). Using this value, and substituting Equation (1) into Equation (14) along with the quantities derived in Chapter 5 for the pertinent parameters, and solving for n, we find a size for the existing defect necessary to account for spontaneous nucleation at M_s for Fe30Ni of n=16. This is greater than the defect size calculated for the $\gamma=0$ criterion by about 3 planes. Since three planes of fault can be derived from one lattice dislocation in the fcc→bcc case, the defect includes only one more dislocation. Inclusion of resistance to dislocation motion, then, does not substantially alter the feasibility of the proposed mechanism for martensitic nucleation in Fe30Ni.

On the other hand, for the fcc-hcp case, if we take the observed critical resolved shear stress of $\sim$5 kg/mm^2 for Fe-Cr-Ni alloys[49] to represent the stress necessary to move Shockley partial dislocations, this does significantly affect the size of the defect that will account for the fcc$\rightarrow$hcp transformation in the Fe-Cr-Ni alloys discussed in Chapter 4. Yet, the absence of hysteresis in the reversibility (on heating and cooling) of the extended-node configurations on which the intrinsic fault-energy measurements were made indicates that no appreciable athermal stress is required for the motion of Shockley partial dislocations in these alloys. The possibility of a "thermal" stress arising from thermally-activated motion of partial dislocations will now be considered.

7.2   Thermally-Activated Dislocation Motion

Theories of thermally-activated deformation[50,51] assume the rate of plastic deformation to be determined by the thermally-activated motion of dislocations. The activation energy, Q, for dislocation motion under an applied stress, τ, can be expressed as:

$$Q = Q_o - (\tau - \tau_\mu)v^* \tag{15}$$

where Q_o is the activation energy in the absence of applied stress, τ_μ is the athermal resistance to dislocation motion, and v* is the "activation volume" defined by:

$$v^* = - \frac{\partial Q}{\partial \tau} . \tag{16}$$

A basic assumption is that v* is independent of strain rate. The stress necessary for a given rate of dislocation motion (or, equivalently, a rate of plastic strain) is then dependent on temperature and the imposed rate. Figure 14 represents the temperature dependence of the applied stress necessary for two strain rates. At high temperatures, this simple model predicts that the applied stress necessary for dislocation motion becomes τ_μ and the dislocation behavior is then essentially athermal in nature.

If we now consider the thermally-activated motion of the partial dislocations bounding the martensitic embryo faults, we find that the resistance stress τ_o in Equation (14) is dependent on the "imposed" rate of growth of the fault, or, alternatively, the rate of growth of the fault is dependent on the stress τ acting on the partial dislocations through the fault energy γ. From the relation of Equation (14), we can now see that the stress associated with the fault energy will be:

$$\tau = \frac{-\gamma}{nb} . \tag{17}$$

Figure 15 schematically illustrates the conditions for martensitic nucleation when the motion of the partial dislocations is thermally activated. The line showing the fault energy necessary to drive the dislocations, $-n\tau_o b$, is split into two curves at low-temperatures representing two rates of growth (in the fault plane) of the faults. The solid
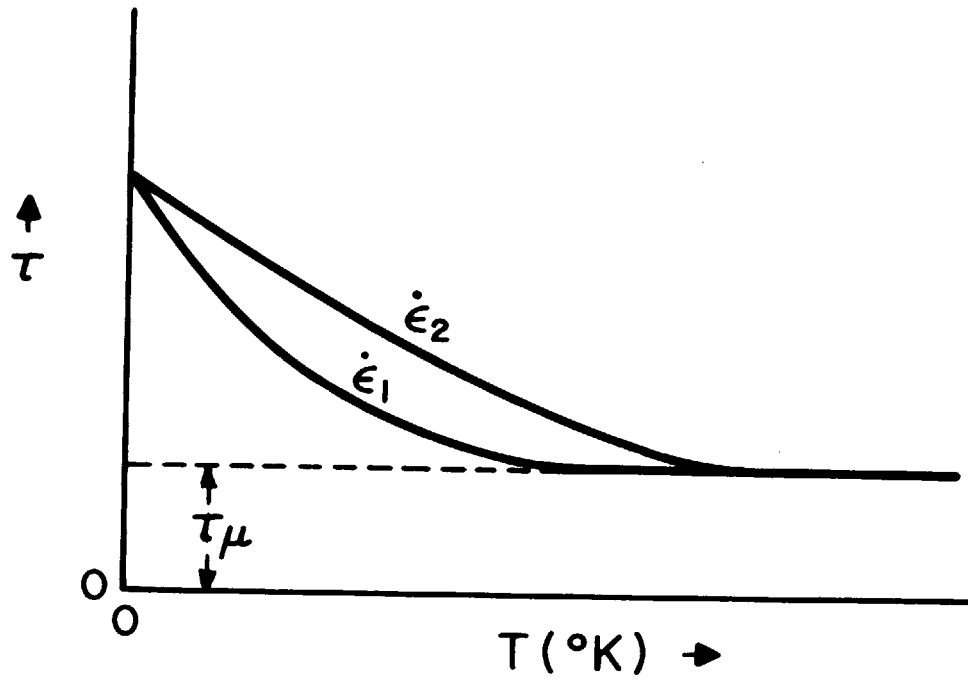
FIGURE 14. TEMPERATURE DEPENDENCE OF THE APPLIED STRESS
NECESSARY FOR TWO RATES OF PLASTIC DEFORMATION
$\dot{\epsilon}_1$ AND $\dot{\epsilon}_2$. $\tau\mu$ REPRESENTS THE ATHERMAL
COMPONENT OF THE STRESS. AFTER CONRAD[50]
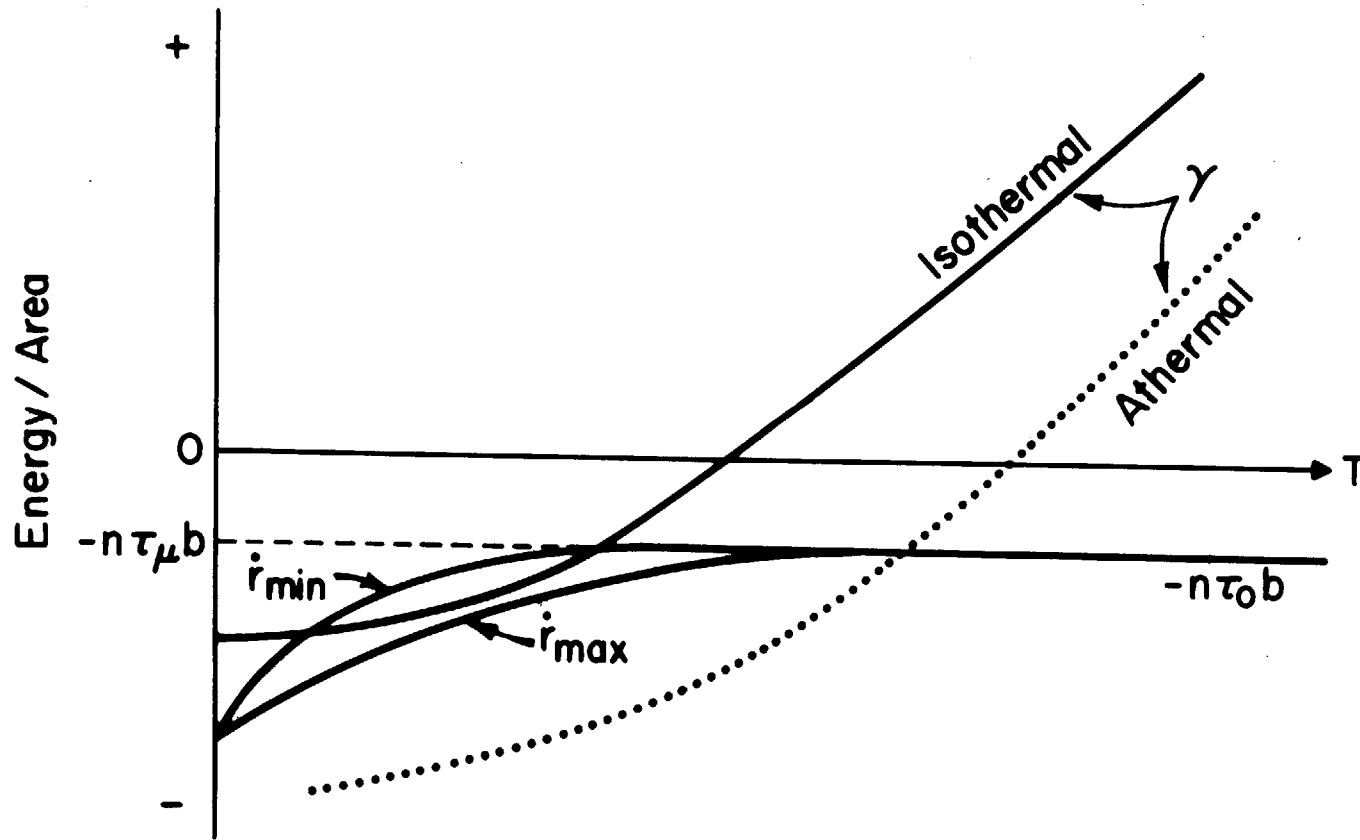
FIGURE 15. SCHEMATIC REPRESENTATION OF THE CONDITIONS FOR MARTENSITIC NUCLEATION WHEN
MOTION OF THE PARTIAL DISLOCATIONS IS THERMALLY ACTIVATED. γ (FAULT
ENERGY) CURVES ARE SHOWN FOR BOTH ISOTHERMAL (SOLID CURVE) AND ATHERMAL
(DASHED CURVE) CONDITIONS. DETECTABLE TRANSFORMATION OCCURS WHEN THE γ
CURVE CROSSES THE $-n\tau_0 b$ CURVE.

γ curve indicates the temperature dependence of the fault energy of a defect of size n as in Figure 4. Equation (14) is satisfied when the γ curve crosses into the region between the $-n\tau_o b$ curves corresponding to $\dot{r}_{min}$ and $\dot{r}_{max}$.* In this region the rate of growth of the fault will vary with temperature, and further, owing to the curvature of the γ curve, there is a temperature where this rate is a maximum. Thus, consideration of thermally-activated motion of the partial dislocations leads to the prediction of isothermal growth of the martensitic embryos and also suggests that the kinetics of this growth can exhibit C-curve behavior.

7.3   Isothermal Nucleation

The observation in Au-Cd (Chapter 6) that an embryo fault must grow to some size (in the fault plane) before a martensitic plate with the macroscopic habit grows from it suggests the possibility that the isothermal growth of these faults could represent the rate-limiting step in isothermal nucleation. Once a particle has reached a condition where it can advance to a later stage in the nucleation sequence (e.g. macroscopic habit) with sharply reduced coherency strain energy, the effective driving force is then greatly increased (γ more negative) and growth may then be very rapid. On the basis that the growth of the embryo faults is the rate-limiting step in isothermal nucleation, the $\dot{r}_{min}$ and $\dot{r}_{max}$ shown in

---

* The significance of $\dot{r}_{min}$ and $\dot{r}_{max}$ will be discussed later.

Figure 15 can be taken as the embryo growth rates which

correspond to the minimum and maximum* detectable isothermal

nucleation rates, respectively. Isothermal behavior can be

detected when the γ curve crosses the $-n\tau_o b$ curve in the region

where it is separated into the $\dot{r}_{min}$ and $\dot{r}_{max}$ branches.† This

simple model of thermally-activated dislocation motion suggests

that for the thermodynamic conditions portrayed by the dashed γ

curve in Figure 15, true athermal behavior can also occur.

With the assumption that the thermally-activated

motion of the partial dislocations bounding the embryo faults

is rate-limiting, we can obtain an expression for the activation

energy, Q, for isothermal martensitic nucleation by substituting

Equations (1) and (17) into Equation (15) to obtain:

$$Q = Q_o + (\tau_\mu + \frac{\rho_A}{b} E^{str} + \frac{2\sigma}{nb}) v^* + (\frac{\rho_A}{b} v^*) \Delta G^{chem}. \qquad (18)$$

Inspection of Equation (18) reveals that the

dependence of the activation energy on the chemical driving

force is determined by the activation volume v^*. This is

similar to the result suggested by Magee[5,52] in treating

the motion of lattice dislocations as the rate-limiting

phenomenon, except that v^* is here the activation volume for

the motion of partial dislocations. If v^* is insensitive to

temperature over the temperature range of the isothermal-nuclea-

tion measurements, the model is in accord with the familiar

---

* The maximum detectable rate of isothermal nucleation is the
  maximum rate distinguishable from athermal behavior.

† Provided autocatalytic effects are not too severe.

experimental result[5,52,53] that the activation energy for isothermal martensitic nucleation is very nearly linearly dependent on the chemical driving force. Moreover, since Q is inversely related to n in Equation (18) and there will be a distribution of existing defects of varying n, a distribution of activation energies is predicted, as experimentally verified by the small-particle experiments of Magee[52].

Expressing the activation energy in the form $Q = A + B\Delta G^{\gamma \to \alpha}$*, the experimentally determined values of A and B are summarized in Table 1. The first two alloys represent results obtained on bulk specimens as summarized by Raghavan and Cohen[53]. The values listed for Fe24Ni3Mn actually summarize results obtained for many Fe-Ni-Mn alloys of similar composition. The activation energies obtained from the bulk-specimen data constitute an "average" activation energy since autocatalysis was present and the quantities were derived assuming a singly-activated process.

The second two alloys represent the results of the small-particle experiments of Magee[52]. Here autocatalytic effects are circumvented and the distribution of activation energies can be taken into account more directly. The activation energies determined were those of the most potent initial nucleation sites. The A and B values listed in Table 1 for these alloys were determined from Magee's data (activation energy versus temperature) by calculating the appropriate

---

* With $\Delta G^{\gamma \to \alpha}$ in ergs/cm^3.

TABLE I

KINETIC PARAMETERS DERIVED FROM ISOTHERMAL NUCLEATION EXPERIMENTS

	A	B	Q_0		v^*	
	ERGS	CM^3	ERGS	eV	CM^3	Ω
BULK SPECIMENS[53]						
Fe24Ni3Mn	3.66×10^{-12}	1.05×10^{-21}	1.84×10^{-12}	1.15	2.44×10^{-22}	21
Fe29.2Ni	8.27×10^{-12}	3.69×10^{-21}	1.89×10^{-12}	1.18	8.56×10^{-22}	73
SMALL PARTICLES[52]						
Fe24.2Ni3.6Mn	3.39×10^{-12}	1.20×10^{-12}	1.32×10^{-12}	0.83	2.78×10^{-22}	24
Fe22.3Ni.49C	4.48×10^{-12}	1.77×10^{-21}	1.42×10^{-12}	0.89	4.11×10^{-22}	35

chemical driving forces using thermodynamic parameters suggested by Kaufman[54].

The values of Q_o and v* necessary to account for the measured A and B values are also given in Table 1. These were obtained through Equation (18) using the values of the parameters derived in Chapter 5 for Fe30Ni and taking n ≈ 15. The magnitude of τ_μ, the athermal component of τ_o, may be significant in deformed austenites (thus accounting for mechanical stabilization effects) but is assumed negligible for the annealed alloys under discussion here (following the considerations described earlier for Shockley partial dislocations). The derived quantities indicate a magnitude of Q_o for the motion of the $\frac{a}{18}$ <112> partial dislocations of ∿1eV. The activation volumes range between 21 and 73 Ω, where Ω is the atomic volume.

Results of deformation studies of Fe30Ni.04C austenite near M_s by Richman and Bolling[55,56] yield values of Q_o = 1.68 eV and v* = 13.7 x 10^{-22} cm^3 or 117Ω for normal slip. With Q_o = 1.68 eV for the motion of lattice dislocations, the proposed value of ∿1eV for the smaller partial dislocations considered here seems reasonable.

When correlating measured activation volumes with specific dislocation mechanisms, an activation area, A*, is derived by theoretical considerations of the mechanism being proposed; the expected activation volume is given by:

$$v* = bA*. \tag{14}$$

If the same activation area for the thermally-activated motion of the $\frac{a}{18}$ <112> partial dislocations as for the lattice dislocations is assumed, an activation volume for the partial dislocations of v* = 2.64 x 10^{-22} cm^3 or 23Ω is predicted. The expected v* for these dislocations thus agrees quite well with the derived values necessary to account for the observed nucleation kinetics of these alloys. Richman and Bolling's measurements also confirm that the activation volume is not strongly temperature dependent at the low temperatures where the isothermal nucleation measurements are made.

7.4   Alternative Rate-Limiting Steps

Several possibilities may be explored for alternative rate-limiting steps in the total nucleation sequence. The spontaneous formation of the interfacial $\frac{a_{bcc}}{8}$ <110> partial dislocations occurring in fcc→bcc nucleation involves motions of atoms from unstable to stable positions under the conditions at hand and so should occur without a barrier. However, the Shockley partial dislocations which must be formed on every eighth plane could require thermal activation in a manner similar to that considered by Kaufman and Cohen[1] and Raghavan and Cohen[3] for the punching out of lattice dislocation loops in a Frank interface. On the other hand, the barrier for the formation of Shockley partial dislocation loops would be much lower than that for lattice dislocation loops, and if we visualize this component of the interface to form, instead, as a

continuous distribution of smaller partial dislocations as
considered in the discussion of the interfacial energy, the
barrier should be negligible.

The lattice-invariant deformation required in the
later stages of nucleation might constitute another possible
rate-limiting step. This is the case represented by the
thermally-activated punching out of lattice-dislocation loops
to form a Frank interface. The assumption has been that twinned
martensites would exhibit similar behavior if we regard the twin-
related regions to be formed by mechanical deformation or
"twinning" (i.e. the passage of twinning partial dislocations)
of regions which have undergone the lattice deformation.
However, it is not clear that the formation of twin-related
regions requires any true additional deformation beyond the
lattice deformation. Referring to Figure 7 we can see that
after the partial dislocations derived from the existing defect
have moved on plane PVQ to produce the intermediate configura-
tion of Figure 7b, the spontaneous displacements necessary to
complete the fcc→bcc lattice deformation can occur on either
plane Q'V'S' or Q'P·'S'. The bcc structures produced by these
two possibilities are twin-related to each other across the
plane QTS. Accordingly, as one set of existing partial
dislocations moves on the fault plane, the selection of
alternating shear systems for the spontaneous motions required
to complete the lattice deformation can result in the formation
of alternating twin-related regions without the necessity of

any further plastic deformation beyond the lattice deformation. The mechanism described can account for the twin-related martensite laths observed in low stacking-fault energy austenites[57]. If the twin-related regions in twinned-plate martensites can be generated by this type of mechanism (the operation of one common set of dislocations together with alternating systems of spontaneous ·motions*), the formation of a twinned plate should not require any (thermally-activated) mechanical twinning.

We have so far not specifically dealt with the kinetics of the dissociation of a dislocation core. However, if we adopt the model of a dislocation core as a distribution of small Burgers vector dislocations[58], such that the required partial dislocations may be viewed as already existing in the core, the problem of <u>dissociation</u> simply reduces to the problem of partial dislocation <u>motion</u> already considered.

There is experimental evidence in support of the motion of partial dislocations as the rate-limiting step in isothermal martensitic nucleation. The observation of isothermal fcc→hcp transformation in Fe-Cr-Ni alloys by Manganon and Thomas[60] and by Breedis and Robertson[49] substantiates this mechanism, since none of the subsequent stages in the general nucleation mechanism are required for

---

* Dislocations formed in the spontaneous "second shear" motions of one variant might perform the "first shear" of a second variant. This could also provide a mechanism of "interfacial" autocatalysis; the $a_{fcc}/6$ [112] partial dislocations formed in the interface of an embryo fault on $(111)_{fcc}$ (Figure 10) might operate to form another embryo fault on $(11\bar{1})_{fcc}$.

the fcc→hcp transformation. Strong evidence in support of the
proposed rate-limiting mechanism for fcc→bcc nucleation is the
direct observation by Magee[5] of the slow isothermal growth of
such embryos on $(111)_{fcc}$ in thin foils under the same conditions
for which isothermal nucleation was known to occur in bulk
specimens.

Though we cannot at this time rule out the possibility
that later stages in the total nucleation sequence might be
rate-limiting, and indeed it is still possible that different
stages of the general mechanism may be rate-limiting in
different systems or conditions, the evidence to-date would seem
to favor the motion of partial dislocations as the most likely
candidate for a general rate-limiting step.

8. THE NUCLEATING DEFECT

The proposed general mechanism of martensitic
nucleation by faulting defines the function of the nucleating
defect. The defect must be able to provide a group of
appropriate partial dislocations of the proper spacing. One can
easily conceive of a variety of structural defects capable of
fulfilling this function. We will here examine those defects
for which direct observations of their operation as martensitic
nucleation sites are available. It should be noted that, although
the required Burgers vector and spacing of the dislocations will
depend on the particular martensitic transformation in question,
the basic features of the necessary defects are common to the
other martensitic transformations. Accordingly, a particular
type of defect which is observed to operate for one martensitic
transformation is expected to be a very likely nucleation site
for the other transformations as well.

8.1   Grain-Boundary Segments

In our discussions of specific transformation
mechanisms thus far, we have considered the example of a finite
symmetric tilt-boundary segment as a kind of prototype nuclea-
tion site. Such a segment could easily exist as part of an
"infinite" tilt boundary having a lower average tilt angle.
In such a case, the considerations of the dislocation
interactions of Chapter 4 must be modified to take into account

the attractive interaction of the partial dislocations of the segment with the rest of the boundary. The segment will still be unstable with respect to embryo formation according to our fault-energy considerations as long as the conditions at the boundary are such that the repulsive interaction of the partial dislocations exceeds this attractive interaction.

More complex "general" grain boundaries could also contain segments in which locally some of the boundary dislocations are in a configuration consistent with these conditions. The sequence of electron micrographs in Figure 16, from the work of Ferraglio and Mukherjee[42] on Au-Cd already discussed, demonstrates martensitic nucleation from such grain-boundary segments. The progress of the transformation in this sequence was controlled by thermal stressing with the electron beam. A martensitic embryo fault on $(011)_{bcc}$ is seen growing from the grain boundary at "A" in Figure 16a, while a subgrain boundary at "I" in Figure 16a gives rise to a martensitic plate at "C" in Figure 16b. Since a grain boundary is thought to possess a somewhat periodic structure of regions of varying misfit, we might expect the regions of the appropriate structure for martensitic nucleation to be arranged in a somewhat periodic fashion. This appears to be the case in Figure 16. The boundary at "A" in Figure 16a is dotted with small dark regions which widen to form embryo faults at later stages in the sequence. The largest fault from this boundary also demonstrates in this sequence that the embryo first grows to some size in the "fault"
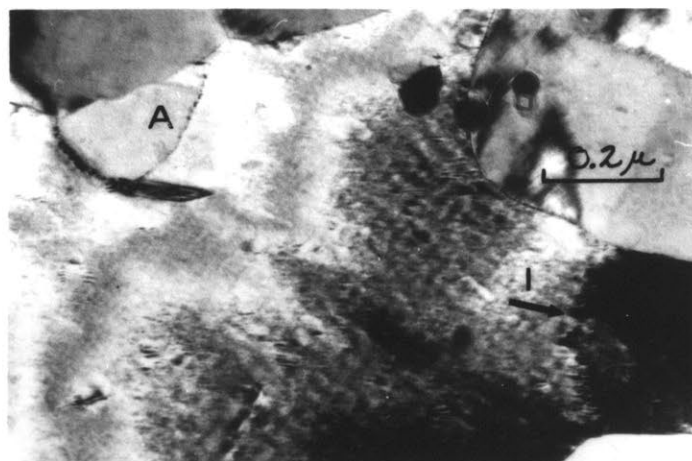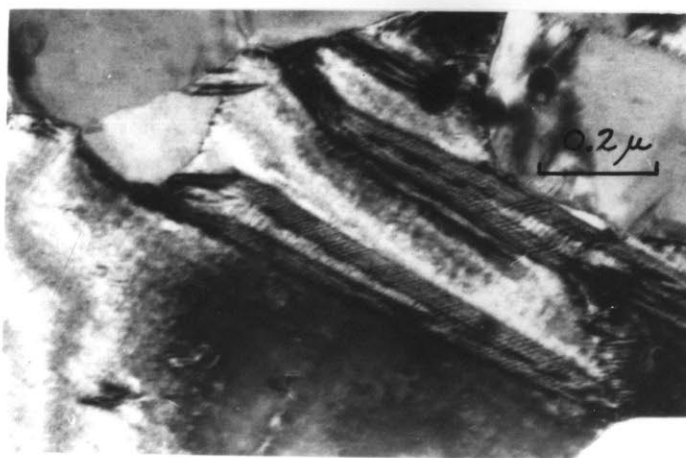
FIGURE 16. SEQUENCE OF ELECTRON MICROGRAPHS SHOWING FORMATION OF
MARTENSITIC EMBRYO FAULTS IN ORDERED AU-CD FROM A GRAIN
BOUNDARY AT "A" AND A SUBGRAIN BOUNDARY AT "I". LARGEST
FAULT AT "A" BOUNDARY IN (A) TAKES ON MACROSCOPIC
MORPHOLOGY DURING LATER GROWTH IN (B) AND (C). FERRAGLIO
AND MUKHERJEE[42].

morphology before a plate with the macroscopic habit grows from it.

8.2   Incoherent Twin Boundaries

An incoherent segment of an fcc twin boundary can be modeled as an array of Shockley partial dislocations, one on each close-packed plane. Hence, such a boundary is a likely source of Shockley partial dislocations on separate planes. The fcc→bcc transformation can be nucleated by the glide of every third dislocation from the boundary (with subsequent core spreading), or alternatively, dissociation of all of the Shockley partial dislocations to produce $\frac{a_{fcc}}{18}$ <112> partial dislocations, leaving $\frac{a_{fcc}}{9}$ <112> partial dislocations in the boundary. Figure 17 illustrates the transmission microscopy observation of Dash and Brown[38] in Fe32.3Ni of such an embryo "M" nucleating from an incoherent twin boundary segment "N" at the "corner" formed with the coherent boundary "C". Such a twin boundary corner is a most probable nucleation site inasmuch as the array of partial dislocations forming the incoherent segment represents a "finite" tilt boundary at that point and is thus most likely to give the desired "superdislocation" behavior.

8.3   Inclusion-Particle Interfaces

The interface of an incoherent inclusion particle might be expected to contain the appropriate "finite boundary" array of dislocations for martensitic nucleation. The earliest
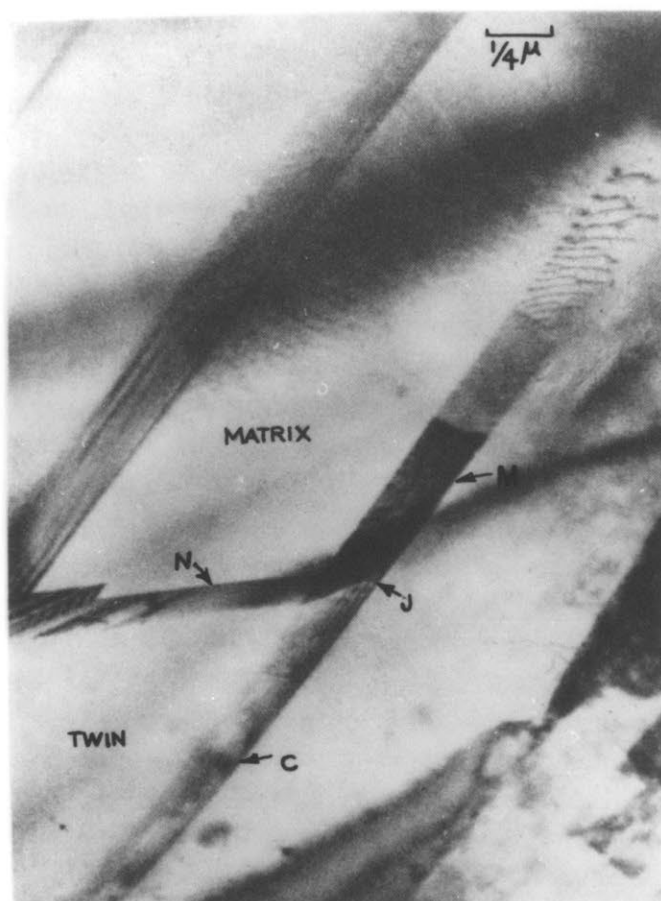
FIGURE 17. MARTENSITIC NUCLEATION AT A TWIN BOUNDARY IN
Fe32.3Ni. EMBRYO FAULT "M" ORIGINATES AT TWIN
CORNER "J" FORMED BY INCOHERENT BOUNDARY "N"
AND COHERENT BOUNDARY "C". DASH AND BROWN[38]

experimental evidence in support of the proposed faulting
mechanism for martensitic nucleation was the transmission
microscopy observation by Gaggero and Hull[37] of such faults
emanating from an inclusion particle in a partially transformed
Fe30Ni austenite foil, as shown in Figure 18.

8.4   Strain-Induced Nucleation Sites

There are numerous observations of special martensitic
nucleation sites which can be produced during plastic deforma-
tion. A rather unique example is the observation of
Easterling and Swann[61] of the martensitic transformation of
small iron precipitates in copper. Small coherent fcc particles
of almost pure iron in a copper matrix were found to be stable
with respect to spontaneous transformation to bcc even at
cryogenic temperatures, presumably due to the absence of
suitable nucleation sites. However, the particles could be
made to transform martensitically by room-temperature plastic
deformation of the copper matrix, and electron microscopy
indicated that the transformation was nucleated when matrix
screw dislocations passed through the particles. This observa-
tion is illustrated in the micrograph of a deformed foil in
Figure 19. Some fully coherent particles still remain, as at
point "A". Many particles are fully transformed (e.g. at "B")
giving a dark contrast, while others marked "C" and "D" are
partially transformed, some with the dislocations still attached.
These experiments comprise rather unusual conditions in that the
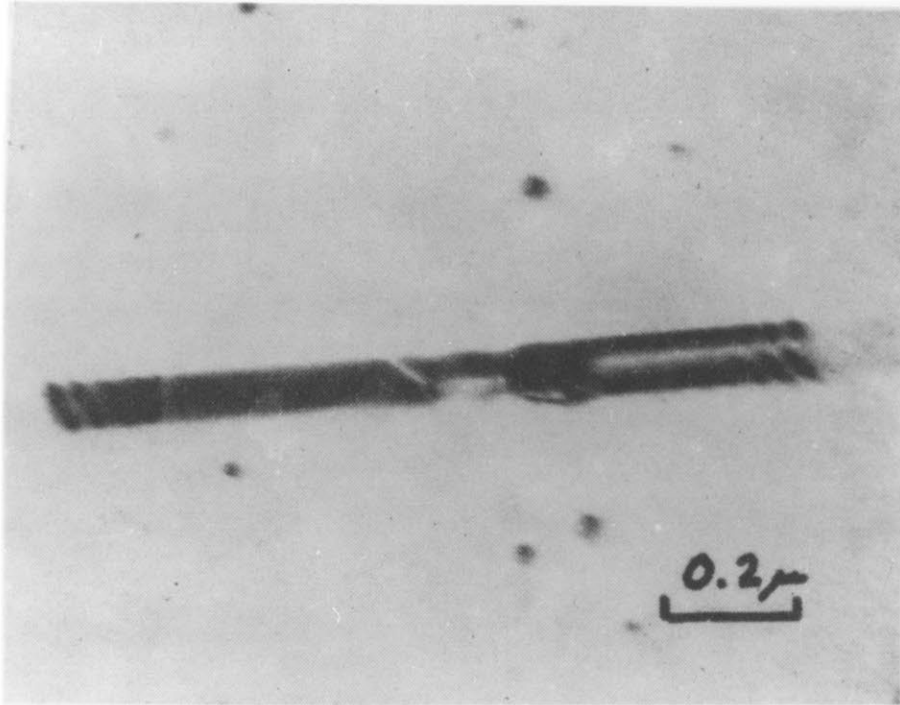
FIGURE 18. FAULTS ASSOCIATED WITH AN INCLUSION PARTICLE IN A PARTIALLY TRANSFORMED Fe30Ni FOIL. GAGGERO AND HULL[37]
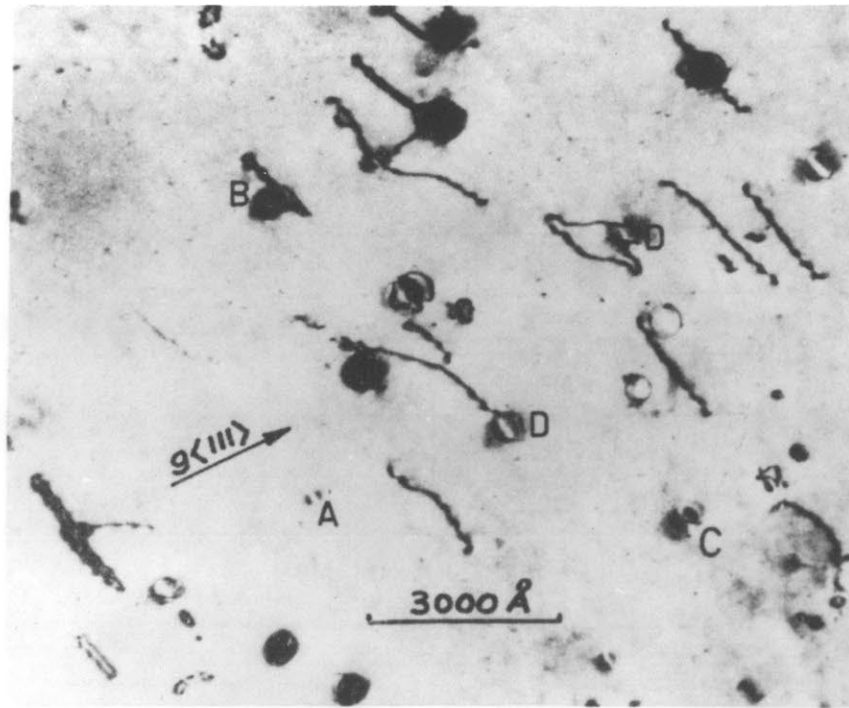
FIGURE 19. DEFORMED COPPER FOIL CONTAINING IRON PRECIPITATES. SOME PARTICLES ARE STILL COHERENT AS AT "A". DARK PARTICLES AS AT "B" ARE FULLY TRANSFORMED WHILE OTHERS AT "C" AND "D" ARE PARTIALLY TRANSFORMED, SOME WITH DISLOCATIONS STILL ATTACHED. EASTERLING AND SWANN[61]

chemical driving force involved was on the order of 1000 cal/mole.
Using this chemical driving force in Equation (7) together with
the parameters developed for Fe30Ni in Chapter 5 suggests that
under such extreme conditions a single dislocation could be an
operative nucleation site. Under the more typical chemical
driving forces encountered in bulk materials, we would expect
that dislocation pile-ups involving several parallel slip planes
might be able to act as nucleation sites in a similar manner.

Cohen and Weertman[62] proposed a cross-slip mechanism
for producing partial dislocations on consecutive close-packed
planes in fcc materials. In this picture, Shockley partial
dislocations in an initially coplanar pile-up of extended
dislocations are visualized to cross-slip onto another close-
packed plane by leaving behind sessile "stair-rod" dislocations.
The sessile dislocations cause the next dislocation to cross-
slip onto another plane parallel to the first, and so on.
Fujita and Ueda[63] have found evidence by transmission
microscopy that such a mechanism operates in the strain-induced
fcc→hcp martensitic transformation in Fe-Cr-Ni alloys. Their
observation is illustrated in Figures 20a-c. Dislocations "D"
running along fcc→hcp interfaces or slip planes in the "X"
direction cross-slip to product faults running in the "Y"
direction. Overlap of such faults is clearly indicated at "S"
in Figure 20b. Fujita and Ueda's interpretation of this process
as a mechanism for producing hcp martensite is illustrated in
Figure 21.
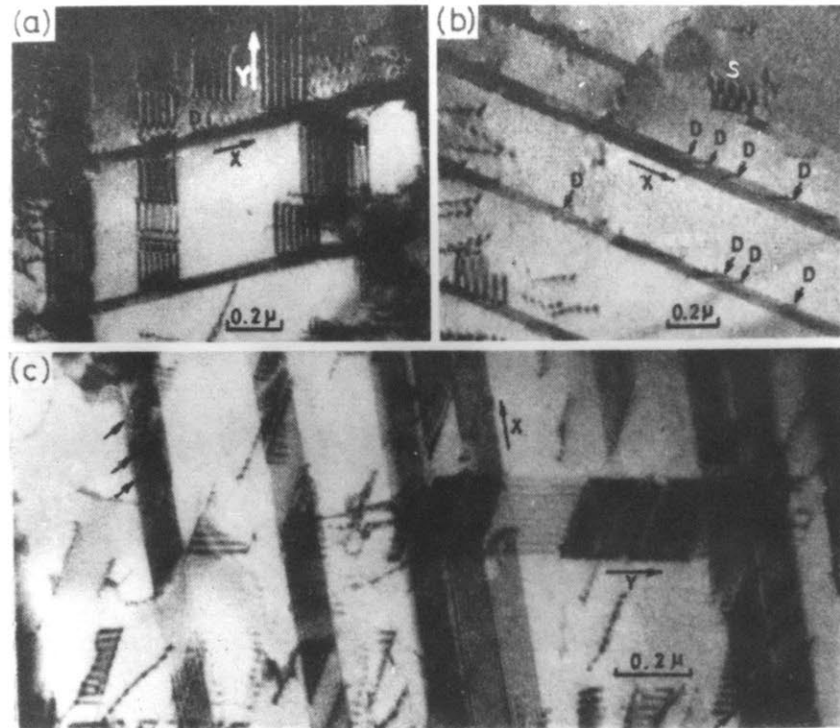
FIGURE 20. FORMATION OF HCP MARTENSITE BY CROSS-SLIP. DIS-
LOCATIONS "D" RUNNING ALONG FCC-HCP INTERFACES
OR SLIP PLANES IN THE "X" DIRECTION CROSS-SLIP
TO PRODUCE FAULTS RUNNING IN THE "Y" DIRECTION.
OVERLAP OF SUCH FAULTS IS INDICATED AT "S" IN
(B). ARROWS IN (C) INDICATE FAULTS ORIGINATING
AT AN FCC-HCP INTERFACE. FUJITA AND UEDA[63]

Stacking faults in the primary slip plane ($\bar{1}11$)

Stacking faults in the cross slip plane ($1\bar{1}1$)

$\frac{a}{6}[12\bar{1}]$

$\frac{a}{6}[1\bar{1}0]$ (Stair – rod dislocation)

$[1\bar{1}0]$

$\frac{a}{6}[21\bar{1}]$ $\frac{a}{6}[12\bar{1}]$

Thin ϵ – crystal

($\bar{1}11$)

$\frac{a}{6}[21\bar{1}]$

$(1\bar{1}1)$

$.2d(1\bar{1}1)$

Pile up of screw dislocations

Interval of several slip planes
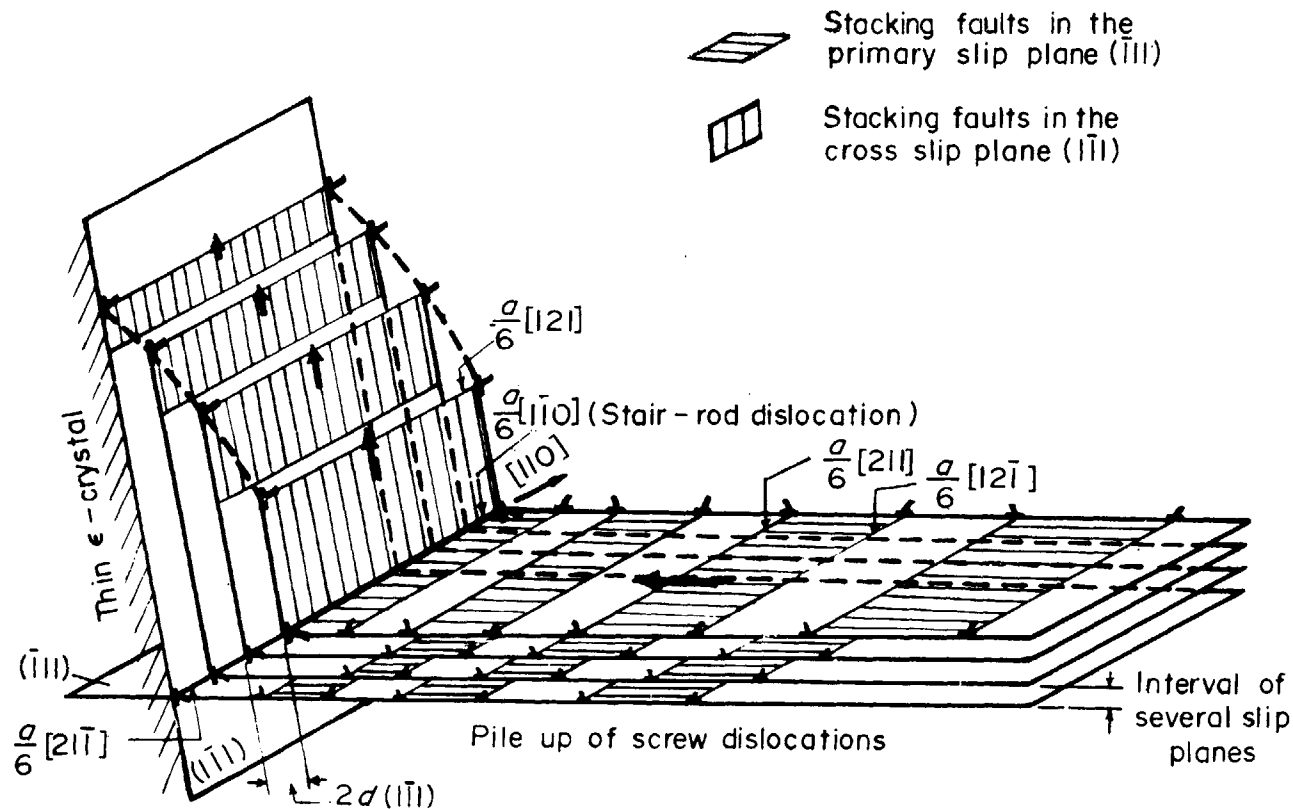
FIGURE 21. SCHEMATIC ILLUSTRATION OF THE CROSS-SLIP MECHANISM OF FIGURE 20. A/6 $[21\bar{1}]$ PARTIAL DISLOCATIONS ON ($\bar{1}11$) CROSS-SLIP ONTO ($1\bar{1}1$) AS A/6 $[12\bar{1}]$ PARTIAL DISLOCATIONS BY PRODUCING A/6 $[1\bar{1}0]$ STAIR-ROD DISLOCATIONS AT THE INTERSECTION OF THE TWO PLANES. OTHER DISLOCATIONS ON ($\bar{1}11$) MUST CROSS SLIP ON DIFFERENT ($1\bar{1}1$) PLANES DUE TO THE SESSILE STAIR-ROD DISLOCATIONS. CROSS-SLIP TO EVERY SECOND ($1\bar{1}1$) PLANE PRODUCES AN FCC STRUCTURE. FUJITA AND UEDA[63]

The most commonly observed[21,26,60,64] strain-induced
nucleation site for the fcc→bcc martensitic transformation is
the intersection of various types of shear bands (ε martensite,
twins, bundles of stacking faults) in austenites of low intrinsic
stacking-fault energy. The observation by Venables[26] of a bcc
martensite embryo produced at the intersection of two ε martensite
plates is shown in Figure 22. Mechanisms by which these inter-
sections can produce the $\frac{a_{fcc}}{18}$ <112> partial dislocations
necessary for the Bogers-Burgers lattice deformation have been
proposed[21,65]. The partial dislocations may be produced by
the spreading of the cores of the Shockley partial dislocations
of the second shear band as they cross the coherent interface
of the first[65], or, treating the interface as incoherent, such
dislocations might be produced by interaction of the crossing
Shockley partial dislocations with the interface (as in the
crossing of a symmetric tilt boundary)[21].

It should be noted that these strain-induced nucleation
sites are largely operational during plastic deformation where
martensite formation is an effective means of plastic
relaxation. Under conditions of an unfavorable chemical
driving force, alternative relaxations can occur at these sites
such that their potency as nucleation sites on subsequent
cooling is substantially reduced.
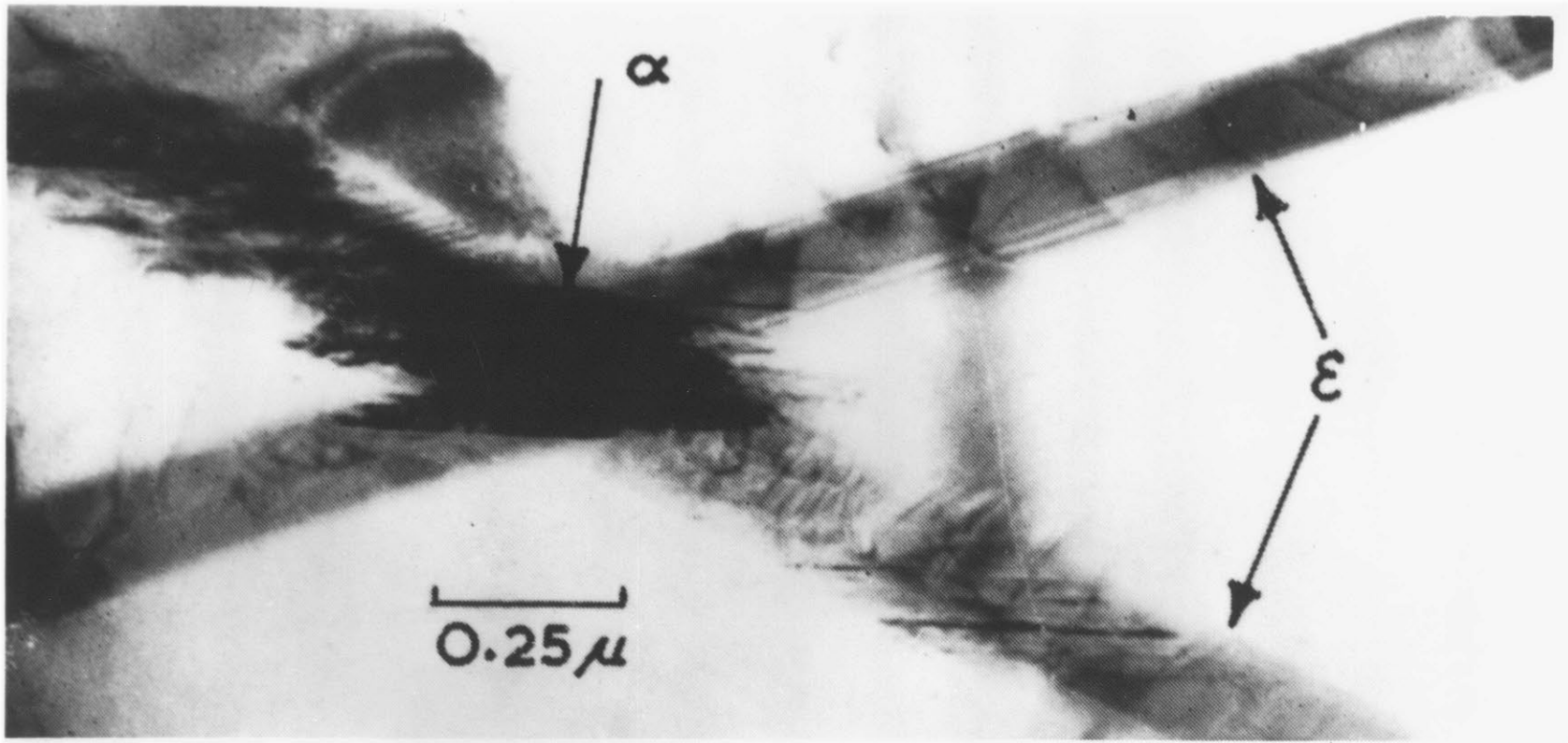
FIGURE 22. NUCLEATION OF α (BCC) MARTENSITE AT THE INTERSECTION OF TWO ϵ (HCP) PLATES IN AN AUSTENITIC (FCC) STAINLESS STEEL. VENABLES[26]

9. <u>CONCLUDING REMARKS</u>

We have now made the case for a general mechanism of
martensitic nucleation by faulting on closest-packed planes, and
have shown this mechanism to be consistent with a wide variety
of experimental observations, many of which were previously
unaccounted for by existing theories. In its essential nature,
the proposed theory can be considered to regard martensitic
nucleation as a type of spontaneous plastic deformation, brought
about not by an externally applied stress, but by an "internal"
chemical stress. The concept is similar to the proposal of
Kaufman and Cohen[1] of <u>formation</u> of dislocations necessary for
the lattice-invariant deformation by a chemical stress, or
Magee's[5] concept of the <u>motion</u> of such dislocations through
chemical stress, but goes beyond these concepts in that the
"plastic deformation" considered is the actual lattice deforma-
tion which brings the primeval embryo structure into existence.

Plastic deformation represents an apt analogy to
martensitic nucleation in several respects. Early theoretical
considerations of the mechanism of plastic deformation led to
the conclusion that to homogeneously distort a crystal into a
"slipped" structure would require an energy far in excess of
that observed to be necessary for plastic flow. To circumvent
this difficulty, the concept of a dislocation was invented.
Rather than homogeneously deforming a large volume, a small
(pre-existing) singularity in displacement is propagated along

the crystal to achieve the same final structure. Similarly, early theoretical considerations of martensitic nucleation led to the conclusion that homogeneous deformation of a region of crystal into the product structure involved an intolerably large energy barrier. Again, we circumvent this difficulty by simply propagating existing dislocations to achieve the lattice deformation.

It should be noted that treating martensitic nucleation as spontaneous plastic deformation leads to a particular type of kinetic behavior. Normal plastic deformation can be viewed as an essentially athermal process which can be <u>assisted</u> by thermal activation; plastic flow can still occur at $0^{\circ}K$ if a high enough stress is applied. Similarly, the considerations of Chapter 7 predict that martensitic nucleation can still occur at $0^{\circ}K$ if the chemical driving force is sufficiently large. Hence, we are led back to the concept originally proposed by Knapp and Dehlinger[4] that martensitic nucleation is to a first approximation an athermal process. Aside from the special cases where the transformation can be made to exhibit isothermal behavior, the role of thermal activation can largely be regarded as a reduction of the magnitude of the chemical stress necessary for this spontaneous deformation.

A few words are in order concerning the possible relevance of "soft phonon-mode" concepts[7,8] to martensitic nucleation. These ideas have had some success in accounting for certain displacive phase transformations (e.g. the ω

transformation[66]) consisting primarily of "atom shuffles"
which do not result in any overall shape change. As pointed out
in Appendix C, the occurrence of a shape change in martensitic
transformations greatly increases the importance of matrix
constraints. Though soft-mode mechanisms may have some
relevance to surface and thin-film martensitic nucleation (as
suggested by recent experiment[9]) where the matrix constraints
are somewhat relaxed, it has not been demonstrated that these
mechanisms can account for martensitic nucleation in the bulk
when the constraint of the matrix opposing the shape change is
fully taken into account. Also, as pointed out in Chapter 1,
these theories do not appear able in their present stage of
development to take into account the known heterogeneous nature
of the transformation in bulk material.

Many lattice deformations involved in martensitic
transformations can be considered as the product of a homogeneous
strain and "atom shuffles." In such cases (e.g. the fcc→hcp
transformation), the mechanisms proposed here accomplish both the
homogeneous strain and shuffles simultaneously by the passage of
an inhomogeneous array of partial dislocations. However, it is
conceivable that in a complex transformation, such as bcc→hcp
which we treated here as a combination of bcc→fcc and fcc→hcp,
the atomic-shuffle component of the transformation might be
accomplished separately by a soft-mode transformation. This
could account for the observation of pre-martensitic effects in
Ti-Ni which have features similar to the ω transformation[67,68].

However, the observation by Perkins[68] of thin embryo faults in partially transformed Ti-Ni foils suggests that even in this complicated material, the basic mechanism of nucleation by faulting still applies.

In summary, both theoretical considerations and experimental evidence lead to the proposition that the general mechanism of martensitic nucleation is a type of faulting on closest-packed planes. The total nucleation process is postulated to comprise a sequence of steps with the first step derived from an existing defect. Taking matrix constraints into account, the first step should be a faulting displacement on a plane of closest packing and subsequent steps are expected to occur in such a way as to leave the fault plane unrotated. Such a general mechanism is consistent with the observed orientation relations and the known heterogeneous nature of martensitic nucleation.

Specific mechanisms have been presented for each of the major lattice changes occurring in alloy systems. The energetic feasibility of these mechanisms has been demonstrated for the known conditions for martensite nucleation, invoking fairly simple defects which may consist of 4 or 5 lattice dislocations of the proper spacing. The predicted kinetic behavior of such a faulting mechanism is consistent with the

observed kinetics of martensite nucleation, both in terms of

the basic athermal nature, and in terms of the correct

activation energy and its dependence on chemical driving force

when isothermal behavior is observed. For each of the major

lattice changes, there are ample direct experimental observations

available of the predicted embryo faults emanating from the

types of nucleation sites where the proposed dislocation

groups are expected.

10. <u>SUGGESTIONS FOR FUTURE WORK</u>

1.   Though the available evidence supports the idea that
the faults observed in partially transformed Fe-Ni austenites
are martensitic embryos, it still remains to be proven that
they are bcc in structure. Further transmission electron
microscopy would undoubtedly be the most fruitful approach to
this problem. Since we have a precise model for the structure
and orientation of such faults (i.e. the semicoherent embryo
of Figure 10c), the expected diffraction contrast can be
computed and tested against contrast experiments. However,
preliminary calculations indicate that the expected displacement
vector is such that the conditions for loss of contrast,
$\vec{g} \cdot \vec{R} = 0$, would be satisfied only for very special combinations
of $\vec{g}$ reflections and fault thickness. Testing these predictions
would require an accurate determination of the number of planes
of thickness of the faults. Since many of these faults are
found to be in direct contact with larger martensitic units, a
simpler test of whether they are bcc might be to examine their
dark-field contrast using $\vec{g}$ reflections from the larger units.
This approach assumes that the faults are in the same
orientation as the larger units, however, and the model
suggests that this would not be strictly correct.

Whereas the faults represent too small a volume to
contribute their own spots to a conventional selected-area
electron diffraction pattern, another approach to structure

determination could be the use of a scanning transmission electron microscope capable of obtaining selected-area diffraction from an area $\sim200\overset{\circ}{A}$ in diameter; faults $\sim20\overset{\circ}{A}$ in thickness might then comprise a large enough fraction of the total diffracting volume to give rise to their own diffraction pattern. Finally, with high-resolution lattice-imaging techniques it might be possible to test the predicted bending of planes on crossing the faulted region.

2.   Having defined the basic structural features of the nucleating defect, it may now be possible to examine thin foils for probable nucleation sites and observe their operation on cooling by cold-stage electron microscopy. Such experiments may now be more fruitful than previous "shot-in-the-dark" attempts where the structure of the defects was completely unknown.

3.   Calculations of the dislocation interactions in the proposed faulting mechanism can be done in more detail. In particular, the interaction of the finite partial dislocation tilt-boundary segments at close separations where the super-dislocation analog is no longer appropriate should be examined. For the case of such segments existing as part of a larger sub-boundary of lower average tilt angle, their interaction with the other dislocations in the boundary should be examined. A useful calculation would be a determination of the largest

average boundary tilt angle for which the repulsion of the finite (partial dislocation) boundary segments is still greater than the attractive interaction with the rest of the boundary.

Another refinement would be an examination of possible "end-effects" in the fault energy (i.e. $\gamma = \gamma(r)$) at early stages of dissociation. A more rigorous calculation of the shape dependence of the strain-energy contribution to the fault energy would be helpful in this connection.

4. The energetics of later stages in the total "nucleation" process should be examined. The critical condition at which a growing semicoherent embryo fault is able to undergo the lattice-invariant deformations determining the invariant line and invariant plane should be considered. Though these steps may occur after the rate-controlling step and thus have no influence on the nucleation kinetics, they may influence morphology and thus determine the final product structure.

5. As for the question of the rate-limiting step in the total nucleation process, an important area for further experimental work is the isothermal fcc→hcp transformation. The kinetics of this transformation should be studied in the same detail as has the fcc→bcc transformation. A much better understanding of isothermal martensitic nucleation may result from a thorough examination of such a special case where the overall transformation mechanism is greatly simplified.

APPENDIX A

COMPARISON OF THERMODYNAMIC AND PAIR-WISE CENTRAL-FORCE INTERACTION APPROACHES TO STACKING-FAULT ENERGY CALCULATION

Since many attempts at theoretical estimates of stacking-fault energy have employed the approximation of pair-wise central-force interactions[28,69], a brief comparison with the predictions of the thermodynamic approach described in Chapter 3 is in order. Considering pair-wise interactions out to 11 neighbor shells (derived from the original fcc 6 neighbor shells), Hirth and Lothe[28] express as sums of interaction energies the following energies (per unit area) relative to perfect fcc: γ_I, the intrinsic stacking-fault energy, γ_H, the energy per (basal) plane of an hcp crystal, γ_E, the extrinsic stacking fault energy, and γ_T, the coherent twin-boundary energy. Comparison of these expressions gives the relations:

$$\gamma_E = 2\gamma_T \qquad (A1)$$

$$\gamma_I = 2\gamma_H - \phi_6 + \phi_6' \qquad (A2)$$

where ϕ_6 and ϕ_6' represent, in Hirth and Lothe's notation, 9th and 10th neighbor interaction energies. The first relation agrees with the thermodynamic prediction for the extrinsic fault energy, and further suggests that there is no inter-action between the coherent twin interfaces since their energy at a separation of two planes is identical to that of isolated boundaries. The second relation is in agreement with

the thermodynamic prediction for intrinsic fault energy if we

take $-\phi_6 + \phi_6'$ to represent twice the fcc-hcp interfacial

energy. However, it is unlikely that the true fcc-hcp

interfacial energy actually arises from 9th and 10th neighbor

interactions, but rather arises from shorter-range interactions

which are not taken into account by the central-force

approximation. Hirth and Lothe suggest that interactions

beyond 8th neighbors need not be considered.

Including interactions out to only 8 neighbor shells

leads to the additional relations:

$$\gamma_I = \gamma_E \qquad \text{(A3)}$$

$$\gamma_T = \gamma_H . \qquad \text{(A4)}$$

These relations are clearly inconsistent with experiment.

Measurements of intrinsic and extrinsic fault energy in the

same alloy indicate that they are in general not equal.

Though the second relation is often suggested, measurement

of the temperature dependence of coherent twin-boundary energy

in platinum[70] and copper[69] shows a positive surface

entropy, whereas the fcc→hcp entropy difference is of opposite

sign[71].

The relations obtained from the approximation of

central-force interactions are clearly not as rigorous as

those obtained from the present, more direct thermodynamic

approach. However, where central-force interactions might be

considered to represent some part of the total forces at play,

this treatment of the problem may be useful in indicating, at

least qualitatively, some additional information beyond that

available from the thermodynamics, e.g. the suggestion of a link
between intrinsic and extrinsic fault energy; materials with
very low intrinsic fault energies might be expected to have low
twin-boundary energies.

APPENDIX B

INFLUENCE OF NUCLEATION CONDITIONS ON MACROSCOPIC HABIT

The semicoherent bcc embryo in an fcc matrix represented in Figure 10c must undergo additional plastic deformations in order to completely relax to its equilibrium lattice parameter. These additional deformations will determine the invariant line and invariant plane which establish the habit of the macroscopic martensitic unit.

We have established the parallelism (or near parallelism) of the closest-packed planes of the two structures, but the final orientation relation will be determined when the invariant line is established, since this line fixes the directions which are parallel in the closest-packed planes of the two structures. In addition to determining the orientation relations, the invariant line may also have a strong influence on the invariant plane or habit plane inasmuch as this plane must <u>contain</u> the invariant line. Accordingly, we can expect a correlation between orientation relations and habit plane.

The three basic types of orientation relations observed in fcc→bcc type martensitic transformations are illustrated in Figure 23. The Kurdjumov-Sachs relation involves parallelism of the close-packed directions of the two structures, $[1\bar{1}0]_{fcc}$ and $[11\bar{1}]_{bcc}$, while the Nishiyama relation involves parallelism of $[1\bar{2}1]_{fcc}$ and $[10\bar{1}]_{bcc}$. The
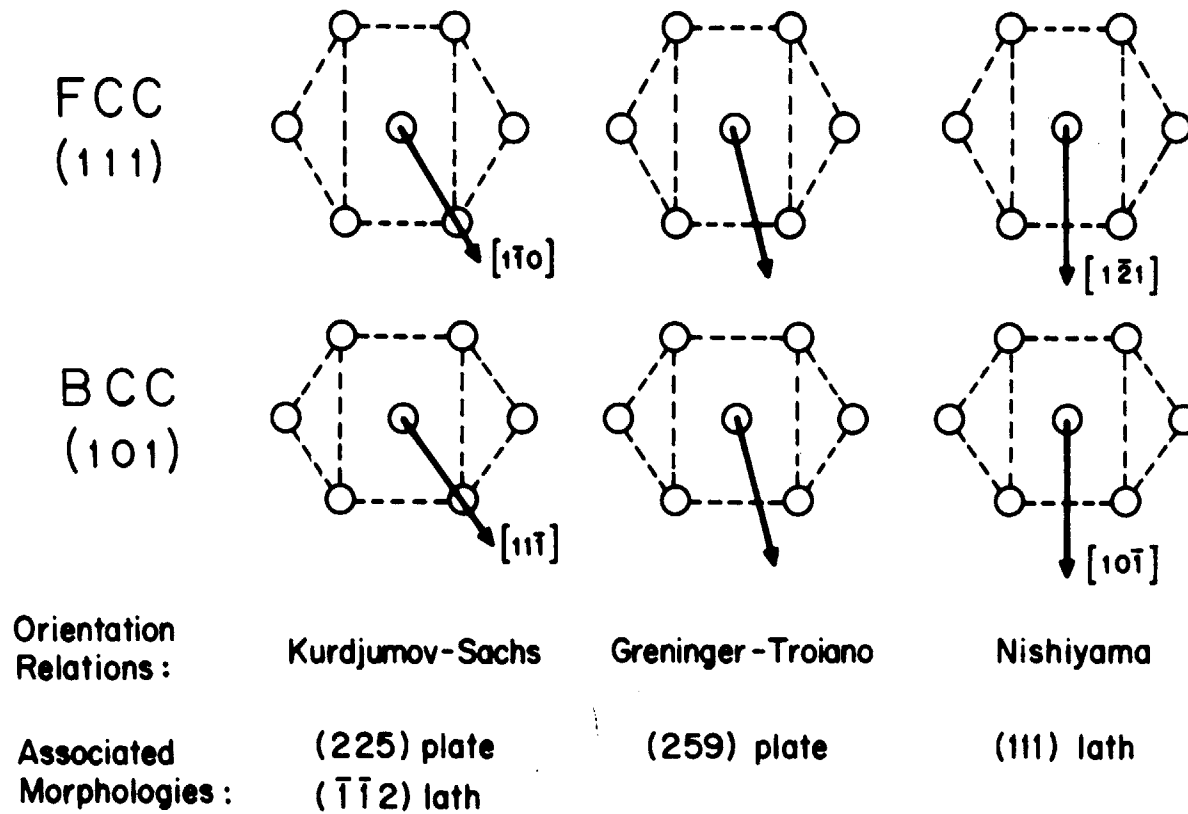
FIGURE 23. REPRESENTATION OF THE DIRECTIONS WHICH ARE PARALLEL IN THE $(111)_{FCC}$ AND $(101)_{BCC}$ PLANES FOR THE THREE BASIC ORIENTATION RELATIONS OBSERVED FOR FERROUS BCC-TYPE MARTENSITES.

Greninger-Troiano relation involves parallelism of directions
approximately midway between these two cases. The macroscopic
morphologies associated with these three relations are also
shown in Figure 23. The Kurdjumov-Sachs relation is found in
the (225) plate martensites as well as in the ($\bar{1}\bar{1}2$) lath
martensites observed in steels of low intrinsic stacking-fault
energy. The Greninger-Troiano relation is generally found in
(259) plate martensites. Determination of the orientation
relations of (111) lath martensites has indicated that they
are closest to the Nishiyama relation[72].

According to the phenomenological theories, once an
invariant line is established by the "total lattice deforma-
tion," the lattice-invariant deformation can produce a macro-
scopic matching of the two structures along a direction normal
to the invariant line, thus defining a macroscopic invariant
plane. Though there may be a true invariant line in the
lattice deformation, the "invariant plane" is only a macro-
scopic concept. Actually, only in the Greninger-Troiano case
is there a true invariant line in the total lattice deformation.
A particle in the Kurdjumov-Sachs or Nishiyama orientation
relations is constrained to match the matrix along directions
which are not equal in length in the two equilibrium
structures and additional deformations are required to
accomplish this matching (macroscopically). In the latter two
cases, the invariant line concept becomes   a macroscopic
concept like the invariant plane, and all directions in the
invariant plane are invariant only macroscopically. The

required additional deformations would account for the more complex substructures of the other morphologies compared to the Greninger-Troiano (259) plate martensites. The semi-coherent embryo in Figure 10c is in the Kurdjumov-Sachs orientation. A small rotation about $[111]_{fcc}$ is required to put the particle in the Greninger-Troiano relation and establish a true invariant line. This can be accomplished by the formation of a grid of additional screw dislocations in the $(111)_{fcc}$ interface. All that is then required to produce the final structure of a (259) plate is the twinning operation on (112) $[11\bar{1}]_{bcc}$. We will now examine possible constraints which could cause the particle to stay in the more "awkward" Kurdjumov-Sachs orientation.

Perhaps the morphology which conforms most closely to the exact Kurdjumov-Sachs orientation relation[21] is the strain-induced martensite produced at the intersection of shear bands in austenites of low intrinsic stacking-fault energy, as illustrated in Figure 22. Clearly the embryo produced at such an intersection of $\{111\}_{fcc}$ bands will be initially rod-shaped with the long dimension along the close-packed $[1\bar{1}0]_{fcc}$ direction. The strain energy of a particle of such a shape is not minimized by establishing an invariant plane but rather by making the direction of its longest dimension an invariant line. Hence, the bcc embryo is plastically "stretched" in the close-packed direction, making this direction macroscopically invariant and thus maintaining the Kurdjumov-Sachs orientation

relation. The complex dislocation structure observed in such martensites is essentially that expected if a bcc crystal is pulled along its $[11\bar{1}]_{bcc}$ three-fold symmetry axis. If a martensitic plate is to grow from such an embryo its habit plane must contain $[1\bar{1}0]_{fcc}$ and must therefore have $(hh\ell)$ indices. Figure 24 illustrates the observation by Venables[26] of such a (225) plate apparently nucleated from the intersection of two ε martensite bands in a deformed stainless steel foil. Hence, we suggest that constraints at the nucleation stage might establish not only the parallelism of close-packed planes but also the invariant line of the total lattice deformation as well, thereby determining the ultimate orientation relations and influencing the macroscopic habit.

The total nucleation process envisioned here can be related to the existing phenomenological theories as follows. In matrix form, Bowles and Mackenzie consider the "total lattice deformation," S_T, which determines the invariant line to be given by:

$$S_T = \delta RB \tag{B1}$$

where B is the "Bain strain" relating the two lattices, R is a rigid-body rotation, and δ is a uniform dilatation which allows some variation of the true invariant line. The existence of such a dilatation is not generally accepted. The total transformation shape change is given by the product of S_T and a lattice-invariant deformation consisting of a single shear.
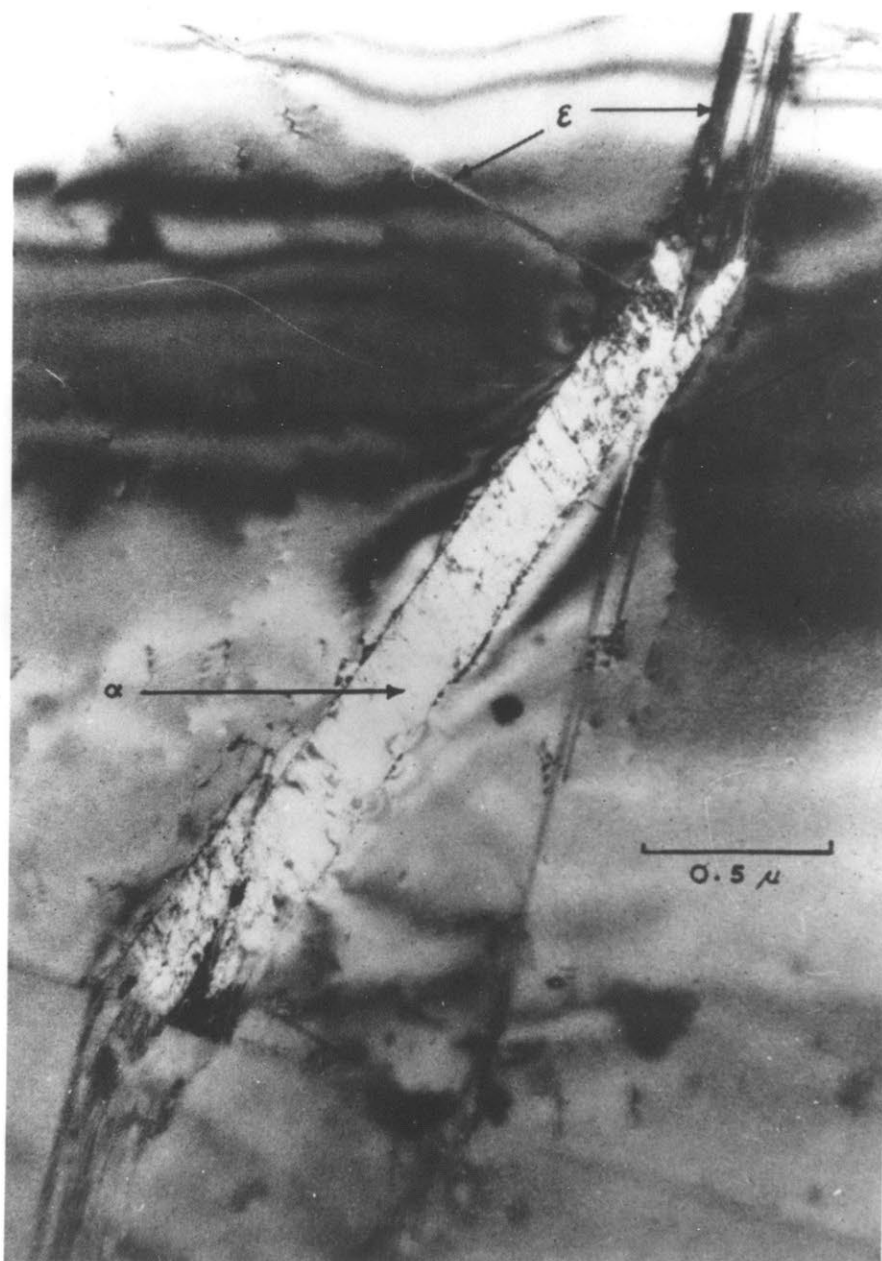
FIGURE 24. {225}-TYPE MARTENSITE PLATE NUCLEATED AT THE
INTERSECTION OF TWO ϵ MARTENSITE BANDS.
VENABLES(26)

In the nucleation process considered here, we substitute for δRB an "effective" total lattice deformation given by:

$$S_T = P\delta'S_2S_1 \qquad\qquad (B2)$$

where S_1 is the first "shear" of the Bogers-Burgers mechanism, S_2 is the modified second "shear," δ' is a uniform dilatation necessary to establish the equilibrium lattice parameter, and P is a plastic deformation which allows a particular (macroscopic) invariant line to be maintained. Though P is actually a lattice-invariant deformation, we here include it in the "effective" total lattice deformation since it performs essentially the same function as the Bowles and Mackenzie diltation parameter, δ. Again, combination of this "effective" total lattice deformation with the conventional single shear lattice-invariant deformation produces the total shape change and thus establishes the invariant plane or habit. In the case of the Greninger-Troiano (259) martensite, P is simply a small rotation about $[111]_{fcc}$ to establish a true invariant line. In the Kurdjumov-Sachs (225) case, it consists of the additional twinning of the multiple-shear theories[73,74] or the complex deformation of the plastic accommodation model[75]. However, in the present context, we consider these additional deformations to take place in the martensite as part of the total lattice deformation rather than occurring in the austenite before the lattice deformation. In other words, we are proposing that the complex deformations

that are necessary to allow habits other than (259) take place

not simply because one type of lattice-invariant deformation

is energetically more favorable than another, but because con-

straints existing at the nucleation stage (and possibly persis-

ting throughout growth) require a particular invariant line to

be produced by the total lattice deformation.

We have already examined how particle shape at the

nucleation stage might influence the invariant line of the total

lattice deformation. It is also possible that such constraints

may have a more basic "mechanistic" origin. If we follow the

orientation of the particle in tracing back the proposed

sequence of steps for the formation of a (259) martensitic plate,

we can describe the sequence as Greninger-Troiano → Kurdjumov-

Sachs → Nishiyama. (The three relations are really equivalent

at the S_1 stage, but the $[1\bar{2}1]_{fcc}$ direction of the Nishiyama

relation is the S_1 shear direction and hence a "special"

direction.) Accordingly, the trend of habit planes corres-

ponding to these three orientation relations of (259) → (225) →

(111) might represent the result of constraints at progres-

sively earlier stages in the lattice-deformation process.

The (111) lath or "massive" martensite morphology is

generally formed at higher temperatures, and is similar to

the martensites formed at higher temperatures in other alloy

systems (e.g. titanium alloys). The analysis of nucleation

kinetics discussed in Chapter 7 and illustrated in Figure 15

suggests that alloys which transform at higher temperatures may

exhibit completely athermal behavior. Further, the kinetic

parameters obtained from isothermal Fe-Ni and Fe-Ni-Mn alloys

indicate that the transition from isothermal to athermal behavior

with increasing transformation temperature will occur in the

vicinity of room temperature, and this is also where the

transition from plate to (111) lath morphology occurs in these

alloys. It may be that an embryo which forms at low

temperatures with some degree of initial isothermal growth may

have an opportunity to relax to a more highly developed form

(e.g. Greninger-Troiano orientation), whereas an embryo which

forms completely athermally at higher temperatures may grow

too rapidly at its inception and its structure and morphology

will resemble that of a more primitive stage of embryo

development (S_1). The more complex deformations required to

maintain this more primitive form might hinder the particle's

growth in the later stages where the plate martensites are

capable of extremely rapid growth, thus accounting for the

smaller size of the final martensitic units in the (111) lath

morphology.

Another possible origin of the constraint leading

to the Kurdjumov-Sachs orientation might be the presence of

the hcp ε phase as an intermediate structure. In the case

of austenites of very low intrinsic stacking-fault energy

where the ε phase is present in appreciable quantities, the

α martensite preferentially nucleates in the ε phase

and forms as ($\bar{1}\bar{1}2$) laths with the Kurdjumov-Sachs orientation. The (225) plate martensites are generally observed in alloys of intermediate stacking-fault energy where the bulk hcp phase is not observed but electron microscopy has revealed the association of intrinsic faults with small embryonic (225) units[76], suggesting that the hcp intermediate structure concept may still play some role in these alloys.

APPENDIX C

ENERGETICS OF INTERMEDIATE CONFIGURATIONS IN THE FCC→BCC LATTICE DEFORMATION

In order to estimate the possible importance of nonlinear elastic effects in the fcc→bcc lattice deformation, the energy necessary to homogeneously deform a bcc lattice into the unrelaxed configuration of the first shear of the Bogers-Burgers mechanism was computed using various interatomic potentials available for pure iron. The results are tabulated in Table C-1. The energies of three configurations were calculated and are represented by the three columns in the table. The first consists of the uniform dilatation ($\Delta V/V \approx 7\%$) necessary to make the bcc atoms of Fe30Ni the same "size" as the fcc atoms. The second consists of the "hard-sphere" shear which converts the bcc structure to the Bogers-Burgers "first-shear" configuration with the atoms in the bcc size. This deformation consists of a shear of 25% along $[0\bar{1}1]_{bcc}$ on $(011)_{bcc}$ accompanied by a 3.6% contraction normal to the shear plane. The third configuration is the product of both the dilatation and "hard-sphere" shear and thus represents the unrelaxed configuration produced by deforming the fcc lattice by the Bogers-Burgers first shear.

The first set of values represents an anisotropic linear elastic calculation for pure iron using a bulk modulus of 1.73×10^{12} dynes/cm^2 and a shear modulus for $[0\bar{1}1]$ (011) shear of $1/2 (C_{11} - C_{12}) = 5.25 \times 10^{11}$ dyne/cm^2. The first

Table C-1

Computed Strain Energy of fcc-bcc Intermediate
Configuration Using Interatomic Potentials
for Pure Iron

	E^{str}, cal/mole		
	dilatation	"shear"	dilatation + "shear"
Linear Elasticity (Anisotropic)	720	3057	3026
Potentials			
Morse (Girifalco and Weizer, 1958)[77]	575	1349	1148
Johnson I (1964)[78]	490	2756	2405
Johnson II (1966)[79]	126	3094	2184
Johnson and Wilson (1971)[80]	674	3840	3391

set of interatomic potential calculations represented are those

obtained from the Morse potential developed for iron by

Girifalco and Weizer[77]. The atomic interactions were summed

over a crystallite 7^3 unit cells in volume. The other

potentials represented in Table C-1 consider only first and

second neighbor interactions. The Morse potential and Johnson

I potential[78] involve only central-force interactions and

thus do not reproduce the elastic constants of iron exactly

since $C_{12} = C_{44}$. For the last two potentials[79,80] a hydro-

static pressure is added to maintain the equilibrium lattice

parameter and the linear elastic constants are reproduced

exactly.

Though the Morse potential calculation gives a strain

energy of approximately half the magnitude of that of the linear

elastic calculation, the other more recent potentials suggest

that the strain energy is not appreciably different from the

linear elastic result. This result is not surprising if we

examine a hard-sphere model. A homogeneous fcc twinning

shear, corresponding to a Shockley partial displacement on

each $(111)_{fcc}$ plane (as illustrated by the displacement "c"

in Figure 12) leads to a twin-related structure with the same

energy as the original undisturbed fcc lattice. The presence

of such a second energy minimum suggests a "softening" of

the elastic constants (at high strain) for displacement in

the $<112>_{fcc}$ direction. However, the deformation of the bcc

lattice considered here corresponds to the displacement "-a"

of Figure 9 on each $(011)_{bcc}$ plane. Such a displacement

brings the hard spheres of one plane in contact with the hard spheres of the plane below in such a way as to hinder further displacement in this direction. If anything, the expected deviation from linearity would be one to make the elastic constants "harder" for displacement in this direction.

The calculated energies in Table C-1 also suggest that to a first approximation the effect of the additional dilatation necessary to maintain a constant sphere size can be neglected in view of the large energy associated with the hard-sphere shear alone. These considerations suggest that a linear elastic calculation of the strain energy of the shear components alone may provide a reasonable picture of the energetics of homogeneously deforming an fcc lattice through the Bogers-Burgers lattice deformation. We can now perform such a calculation for Fe30Ni at the M_s temperature.

The appropriate shear modulus for $[1\bar{2}1]$ $(111)_{fcc}$ shear is $\frac{1}{3}(C_{11} - C_{12} + C_{44})$. Using the elastic constants determined near the M_s temperature for Fe30Ni by Kayser[81] gives a value of $.48 \times 10^{12}$ dyne/cm^2 for this shear modulus. By the considerations discussed earlier, the strain energy associated with a homogeneous shear strain γ_1 on this system should be of the form represented in Figure 25a. Position A is the equilibrium fcc lattice and A' represents the twin-related lattice obtained by a complete twinning shear. The dashed line represents the linear elastic calculation while the solid line reflects the expected "softening" due to the
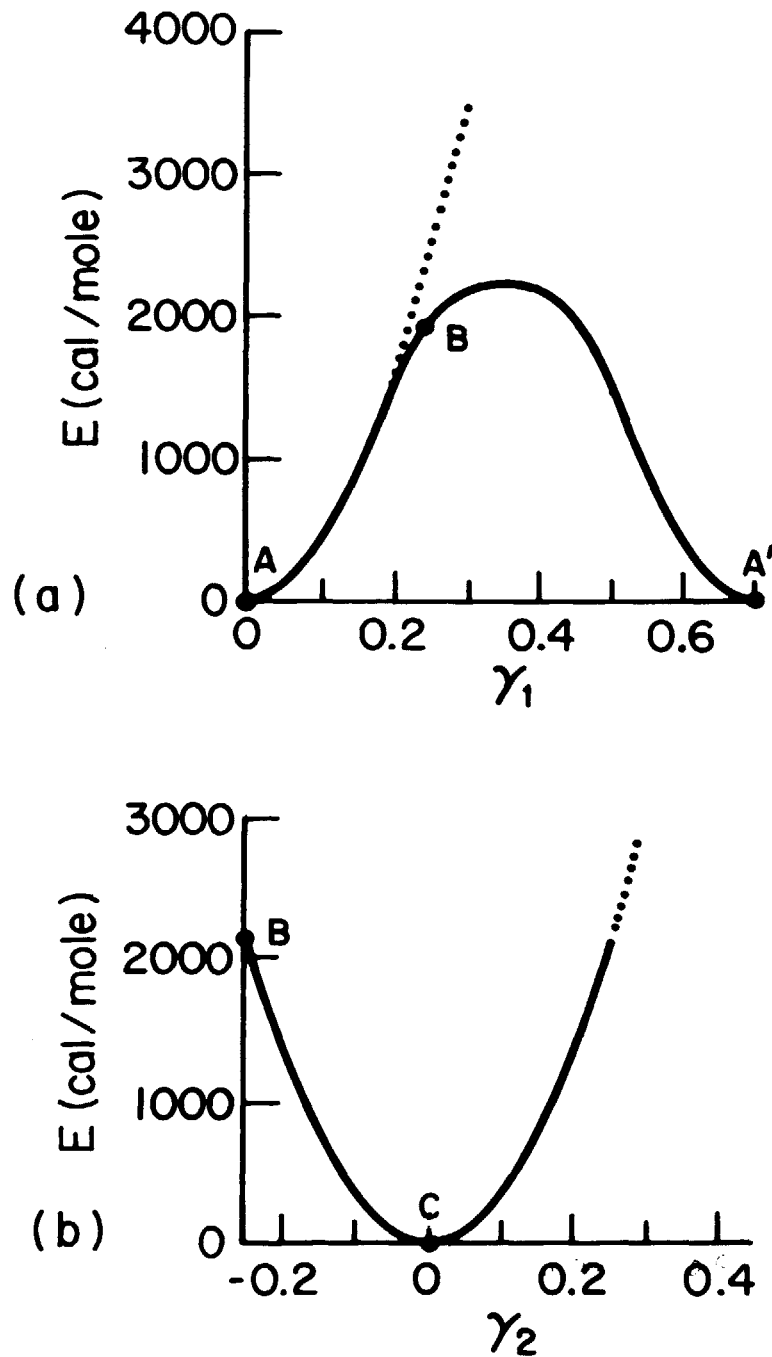
FIGURE 25. STRAIN-ENERGY CURVES FOR SHEAR ON THE TWO SHEAR
SYSTEMS OF THE BOGERS-BURGERS FCC-BCC LATTICE
DEFORMATION MECHANISM
(A) ENERGY VS. SHEAR STRAIN γ_1 ON $[1\bar{2}1]$ $(111)_{FCC}$.
(B) ENERGY VS. SHEAR STRAIN γ_2 ON $[01\bar{1}]$ $(011)_{BCC}$.

presence of the second minimum at A'. Position B represents one-third of a twinning shear and is thus the configuration of the first Bogers-Burgers shear.

The shear modulus for $[01\bar{1}]$ $(011)_{bcc}$ shear used in Chapter 5 gives a strain energy for a shear strain γ_2 on this system in the bcc lattice of the form represented in Figure 25b. Here position C is the equilibrium bcc lattice and position B is again the configuration of the first Bogers-Burgers shear which can be equivalently obtained by a 25% shear strain of the bcc lattice on this system. The interatomic potential calculations and the hard-sphere considerations discussed earlier suggest that there will not be a large deviation from linear elastic behavior in this case. The deformation from position B to position C represents the second shear of the Bogers-Burgers lattice deformation.

Because of the chemical free-energy difference between the two structures the energy of position C of Figure 25b must be 300 cal/mole lower than that of position A in Figure 25a. Also, because position B represents the same structure in both cases the deviations from linear elasticity must be such that the energy of this configuration is the same referred to either lattice. Accordingly, the energetics of homogeneously deforming the fcc lattice through the Bogers-Burgers lattice deformation can be represented by the three-dimensional plot of Figure 26 where the γ_1 and γ_2 axes represent deformations along the two shear systems as in

2500

2000

B

1500

E (cal/mole)

1000

500

0

A   A′ γ_1

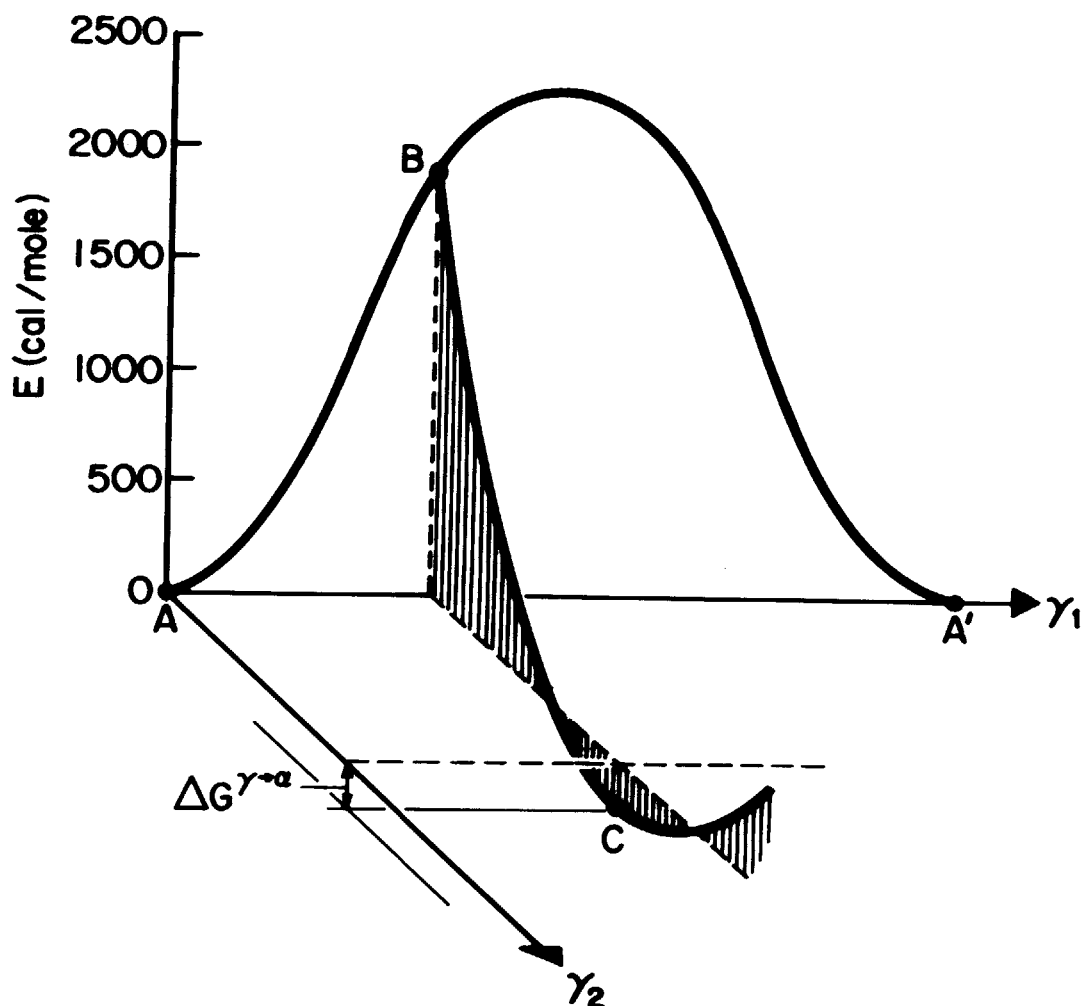$\Delta G^{\gamma \to \alpha}$

C

γ_2

FIGURE 26. COMPOSITE REPRESENTATION OF ENERGY OF HOMOGENEOUS DEFORMATION OF AN FCC LATTICE TO BCC BY THE γ_1 AND γ_2 STRAINS OF FIGURE 25.

Figure 25. We can immediately see than an fcc lattice homogeneously deformed along γ_1 to position B will be unstable with respect to spontaneous deformation along γ_2 to produce the bcc lattice of position C. It should be noted that the energies considered here are for homogeneous deformation of an <u>unconstrained</u> lattice. In considering the formation of a bcc embryo in an fcc matrix, surface and strain energy must be included in the total energy and these will raise position C. Only for the conditions of a negative fault energy established in Chapter 5 will position C be lower than A in the total energy balance. Under such conditions, existing dislocations capable of moving atoms from the A position to the B position will experience a force causing them to move, thus imparting the necessary γ_1 displacement such that the γ_2 displacement may occur spontaneously.

The energy curves in Figure 26 represent sections through an energy surface. If this entire surface were constructed, a lower energy path might be found between points A and C. However, the actual path and the magnitude of the energies involved are unimportant to the nucleation mechanism considered here. The partial dislocations derived from the nucleating defect will accomplish the γ_1 component of the lattice deformation <u>regardless</u> of the energy involved, and the γ_2 component occurs spontaneously. If there is a lower energy path between A and C, the spontaneous γ_2 deformation may begin to occur as the structure is deformed along γ_1 by the partial dislocations even before point B is reached.

By the proposed mechanism these intermediate configurations will only exist at the particle interfaces. The actual magnitude of the energies of the intermediate configurations in the fcc→bcc lattice deformation thus will only influence the core energies of the partial dislocations which form the particle-matrix interfaces.

The exact shape of the energy surface of Figure 26 is important to the proposed alternative approaches to the martensitic nucleation problem which invoke higher-order elastic constants (e.g. localized soft phonon-mode theories[7]). However, it should be noted that higher-order elastic constants derived from such an energy surface for the homogeneous deformation of an unconstrained lattice are not entirely relevant to the nucleation problem. The surface energy and coherency strain energy associated with nucleation in a matrix will severely distort this energy surface (especially where a large macroscopic shape change is involved) and the resultant modification of the effective higher-order elastic constants must be properly taken into account if the martensitic nucleation problem is to be dealt with at all realistically.

It is interesting to consider that the core of an fcc lattice dislocation with partial displacements on the γ_1 shear system is likely to possess atoms in positions near B in Figure 26. Under conditions where position C is of higher energy than A (in the total energy balance of surface, strain, and volume chemical free energy) and thus the formation of a

martensitic embryo is energetically unfavorable, atoms near the B position might still be able to lower their energy somewhat by relaxing toward C on the γ_2 shear system. Since this involves a second shear plane, the dislocation core would thus adopt a partially "cross-slipped" configuration and this may influence dislocation mobility and the resulting mechanical behavior. Such an effect might account for the previously unexplained observation by Breedis and Robertson[49] of a strengthening effect at temperatures slightly above the region of spontaneous stress-assisted martensitic nucleation. The effect was clearly shown by a comparison of the temperature dependence of the critical shear stress for slip in single crystals of an unstable Fe-Cr-Ni alloy with that of a stable Fe-Cr-Ni alloy with comparable solid-solution strengthening. Electron microscopy could reveal no evidence of actual martensitic transformation in the region where the strengthening was observed. Such a strengthening effect might thus be attributed to the dislocation cores adopting the proposed partially "cross-slipped" configuration as the thermodynamic conditions for spontaneous martensitic nucleation are approached.

REFERENCES

1. L. Kaufman and M. Cohen, Prog. Metal Phys., 7 (1958) 165.

2. R. E. Cech and D. Turnbull, Trans. AIME, 206 (1956) 124.

3. V. Raghavan and M. Cohen, Acta Met., 20 (1972) 333.

4. H. Knapp and U. Dehlinger, Acta Met., 4 (1956) 289.

5. C. L. Magee, in Phase Transformations, ASM (1970) 115.

6. V. Raghavan and M. Cohen, Scripta Met., 7 (1973) 591.

7. P. C. Clapp, Phys. Stat. Sol. (b), 57 (1973) 561.

8. H. E. Cook, Acta Met., 21 (1973) 1431.

9. I. Cornelis, R. Oshima, H. C. Tong, and C. M. Wayman, Scripta Met., 8 (1974) 133.

10. L. Kaufman, A. Leyanaar, and J. S. Harvey, Acta Met., 8 (1960) 270.

11. S. V. Radcliffe and M. Schatz, Acta Met., 10 (1962) 201.

12. M. K. Korenko, Sc.D. Thesis, M.I.T. (February 1973).

13. J. W. Christian, in The Mechanism of Phase Transformations in Crystalline Solids, Institute of Metals Monograph No. 33 (1969) 129.

14. M. S. Wechsler, D. S. Lieberman, and T. A. Read, Trans. AIME, 197 (1953) 1503.

15. J. S. Bowles and J. K. Mackenzie, Acta Met., 2 (1954) 129.

16. R. W. Guard and M. E. Fine, Trans. TMS-AIME, 233 (1965) 1383.

17. J. P. Hirth, Met. Trans., 1 (1970) 2367.

18. R. de Wit and R. E. Howard, Acta Met., 13 (1965) 655.

19. A. P. Miodownik, to be published.

20. J. W. Gibbs, The Scientific Papers of J. Willard Gibbs, Dover (1961).

21. F. Lecroisey and A. Pineau, Met. Trans., 3 (1972) 387.

22. F. Lecroisey, Doctoral Thesis, University of Nancy, France (1971).

23. J. F. Breedis and L. Kaufman, Met. Trans., 2 (1971) 2359.

24. T. Ericsson, Acta Met., 14 (1966) 853.

25. A. Pineau, private communication.

26. J. A. Venables, Phil. Mag., 7 (1962) 35.

27. E. Votava, Acta Met., 8 (1960) 901.

28. J. P. Hirth and J. Lothe, Theory of Dislocations, McGraw-Hill (1968).

29. J. D. Eshelby, Roy. Soc. London Proc., A241 (1957) 376.

30. A. E. H. Love, The Mathematical Theory of Elasticity, Cambridge University Press, Cambridge (1927).

31. A. J. Bogers and W. G. Burgers, Acta Met., 12 (1964) 255.

32. K. C. Russell, Met. Trans., 2 (1971) 5.

33. A. J. Goldman and W. D. Robertson, Acta Met., 13 (1965) 391.

34. A. Sherman, Ph.D. Thesis, MIT (August 1972).

35. H. Brooks, Metal Interfaces, ASM (1952) 20.

36. F. C. Frank, Acta Met., 1 (1935) 15.

37. J. Gaggero and D. Hull, Acta Met., 10 (1962) 995.

38. S. Dash and N. Brown, Acta Met., 14 (1966) 595.

39. L. Delaey and I. Cornelis, Acta Met., 18 (1970) 1061.

40. H. Warlimont and L. Delaey, Progress in Materials Science, in press.

41. P. R. Swann and H. Warlimont, Acta Met., 11 (1963) 511.

42. P. L. Ferraglio and K. Muhkerjee, to be published in Acta Met.

43. S. D. Kulkarni, _Acta Met._, _21_ (1973) 1461.

44. D. P. Dunne and C. M. Wayman, _Met. Trans._, _4_ (1973) 137.

45. J. C. Williams, in _Titanium Science and Technology_, Vol. 3, ed. R. I. Jaffee and H. M. Burte, Plenum Press (1973) 1433.

46. J. W. Cahn and W. Rosenberg, _Scripta Met._, _5_ (1971) 101.

47. J. R. Patel and M. Cohen, _Acta Met._, _1_ (1953) 531.

48. V. Vitek, R. C. Perrin, and D. K. Bowen, _Phil. Mag._, _21_ (1970) 1049.

49. J. F. Breedis and W. D. Robertson, _Acta Met._, _11_ (1963) 547.

50. H. Conrad, _Journal of Metals_ (July 1964) 582.

51. J. E. Dorn, in _Dislocation Dynamics_ ed. A. R. Rosenfield, G. T. Hahn, A. L. Bement and R. I. Jaffee, McGraw-Hill (1968) p. 27.

52. C. L. Magee, _Met. Trans._, _2_ (1971) 2419.

53. V. Raghavan and M. Cohen, _Met. Trans._, _2_ (1971) 2409.

54. L. Kaufman, private communication.

55. G. F. Bolling and R. H. Richman, _Phil. Mag._, _19_ (1969) 247.

56. R. H. Richman, private communication.

57. J. F. Breedis, _Trans. TMS-AIME_, _230_ (1964) 1583.

58. V. Vitek and F. Kroupa, _Phil. Mag._, _19_ (1969) 265.

59. G. Fontaine, Thesis, University of Paris (1968).

60. P. L. Manganon and G. Thomas, _Met. Trans._, _1_ (1970) 1577.

61. K. E. Easterling and P. R. Swann, in _The Mechanism of Phase Transformations in Crystalline Solids_, Institute of Metals Monograph No. 33 (1969) 152.

62. J. B. Cohen and J. Weertman, _Acta Met._, _11_ (1963) 996.

63. H. Fujita and S. Ueda, Acta Met., 20 (1972) 759.

64. R. Lagneborg, Acta Met., 12 (1964) 823.

65. G. B. Olson and M. Cohen, J. Less-Common Metals, 28 (1972) 107.

66. D. deFontaine, N. E. Paton, and J. C. Williams, Acta Met., 19 (1971) 1153.

67. G. D. Sandrock, A. J. Perkins, and R. F. Hehemann, Met. Trans., 2 (1971) 2769.

68. J. Perkins, Met. Trans., 4 (1973) 2709.

69. L. E. Murr, Scripta Met., 6 (1972) 203.

70. M. McLean and H. Mykura, Phil. Mag., 14 (1966) 1191.

71. L. Kaufman and H. Bernstein, Computer Calculation of Phase Diagrams, Academic Press, New York, 1970.

72. W. S. Owen, F. J. Schoen, and G. R. Srinivasan, in Phase Transformations, ASM (1970) p. 157.

73. N. H. D. Ross and A. G. Crocker, Acta Met., 18 (1970) p. 1405.

74. A. F. Acton and M. Bevis, Mater. Sci. Eng., 5 (1969) p. 19.

75. J. S. Bowles and D. P. Dunne, Acta Met., 17 (1969) p. 677.

76. K. Shimizu, M. Oka, and C. M. Wayman, Acta Met., 18 (1970) p. 1025.

77. L. A. Girifalco and V. G. Weizer, Phys. Rev., 114 (1959) p. 687.

78. R. A. Johnson, Phys. Rev., 134 (1964) p. A1329.

79. R. A. Johnson, Phys. Rev., 145 (1966) p. 423.

80. R. A. Johnson and W. D. Wilson, in Interatomic Potentials and Simulation of Lattice Defects, ed. R. I. Jaffee, Battelle Memorial Institute (1972) p. 301.

81. F. Kayser, private communication.

Biographical Note

Gregory B. Olson was born on April 10, 1947 in Brooklyn, New York. Raised in Huntington, Long Island, and educated in their primary and secondary school systems, he graduated from Huntington High School in 1965 and entered M.I.T. He received simultaneously the S.B. and S.M. Degrees in Metallurgy in 1970, with a Thesis entitled "The Design and Construction of an Ultra-High Vacuum Field-Ion Microscope," and directly entered a doctoral program in Metallurgy with a minor in music composition. While at M.I.T. he has been active in the M.I.T. Jazz Band, Concert Band, and Sports Car Club.